SPECIAL REPORT 90-40

(12)

CRREL

Ice Formation In Frequently Transited Navigation Channels

Robert Ettema and Hung-Pin Huang

December 1990

For conversion of SI metric units to U.S./British customary units of measurement consult ASTM Standard E380, Metric Practice Guide, *published by the American Society for Testing and Materials, 1916 Race St., Philadelphia, Pa. 19103.*

Special Report 90-40

U.S. Army Corps of Engineers
Cold Regions Research & Engineering Laboratory

Ice Formation In Frequently Transited Navigation Channels

Robert Ettema and Hung-Pin Huang

December 1990

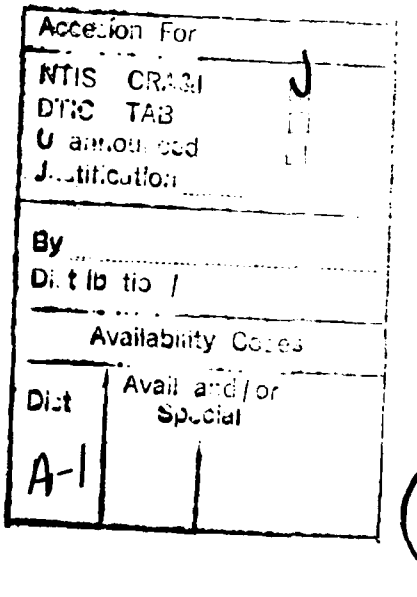

Prepared for
OFFICE OF THE CHIEF OF ENGINEERS

PREFACE

This report was prepared by Robert Ettema, Research Engineer, and Hung-Pin Huang, Research Assistant, Iowa Institute of Hydraulic Research, College of Engineering, The University of Iowa, Iowa City, Iowa. The project was funded by the Office of the Chief of Engineers, Directorate of Civil Works, under the River Ice Management Program, Work Unit CWIS 32292, *Travel Frequency Effects on the Formation of River Ice.*

This report was technically reviewed by Dr. Jean-Claude Tatinclaux and Dr. George Ashton of CRREL and by James Sandkvist of SSPA Maritime Consulting AB, Gothenburg, Sweden.

CONTENTS

ILLUSTRATIONS

Figure

TABLES

Nomenclature

B beam of vessel
C constant
$C_{1,2,3..}$ coefficients
D draft of vessel
D' thickness for determining the loss rate $\{ = \eta_i B/[(1-p)\tan\theta_w)]\}^{0.5}$
d_e equivalent dimension of ice pieces median dimension of brash ice
d_{e16} value of d_e for which 16% of the brash-ice pieces are finer in size
d_{e84} value of d_e for which 84% of the brash-ice pieces are finer in size
$d_{x,y,z}$ orthogonal dimensions of ice pieces
$f_{1,2,3..}$ functions
f_n frequency of sequences within a navigation period
F_r Froude number
F_r^* modified densimetric Froude number $[= F_r y_o/(y_o - D)]$
F_{rc}^* critical densimetric Froude number
f_s frequency of transits within a navigation period
f_t frequency of transits within a sequence period
g gravitational acceleration
h thickness of brash-ice accumulation
h_{ia} heat transfer coefficient between ice and air
i index
j index
K maximum number of layers to form residual ice
k_i conductivity of ice
L_i latent heat of ice fusion
ℓ major length of ice block
L length of barge
m layer number
N number of equivalent dimensions of brash ice
N_i number of cooling temperature for i^{th} transiting interval
n number of transits in the convoy time
p porosity; ratio of water volume to total volume
P_o period between sequences
P_i initial period of ice formation
P_n navigation period $(= P_s + P_o)$
P_s sequence period
P_T total period $[= P_i + \Sigma (P_s + P_o)]$
P_t period between transits
R mean total resistance
R resistance in open water track
R_i mean ice resistance $(= R - R_o)$
t time
T_a air temperature
T_f freezing temperature of water
t_p time for water to calm before regrowth commences after a transit
T_s surface temperature
u_* shear velocity of water flow
u_{*c} critical shear velocity of water flow
V barge speed or flow velocity
mean velocity of water flow
V_{ri} volume of ridge after i^{th} transit
W width of channel
W_r width of ridge after i^{th} transit
y_o water depth
Z_w distance between the upper ice and the water surface
α Stefan coefficient
β areal concentration; ratio of open water to track area
β_o initial β value
ΔT temperature difference
ΔV_r increased volume in ridge between transits
$\Delta\eta_i$ increased average thickness during the i^{th} transit
ε_i loss rate of ice from track to both sides during i^{th} transit
η ice sheet thickness at time t; thickness of ice block
η_o initial ice thickness
η_a residual or additional thickness of ice under the pack
η_b accumulation of brash ice in the track
volume of solid ice in the track per unit layer of track surface
η_i equivalent thickness of ice formation
η_n thickness of ice regrowth over open water in the track
η_p plug thickness of brash ice
η_{ri} ridge thickness
η_s thickness of the ice slabs composing the layer
θ stem angle of barge flow
θ_a accumulation slope ahead of barge
θ_r angle of static repose of the brash ice
θ_w flare angle
λ wavelength of wave
λ_D scale of draft
λ_{hia} scale of h_{ia}
λ_{ki} scale of k_i
λ_L scale of L
λ_ℓ length scale
λ_t time scale
$\lambda_{\Delta T}$ scale of temperature difference
λ_η scale of η
λ_ρ scale of ρ
μ_b coefficient of static friction between ice and hull
μ_i coefficient of static friction between ice blocks
υ kinematic viscosity of water
ρ mass density of water
ρ_i mass density of ice
ΣS_d cumulative cooling time
σ_g geometric standard deviation of ice block
$\phi_{1,2,3..}$ functions
ϕ_i heat flux by conduction through the ice cover
ϕ_{ia} heat flux from ice to air
ϕ_{wi} heat flux from water to ice

Ice Formation In Frequently Transited Navigation Channels

ROBERT ETTEMA AND HUNG-PIN HUANG

INTRODUCTION

Among ice navigators an old adage runs "an ice-breaker is an ice-maker" (Keating 1970). What is implied is that a vessel moving through an ice-covered channel creates an open water track over which ice may regrow. If an ice-covered channel is transited many times along more or less the same track so that numerous cycles of icebreaking and regrowth occur, then considerably more ice may grow in the channel than if it were not transited.

The effects of frequent vessel transit on ice-cover formation pose important concerns for winter navigation of heavily trafficked river, harbor and coastal channels. Of prime concern is the likelihood that frequent transits may cause the channels to become clogged and frozen over with thick accumulations of broken ice, usually termed brash ice, possibly until they become unnavigable. Another concern is that transits may prevent or disrupt the initial establishment of an ice cover over a river, with potentially troublesome consequences if the river water becomes supercooled and generates large amounts of frazil ice. Also, when an ice cover breaks up, the increased volume of ice grown as a result of transiting may increase the potential for ice jamming. Increased ice volume may also exacerbate difficulties associated with passing broken ice at dams.

This study examines the effects of frequent vessel transit on ice formation in navigation channels. It was conducted under the U.S. Army Corps of Engineers' (COE) River Ice Management (RIM) program. The RIM program is aimed at developing engineering methods for managing navigable rivers that become ice covered during winter. In accordance with this aim, this study places special focus on transits of river channels by tow vessels, such as those that ply navigable channels in the upper basin of the Mississippi River. Tow vessels typically comprise a towboat and one or more flat-bottomed barges (Fig. 1). The results of the study are sufficiently generic, however, so as to apply to ice-covered channels in general.

The study's principal contributions include detailed descriptions and a predictive model of the effects of frequent vessel transit on ice-cover formation over navigable channels. The descriptions are founded on computer-based numerical modeling and the results of extensive laboratory experiments conducted in an ice tank with scale-model hulls used to simulate tow-barge and ship-form hulls. The numerical model can be used for predicting ice formation in channels under ranges of meteorological conditions and transit frequencies. It can give information on volumes of ice grown as well as on distributions of broken ice at typical channel cross sections. Its development and calibration were guided by the results of the ice-tank experiments. Though prior studies have used numerical modeling of ice formation, to the best of the authors' knowledge, this is the first for which frequent-transit effects were studied using an ice tank. The numerical modeling and ice-tank experiments were also conducted to determine if there are optimum schedules of vessel transits that would reduce or ameliorate some of the problems attributable to frequent transiting.

A troublesome feature of transiting tows is their propensity to accumulate broken ice beneath their flat-bottomed hulls. Such accumulations may significantly increase transiting resistance and, for shallow channels, may cause tows to ground. Also, when moving through thinly refrozen brash ice or brash that is not refrozen, tows can develop and shove extensive false bows of broken ice. This study also investigated the mechanics of ice accumulation beneath and ahead of tows.

LITERATURE REVIEW

The literature on ice formation in navigation channels is not extensive, though recently it has

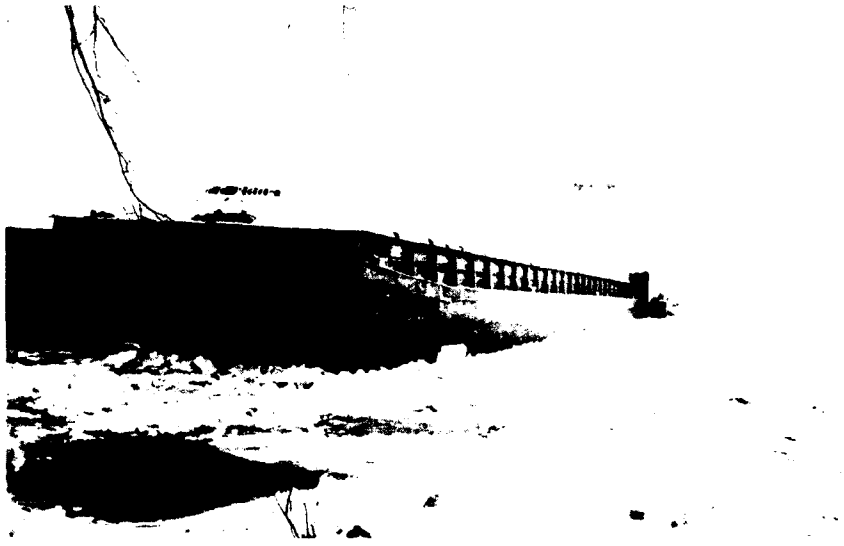

Figure 1. Tow moving through a brash-ice-covered channel in the Mississippi River.

burgeoned in response to heightened interests in developing or improving the use of navigation channels during frigid winter conditions. The potential concerns incurred with vessel transit of ice-covered channels are fairly well recognized, but few in-depth studies have been conducted to address them. Especially lacking are adequate descriptions and knowledge of the ways that frequency of transiting, hull forms of vessels, vessel maneuvering activities, channel geometry and water currents affect ice-cover formation.

This review gathers the sparse information on ice formation in navigation channels. It begins with the standard formulation of ice-cover growth leading to the well-known Stefan equation, which is the basis of prior predictive models of ice formation in frequently transited channels. A digest of field observations on ice formation in navigation channels follows for both river channels and harbor and coastal channels. The review also examines the formulations of prior predictive models of ice formation in vessel tracks opened through ice-covered channels.

Useful assessments of the engineering concerns faced in developing and maintaining navigation of ice-covered channels are given by Ashton (1974), Mellor et al. (1978), Vance (1980), Eranti et al. (1983a,b), Beurket and Argiroff (1984), Tronin et al. (1984), Argiroff and Weigum (1986) and Sölve (1986). These publications are not reviewed here, although some are referred to when they provide insight on how vessel transits affect ice formation. Also not reviewed are publications dealing with the strength properties of brash ice or with the resistance encountered by vessels transiting channels filled with brash or broken ice. These topics are germane to vessel transiting of navigation channels, but they exceed the scope of the present study. Appendix A, however, does deal briefly with the resistance encountered by tows transiting layers of brash ice. Brash-ice strength properties are discussed by Tatinclaux and Cheng (1978), Mellor (1980) and Urroz and Ettema (1987). Further information on brash-ice resistance is available from Voelker and Levine (1972), Ashton et al. (1973), Kotras et al. (1977), Mellor (1980), Eskola (1983), Ettema et al. (1985) and Forsman and Sandkvist (1986).

Ice-cover growth

The rate at which an ice cover thickens thermally, or "statically," as an ice sheet is determined mainly by the net flux of heat through it, as is indicated in Figure 2. Formulation of thickening (or growth) rate usually involves the following assumptions:

- The temperature profile through the ice cover is linear;
- The heat fluxes of water and ice are negligibly small compared with heat fluxes through solid ice covers; and
- The heat-transfer coefficient between ice and air h_{ia} is large relative to the ice conductivity per unit ice thickness k_i/η.

In accordance with these assumptions, the heat

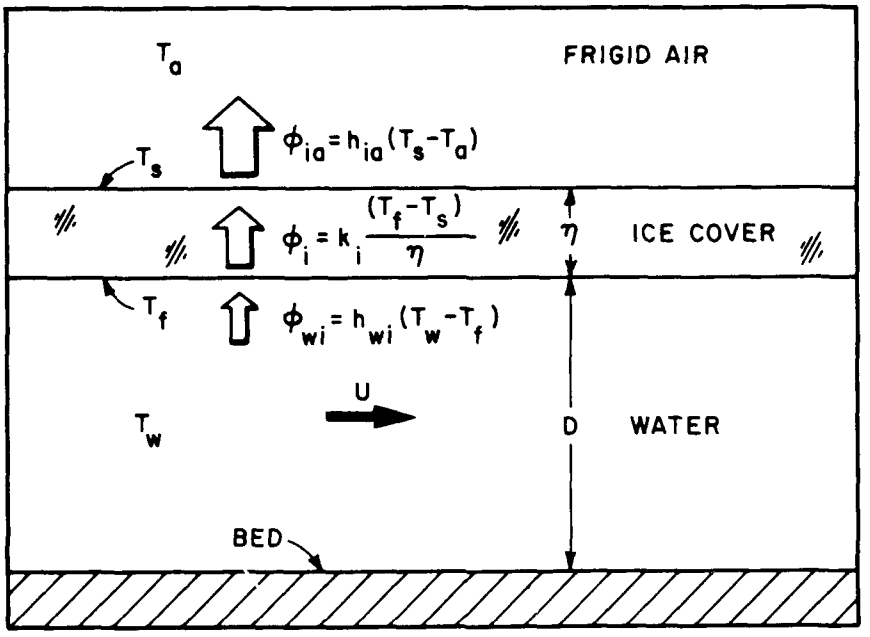

Figure 2. Energy fluxes associated with the thermal growth of ice covers.

balance at the interface between an ice cover and water can be expressed as

$$\phi_i - \phi_{wi} = \rho_i L_i \frac{d\eta}{dt} \tag{1}$$

where ϕ_{wi} = thermal-energy flux from water to ice
ϕ_i = flux by conduction through the ice cover
ρ_i = density of ice
L_i = latent heat of ice fusion
η = ice sheet thickness at time t.

Also,

$$\phi_i = -k_i \frac{(T_s - T_f)}{\eta} \tag{2}$$

where k_i = thermal conductivity of the ice cover
T_s = surface temperature of the ice cover
T_f = freezing temperature of water (0°C or 32°F, for pure water).

If the insulating effects of snow precipitation on ice growth can be neglected, ϕ_i is usually equated to the flux of thermal energy from ice to air ϕ_{ia}:

$$\phi_i = \phi_{ia} = h_{ia}(T_s - T_a) \tag{3}$$

where h_{ia} is the coefficient of heat transfer between ice and air, and T_a is the air temperature. Combining eq 1, 2 and 3 and eliminating T_s yields

$$\phi_i - \phi_{wi} = \frac{T_f - T_a}{\frac{\eta}{k_i} + \frac{1}{h_{ia}}} \tag{4}$$

If ϕ_{wi} is negligibly small, the following relationship is arrived at for ice cover thickening:

$$\phi_i \cong \frac{T_f - T_a}{\frac{\eta}{k_i} + \frac{1}{h_{ia}}} = \rho_i L_i \frac{d\eta}{dt} \tag{5}$$

Integration of eq 5 gives

$$\eta^2 + \frac{2k_i}{h_{ia}}\eta - \frac{2k_i}{\rho_i L_i}\int_0^t (T_f - T_a)\,dt + C = 0 \tag{6}$$

where C is a constant of integration. If $\eta = 0$ at time $t = 0$, eq 6 is reduced to

$$\eta = -\frac{k_i}{h_{ia}} + \left[\left(\frac{k_i}{h_{ia}}\right)^2 + \alpha^2 \sum_{j=1}^{N_i} S_d\right]^{0.5} \tag{7}$$

where α is a growth coefficient [sometimes called air freezing index (Lunardini 1981)], which is usually less than its face value of $(2k_i/\rho_i L_i)^{0.5} = 34$ mm/(°C-days)$^{0.5}$; and ΣS_d is the accumulated degree-days of air temperature below the temperature at which water freezes.

When

$$\alpha^2 \sum_{j=1}^{N_i} S_d < \left(\frac{k_i}{h_{ia}}\right)^2$$

then eq 7 becomes

$$\eta = -\frac{k_i}{h_{ia}} + \frac{k_i}{h_{ia}}\left[1 + \left(\frac{\alpha h_{ia}}{k_i}\right)^2 \sum_{j=1}^{N_i} S_d\right]^{0.5}$$

$$= -\frac{k_i}{h_{ia}} + \frac{k_i}{h_{ia}}$$

$$\left[1 + \frac{1}{2}\left(\frac{\alpha h_{ia}}{k_i}\right) \sum_{j=1}^{2N_i} S_d - \frac{1}{8}\left(\frac{\alpha h_{ia}}{k_i}\right)^4 \left(\sum_{j=1}^{N_i} S_d\right)^2 + \ldots\right]$$

$$\cong \frac{1}{2}\frac{h_{ia}\alpha^2}{k_i} \sum_{j=1}^{N_i} S_d \quad . \tag{8}$$

If

$$\alpha^2 \sum_{j=1}^{N_i} S_d \gg \left(\frac{k_i}{h_{ia}}\right)^2$$

eq 7 is reduced to the well-known Stefan equation:

$$\eta = \alpha \left(\sum_{j=1}^{N_i} S_d\right)^{0.5} \quad . \tag{9}$$

Equation 9 is the basis for all prior predictors of ice growth in navigation channels.

Ashton (1986) and Hausser and Parkinson (1986) pointed out that the presence of a "thermal boundary layer" of air above a thin ice cover should be considered in the foregoing formulation. This refinement is not widely used, and it diminishes in importance once an ice cover is more than a few centimeters thick. The usual practice is to assign values that have been proven representative of particular conditions of ice growth. Michel (1971), for example, recommended using an α value of 28 mm/(°C-days)$^{0.5}$ for windy lakes without a snow cover (the thermal boundary layer is thin). For average rivers with snow and sheltered small rivers (the thermal boundary layer is thick), he suggested α values of 17–13 mm/(°C-days)$^{0.5}$ and 14–7 mm/(°C-days)$^{0.5}$, respectively.

Ice formation in navigation channels

Ice covers over frequently transited navigation channels do not form or remain as monolithic covers. Instead, they become riven with the tracks of vessels, sometimes to the extent that they consist only of broken ice, which is usually in the brash-ice size range. Vessel tracks, and occasionally entire channels, may fill with brash ice, which consists of ice fragments that typically are about 0.02–2 m in major dimension (Mellor 1980, Welsh and Kingsbury 1975). Brash ice normally results when broken ice, often originating as broken sheet ice, is further abraded and fragmented. Few profiles have been measured of brash-ice accumulations in navigation channels. Fewer measurements have been made of the size distribution and micromorphology of brash ice in vessel tracks and navigation channels. What is clear, however, is that, in addition to meteorological conditions, ice formation in navigation channels is influenced by the hull geometry and speed of transiting vessels, the frequency of transits, the channel geometry and water currents. None of these influences appears to have been examined extensively.

For channels of quiescent water, initial ice covers may form as level ice sheets that thicken thermally. For channels with significant water currents, ice covers may establish initially as accumulations of drifting ice floes, broken ice or frazil ice (Ashton 1986) that consolidate, then thicken thermally. The initial establishment of an ice cover over a heavily trafficked channel may be accompanied by the simultaneous formation of a track or tracks opened by transiting vessels. Vessel tracks through moderately or lightly trafficked channels may form through already established ice covers. In either case the track width and the amount of broken ice left in it depend on icebreaking patterns created by the transiting vessel, as well as the speed and hull form of the vessel.

Several detailed measurements of icebreaking patterns and ice-fragment sizes have been made for vessels moving through level sheets of ice. Kashteljan et al. (1968), Lewis and Edwards (1970), Enkvist (1972) and others have published descriptions of ship tracks through ice sheets. Ashton et al. (1973) described tracks typically formed by tows navigating ice-covered rivers. The track left by a vessel moving through an ice sheet is slightly wider than the vessel and for most ship-form hulls may have cuspate edges. The tracks left by tows are characteristically relatively straight-edged and, for thin ice, can have widths equivalent to tow beams (Ashton et al. 1973), although this depends on the tow configuration and the occurrence of wave-induced icebreaking. The size of the ice fragments left in a vessel track depends on ice thickness, ice strength and hull speed, as well as hull bow and form.

Generally ice fragments increase in size (plan dimensions) with increasing thickness and strength of the ice sheet transited by vessels. Somewhat

smaller fragments can occur for greater hull speeds (e.g. Enkvist 1972), and larger fragments occur for larger bow flare angles. McKindra and Lutton (1981) statistically analyzed measurements of broken ice in tracks formed by an icebreaking tug during a single transit through level ice sheets and ice covers composed of refrozen brash ice on Lake Superior. They found that refrozen brash ice broke into pieces about 30% smaller than did ice sheets. The mean size of ice-sheet pieces decreased with hull speed, but the mean size of refrozen brash-ice fragments increased slightly with hull speed. For both types of ice cover, they found the size distributions of broken ice to be log normal. Tuovinen (1978) reached the same conclusion during a study of channels cut through ice sheets on the Baltic Sea.

There are few published studies dealing with ice formation in frequently transited navigation channels or vessel tracks. The most informative studies are those by Ashton et al. (1973), Kannari (1983) and Sandkvist (1986). However, these are limited to field investigations of particular channels traversed at irregular frequencies by vessels of quite different hull forms. The field study reported by Sandkvist constitutes perhaps the most detailed set of field observations on ice formation in a frequently transited navigation channel. His study was conducted with an icebreaker that, at irregular frequencies, plied two channels at Luleä Harbor in coastal northern Sweden. Kannari's study involved several icebreakers and ice-worthy cargo ships that transited coastal channels in Finnish waters off the Gulf of Bothnia. Ashton et al. gave an extensive account of tow transits through diverse conditions of ice-covered channels in the upper Mississippi River.

Significant differences in the observations reported by the three studies, mainly brought about by the radically different hull forms and channel conditions that each involved, suggest that river channels should be viewed separately from harbor and coastal channels. River channels are characteristically shallow and often narrow. They contain flowing water, are prone to becoming supercooled and generating frazil ice, and may be punctuated by barriers such as locks and dams. Furthermore, they nearly always are transited by shallow-draft vessels that are relatively bluff-bowed and flat-bottomed, such as tows, barges, scows and, for the St. Lawrence and St. Marys rivers, Great Lakes bulk carriers. Harbor and coastal channels, on the other hand, are usually (though not exclusively) comparatively deep, adjoin large water bodies that are less readily supercooled than are rivers, and are transited by relatively deep-draft, ship-form hulls. There is, of course, some overlap of the two categories of channel, as they have many common features of ice formation. On occasion, barges are used for coastal transportation, and sea-going ships may transit portions of the St. Lawrence River (Canada), the Saimaa Canal (Finland) or the Trollhätte Canal (Sweden).

Transit of river channels

The only substantial account of ice formation in river channels transited by tows is given by Ashton et al. (1973). Their description of the effects of repeated tow transiting on ice formation is complicated by the fact that their observations were made during comparatively few transits by eight different configurations of tow. Nonetheless, their study indicates that, as the result of water current and tow entrapment and shoving of brash ice, brash ice accumulates very nonuniformly in tracks made by tows. They observed that brash ice in tracks tended to consolidate at certain locations separated by extensive areas of open water, as illustrated in Figure 3. It is at these locations, which often seem to coincide with a channel constriction, that tows had great difficulty in transiting thick accumulations of brash ice. Ashton et al. (1973) found that thick accumulations of brash ice almost halted tow transit at two especially difficult locations (Fig. 4).

Ashton et al. (1973) described the tracks left by tows transiting ice sheets, which were about 0.20–0.25 m thick, as being "cleanly edged" and about the same width as the tow. Much of the broken or brash ice created during the transit was either cast to the sides of the tow, with very little remaining in the track, or accumulated beneath barges. They detected this feature from an extensive trail of brash ice that, on one occasion, was left behind a tow once it had entered open water. They noted that, once an accumulation was in place, it required increased tow speed to entrain it.

The form of the tracks opened by tows and the amounts of brash ice accumulated in them varied with tow arrangement, tow speed, extent of maneuvering and ice-sheet thickness. Ashton et al. (1973) reported that "while an initial passage through an unbroken ice cover may result in a track with considerable open water areas, after several passages the track becomes entirely covered with brash." They qualified this description by noting that the increased areal concentration of brash ice was due in great part to the additional breaking of ice bordering the track by the bow wave produced by a tow during a subsequent

▲ *a. Mississippi River.*

◀ *b. Illinois River at its confluence with the Mississippi River.*

Figure 3. Tow tracks through an ice cover.

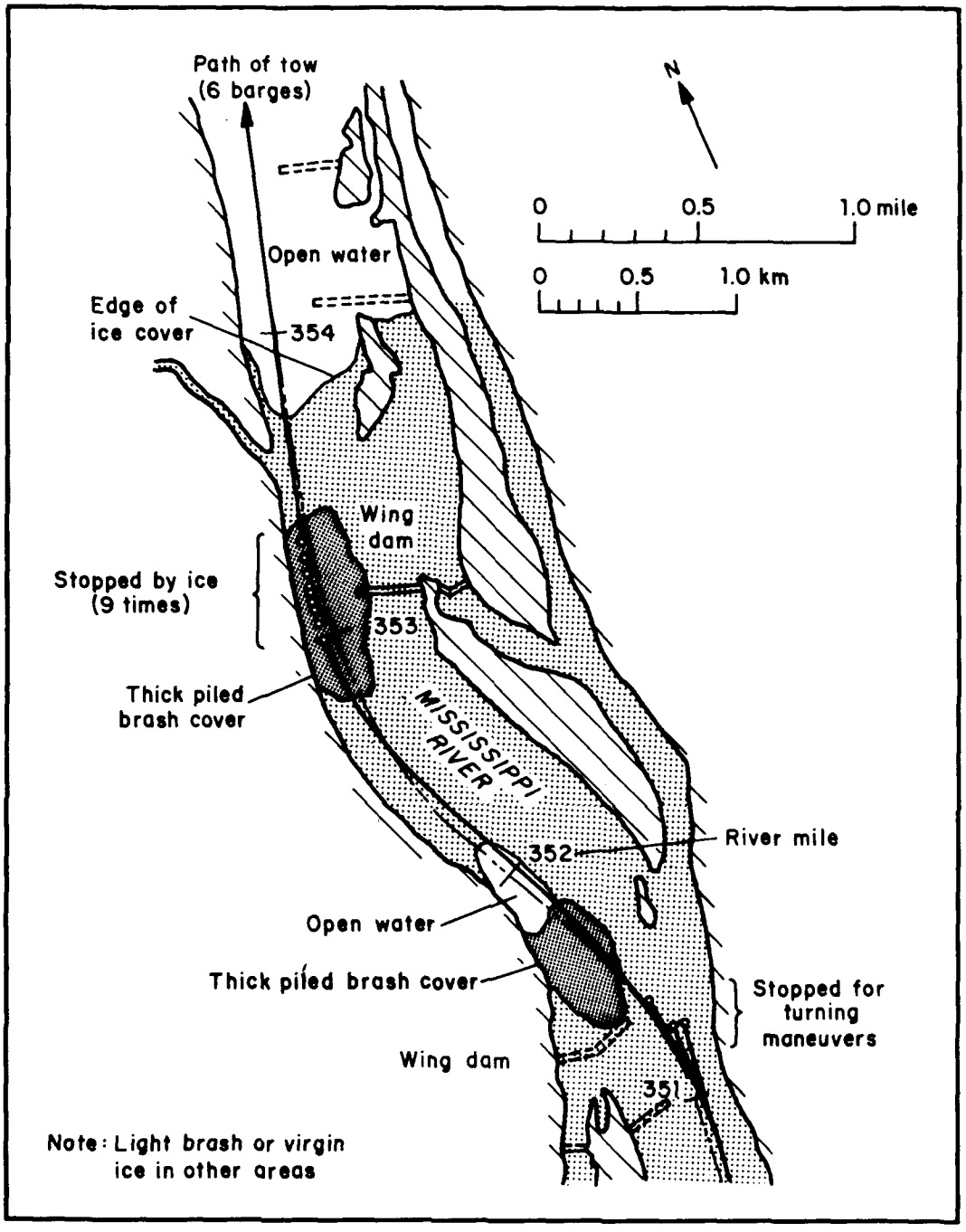

Figure 4. Local areas of thick brash-ice accumulations in the Mississippi River. (From Ashton et al. 1973.)

passage of the track. They did mention, though, that the arrangement involving the towboat alone resulted in more brash ice remaining in the track; about 95% of the track was covered by brash ice. These observations suggest that for tow hulls, hull length influences the displacement of brash ice from a track and therefore affects ice formation in a frequently transited channel.

Entrapment and shoving of broken ice seems to be a characteristic feature of tow transit through ice-covered channels. In addition to collecting broken ice beneath their hulls, tows moving through loose (not refrozen) covers of brash ice develop false bows of brash ice. False-bow and under-hull accumulations of ice rubble may cause especially severe problems for tows attempting to

Figure 5. Tow shoving brash ice while approaching a lock.

pass through locks. Brash ice accumulated ahead of a lead barge can be pushed into locks, creating problems for operation of their miter gates. Ice accumulated beneath barges may cause them to become stuck on the exit sill of locks. Figure 5 illustrates the amount of ice that a tow can shove ahead of itself, especially when moving through a narrow or confined channel. Under-hull accumulations of ice not only increase the resistance experienced by tows, but they may also cause them to ground in shallow channels. Reports prepared by the U.S. Army Corps of Engineers (1976, 1978) and Borland (1987) cite frequent instances of tows grounding on ice under the hull. One report (U.S. Army Corps of Engineers 1978) mentions an incident in which a tow grounded on an accumulation that was about 6.1 m thick. Another (U.S. Army Corps of Engineers 1976) documents an incident in which a tow grounded on about 3.9 m of brash ice when attempting to pass through Lock and Dam No. 26 in the Mississippi River. Figure 6 shows ice removed from beneath a tow and left in a lock after a difficult lockage. Operators of tows in the waterways of the upper Mississippi River report

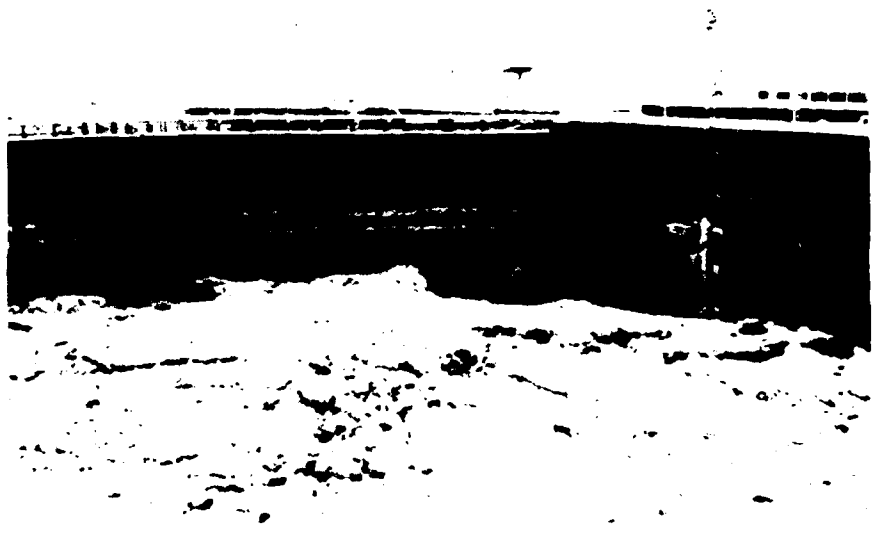

Figure 6. Ice removed from beneath a tow as it left a lock.

that accumulation problems can be particularly severe for tows with empty, open barges in frigid conditions, because brash ice may adfreeze to them. Incidents of grounding, especially in locks, have become of such concern to the Corps of Engineers, as well as to tow operators, that at Lock and Dam No. 26 the Corps of Engineers has installed sonar transducers for monitoring ice accumulation beneath tows (Borland 1987).

One river that regularly poses problems for winter navigation is the St. Marys River linking Lakes Superior and Huron. Kotras et al. (1977), Mellor et al. (1978) and Vance (1980) described the difficulties experienced by Great Lakes bulk carriers in transiting relatively thick accumulations of brash ice that form along the St. Marys River. Although these studies did not explicitly identify the origin of the brash-ice accumulations, they did infer that the accumulations are attributable to the water current and the shoving of ice by bluff-bowed bulk carriers. Mellor et al. ventured some concepts on how best to manage brash-ice accumulations, as did Vance. Scheduling of transits was not considered. Kotras et al. also provided some anecdotal information on transits of brash ice in vessel tracks through ice covers on Lake Superior. The brash-ice layers were thin and posed no significant problem except when wind-driven ice sheets pressurized the layers.

Transit of harbor and coastal channels

Field studies indicate that ice formation in ship tracks through ice-covered harbor and coastal channels is more orderly than in tracks through ice-covered river channels transited by tows. The greater orderliness can be attributed to the inability of typical ship-hull forms to entrap and shove broken ice, and to the absence of significant water currents, which would cause brash ice to drift and collect as locally thick accumulations.

Detailed field studies of ice formation in specific harbor and coastal channels have been reported by Sandkvist (1978, 1980, 1981, 1982, 1986), Tuovinen (1978) and Kannari (1983). These studies show that frequent transits of harbor and coastal channels result in ship tracks that fill with more-or-less uniform layers of brash ice flanked by inverted linear mounds or ridges of brash ice accumulated beneath the ice-cover edges adjoining the tracks. Figure 7 depicts a typical cross section of a brash-filled track. Their studies indicate that layers and ridges of brash ice resulted largely from repeated cycles of ice regrowth and icebreaking, rather than from brash ice conveyed and collected by the water current or by vessel shoving.

Sandkvist, who studied ice formation in two 200-m-long channels at Luleä Harbor, Sweden, obtained information on the rates at which layers of brash ice formed and thickened in ship tracks, their cross-sectional profiles, size distributions of their constituent brash ice, and layer porosities. He used the data on layer thickening (Fig. 8) to develop a fairly simple predictor of ice formation. The two channels were ostensibly transited at different frequencies, but there were no major

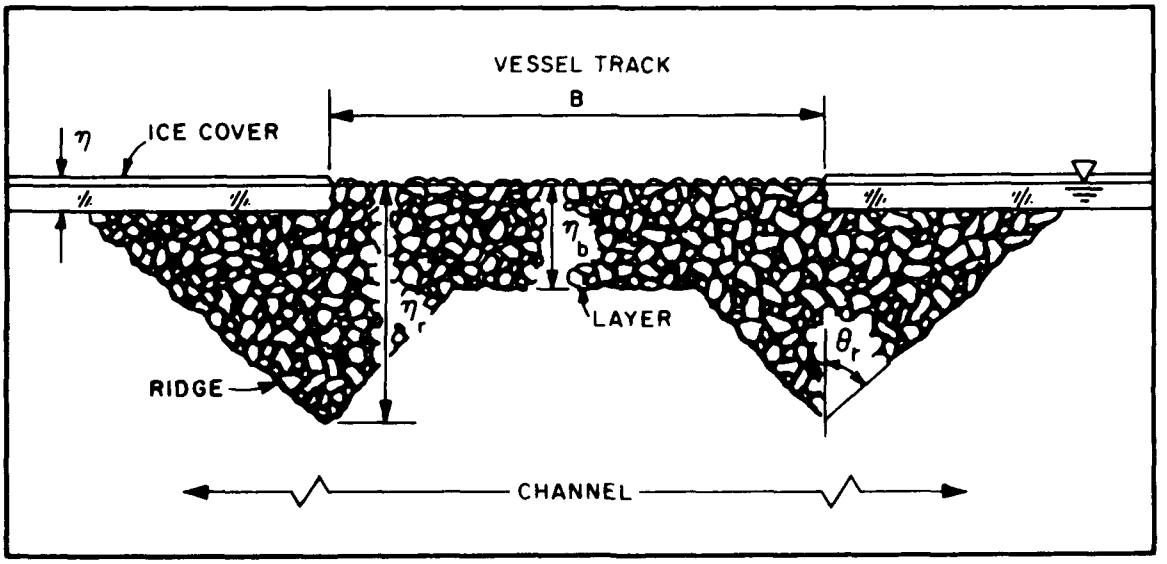

Figure 7. Typical cross section of a vessel track filled with brash ice.

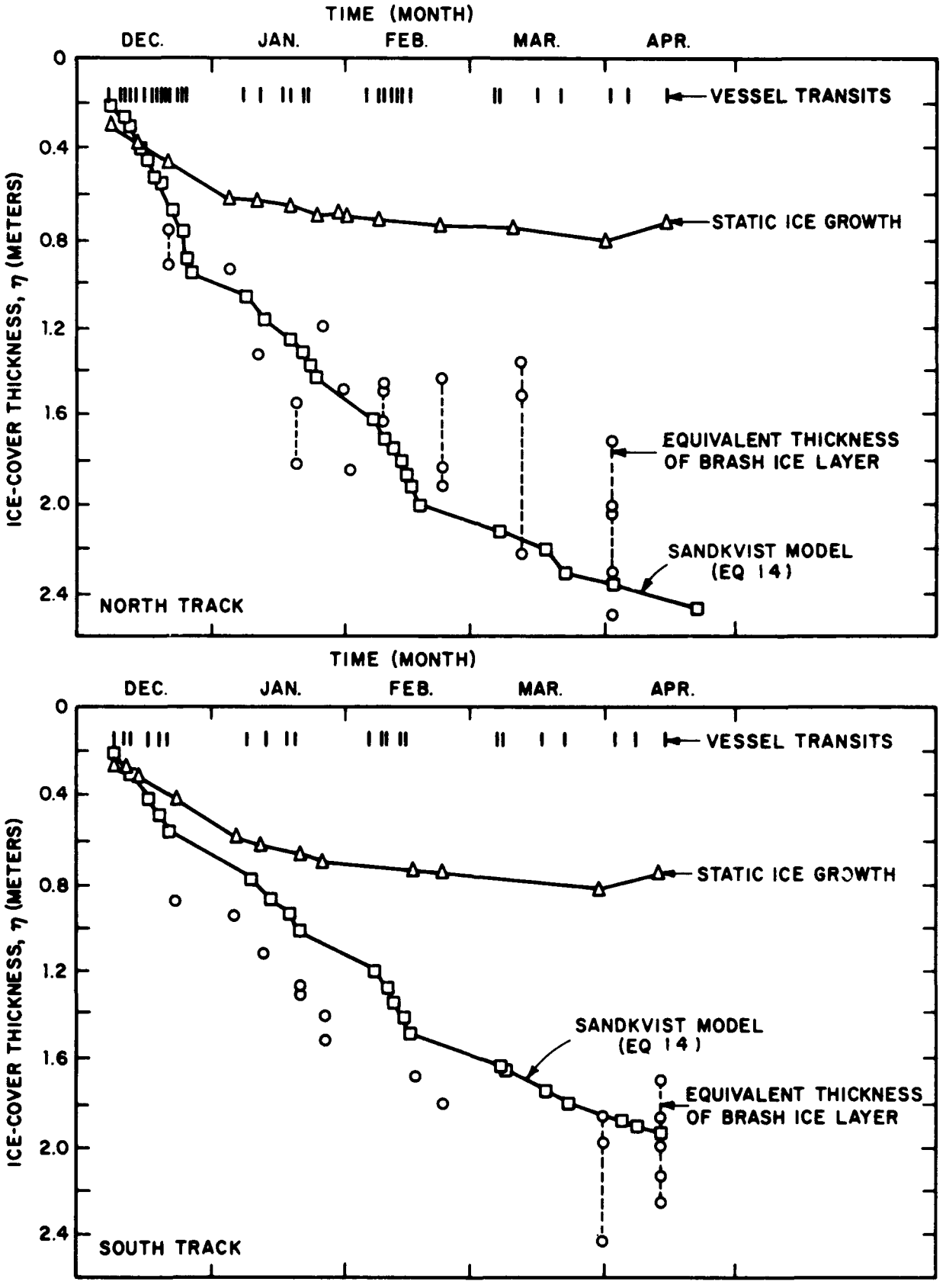

Figure 8. Field data on brash ice and ice-cover thicknesses in ship tracks formed in Luleä Harbor, Sweden (Sandkvist 1986).

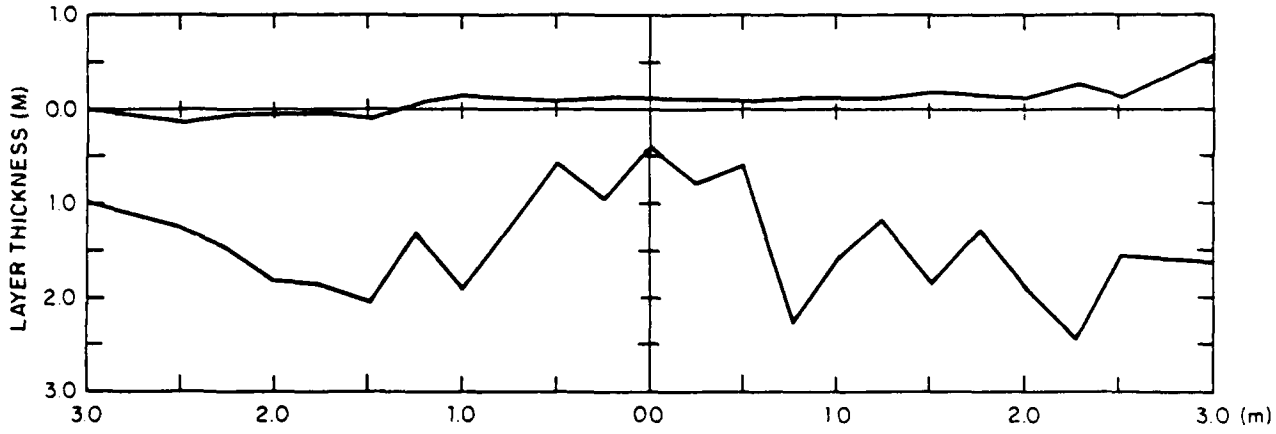

Figure 9. Cross section of a navigation channel covered with brash ice. (From Kannari 1983.)

differences in ice formation.

Tuovinen and Kannari studied ice formation in coastal channels in Finnish waters of the Gulf of Bothnia. They characterized the dimensions and mechanical properties (primarily shear strength and friction) of brash-ice layers in what they termed ice-clogged ship tracks. The brash-ice accumulations in the navigation channels monitored by Sandkvist and Kannari are typified by the cross-sectional profile shown in Figure 7. However, depending on the relative magnitudes of navigation-channel width and vessel beam, the profiles may be more irregular, as shown in Figure 9. Unsteady speeds or maneuvering may cause longitudinal profiles of brash-ice accumulations to be somewhat irregular or undular, as indicated in Figure 10.

With each transit of a vessel through a navigation channel, brash ice is displaced sideways beneath the bordering ice cover. There, brash ice accumulates to form inverted, linear mounds or ridges that run more-or-less parallel to the track so as to confine brash ice in the track. The ridges solidify due to freezing from above and local freezing at contact points between ice pieces. If the channel is relatively wide compared to the vessel beam (maximum width), an irregular series of furrows may form between the ridges. Brash-ice accumulations may be particularly irregular if vessels do not follow exactly the same track or if vessels of different sizes ply the channel.

Detailed measurements of the sizes of individual brash-ice pieces led Sandkvist to conclude that the distribution of brash-ice thickness was not log-normal, as had been found for the distribution of horizontal lengths of freshly broken ice pieces. He also deduced that additional breaking caused the mean plan size of brash ice to decrease gradually with increasing number of transits until it attained some constant value. He reported further that brash-ice pieces become more spherical and that the average thickness or vertical dimension increased to an asymptotic value, called the equilibrium vertical block thickness (Sandkvist 1982). Sandkvist's measurements of brash-ice fragment thickness are reproduced in Figure 11. Tuovinen (1978), Greisman (1981) and Kannari (1983) also reported that brash ice in ship tracks becomes

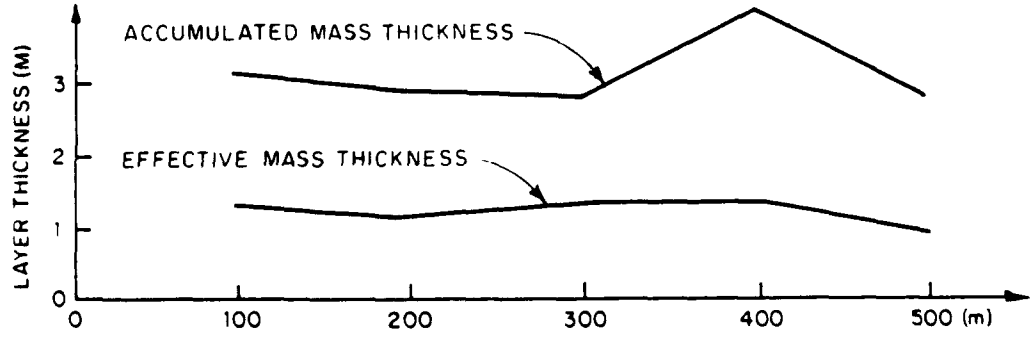

Figure 10. Longitudinal profile of a navigation channel covered with brash ice. (From Kannari 1983.)

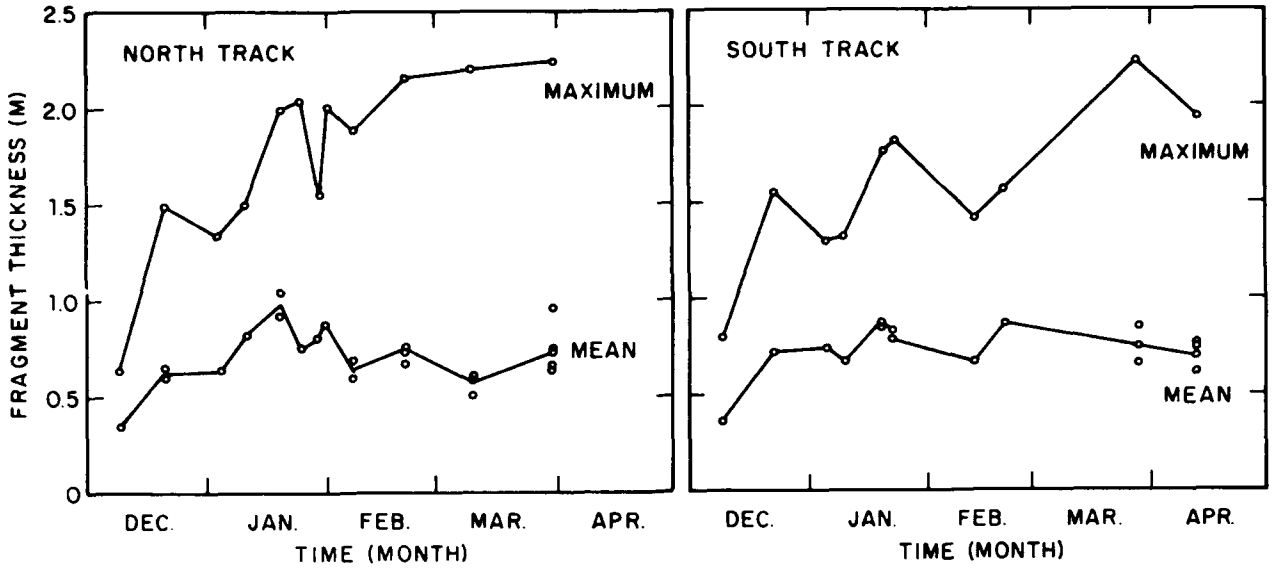

Figure 11. Thickness distribution of brash-ice fragments. (From Sandkvist 1983.)

rounded. Greisman coined the term "cannonball ice" for such ice. Kannari presented data on measured sizes of brash ice in channels in coastal regions of the Gulf of Bothnia (Fig. 12). He concluded that the size distribution is affected by ΣS_d and by the number of transits.

Prior formulations

Five semi-empirical formulations of ice formation in ship tracks have been proposed (Ashton 1974, Bérenger and Michel 1975, Vance 1980, Sandkvist 1981, Hamza 1985). Each formulation is based on eq 7 and invokes the assumption that ice covers regrow over a porous layer of uniformly distributed brash ice. In accordance with this assumption, each formulation yields only an average, or equivalent, thickness of ice accumulation in ship tracks.

Ashton (1974) modified eq 9 and proposed the following expression for the average thickness of ice regrown and accumulated in an ice-covered track:

$$\eta = \beta\alpha \left(\sum_{j\ 1}^{N_i} S_d \right)^{0.5}$$

$$+(1-\beta)\left[\left(\frac{\eta_{i-1}}{1-\beta} \right)^2 + \alpha^2 \sum_{j=1}^{N_i} S_d \right]^{0.5} . \qquad (10)$$

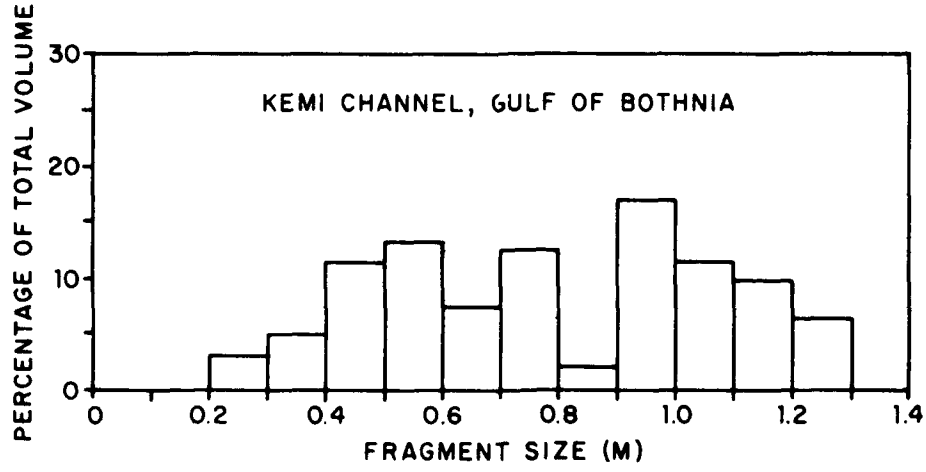

Figure 12. Size distribution of brash-ice fragments. (From Kannari 1983.)

The first term is the thickness of ice grown on open water, which occupies a fraction β of the track's surface area; the second term is the equivalent thickness of the ice cover (occupying 1-β of the track's surface) over the track prior to the i^{th} transit of a vessel through the track; and the third term relates to the additional thickening of the ice fragments floating in the track. Thickness η_i is actually a length index that is equivalent to the accumulated volume of ice grown per unit surface area of track prior to the i^{th} vessel transit. Ashton suggested $\alpha = 24$ mm/(°C-day)$^{0.5}$, based on observations of ice growth at sections of the Mississippi River. He also suggests using $\beta = 0.25$, at least for initial transits. Bérenger and Michel (1975) developed a considerably more complicated expression for ice accumulation in a track. They proposed that the increased average thickness $\Delta\eta_i$ of ice formation between transits be calculated as

$$\Delta\eta_i = \frac{p}{1-p} \left\langle (\eta_s - Z_w) + C_1 \left[\alpha \left(\sum_{j=1}^{N_i} S_d \right)^{0.5} - (\eta_s - Z_w) \right] \right\rangle + p \sum_{m=2}^{K} \left\langle \left[(i-1)^2 \eta_s^2 + \alpha^2 \sum_{j=1}^{N_i} S_d \right]^{0.5} - (i-1)\eta_s \right\rangle + C_2 (1-p)^{m-1} \left(\left[(m\eta_s + \eta_a)^2 + \alpha^2 \sum_{j=1}^{N_i} S_d \right]^{0.5} - (m\eta_s + \eta_a) \right) \quad (11)$$

where p = ratio of water volume to total volume (porosity)
η_s = thickness of individual ice fragments composing a brash-ice layer
Z_w = distance between the upper ice and the water surface
η_a = additional or residual thickness of ice formed under the layer
m = layer number

$$C_1 = 1, \text{ for } \alpha \left(\sum_{j=1}^{N_i} S_d \right)^{0.5} \leq (\eta_s - Z_w)$$

or

$$C_1 = p, \text{ for } \alpha \left(\sum_{j=1}^{N_i} S_d \right)^{0.5} > (\eta_s - Z_w)$$

$$C_2 = 1, \text{ for } m \leq K$$

or

$$C_2 = 0, \text{ for } m > K$$

K = maximum number of layers to form the residual ice $\{1/[p\,(1-p)]\,m\}$.

In eq 11, the first term is ice growth over open water at the surface of the track; the second term is the ice growth within the pores of layers of ice fragments; and the third term is the additional, or residual, ice grown beneath a layer of brash ice. For periods of regrowth P_n, or M ($=\Sigma n$) transits, the total volume of ice grown per unit plan area of the track is estimated from

$$\eta_i = \sum_{i=1}^{M} \Delta\eta_i \quad . \quad (12)$$

A difficulty in applying Michel and Bérenger's formulation is that m and K are difficult to assess.

Vance (1980) suggested the following expression for estimating η_i:

$$\eta_i = (1-\beta) \left[\eta_{i-1} + \alpha \left(\sum_{j=1}^{N_i} S_d \right)^{0.5} \right] + \alpha \left(\sum_{j=1}^{N_i} S_d \right)^{0.5} . \quad (13)$$

The first two terms relate to continuous thickening of brash-ice pieces; the third term is ice growth over open water. A comparison of eq 10 and 13 shows that eq 13 is misformulated and would lead to a significant overprediction of ice regrowth. In eq 13 the summation of the first two terms, combined, should be to the power 0.5, as is the case for the second and third terms in eq 10. Also, the third term in eq 13 should be multiplied by β, as is the first term in eq 10.

Sandkvist adapted eq 9, the Stefan equation, and proposed the following simple formulation

for the average or "equivalent" thickness of ice formation η_i, which he defined as the resulting thickness of brash ice accumulated in a vessel track, of width equal to the vessel beam, if all brash ice is contained in the track, as depicted in Figure 13:

$$\bar{\eta}_i = \eta_o + \sum_{i=1}^{M} \alpha \left(\sum_{j=1}^{N_i} S_d \right)^{0.5} . \qquad (14)$$

The first term is the initial ice-cover thickness before the first transit ($i = 0$); the second term is the equivalent thickness of ice formation for M transits of a channel. By setting $\alpha = 12\,\text{mm}/(°\text{C-days})^{0.5}$, Sandkvist was able to fit eq 14 with field measurements of brash ice accumulation in two test channels at Luleä Harbor in northern Sweden. The result is shown in Figure 8. Eranti et al. (1983b) reported using eq 14, with $\alpha = 6.5\,\text{mm}/(°\text{C-days})^{0.5}$, in estimating ice formation in a 30-m-wide channel transited by 12-m-beam ships (Saimaa Canal, Finland).

Hamza (1985) proposed the following expression for accumulated brash-ice thickness $\Delta\eta_i$ between two successive transits:

$$\Delta\eta_i = \alpha \left(\sum_{j=1}^{N_i} S_d \right)^{0.5} + \left[(\eta_{i-1})^2 + \alpha^2 \sum_{j=1}^{N_i} S_d \right]^{0.5} - \eta_{i-1} . \qquad (15)$$

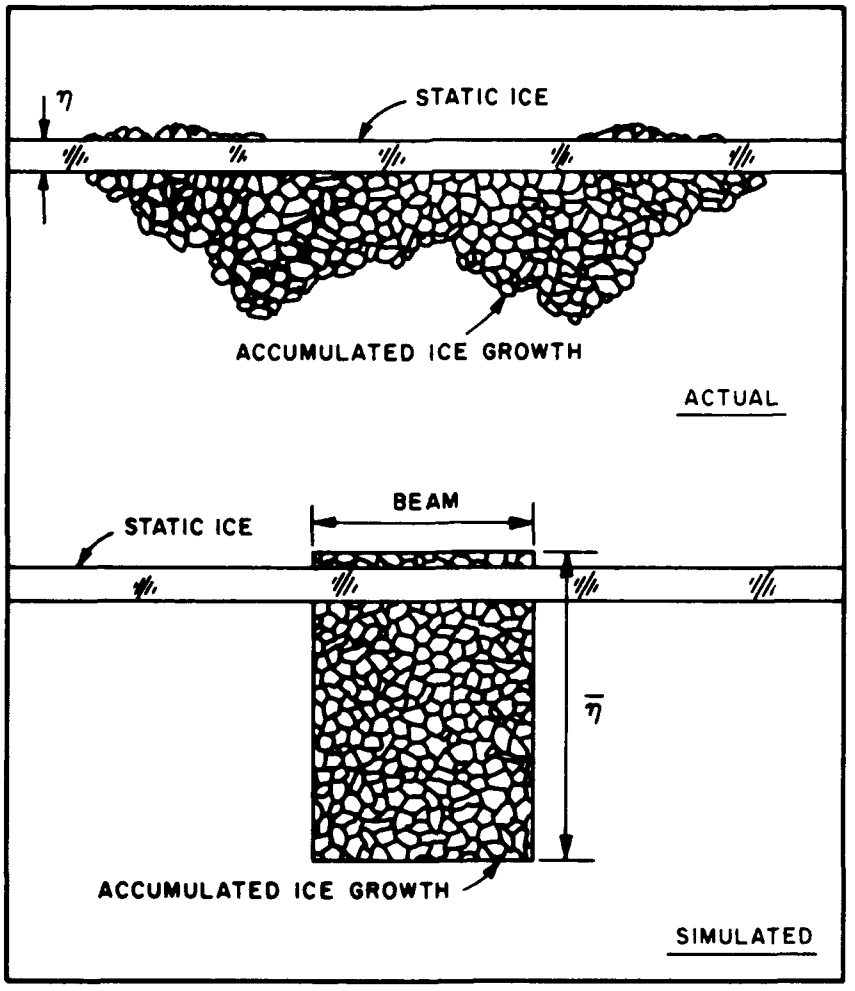

Figure 13. Sandkvist's model of brash-ice accumulation.

The first term is the ice growth over open water, and the second term is the continuous thickening of ice fragments in the channel. The thickness of accumulated brash ice after the i^{th} passage is

$$\eta_i = \frac{1}{1-\beta}\left(\Delta\eta_o + \Delta\eta_1 + \ldots + \Delta\eta_{i-1}\right). \quad (16)$$

Equation 15 is faulty and leads to an overestimation of ice regrowth, because the first term should be multiplied with β, and the second term with $(1-\beta)$, as in eq 10. Equation 16 is also incorrect because it involves $(1-\beta)^{-1}$ as a coefficient for η_i, which has involved the fraction of open water β in eq 15. Unlike the other models cited, Hamza considered that β (= p) is not constant but depends on the frequency of transit. He suggested that β decreases with the increasing frequencies of transit. The accelerated thickening of an ice cover with an underlayer of frazil ice is similar to the regrowth of ice in a navigation channel filled with brash ice. Calkins (1979) modified eq 5 to include the effect of an underlayer of frazil-ice slush on a statically thickening ice cover. He assumed that with a layer of slush present, $\phi_{wi} = 0$, and proposed allowing for slush-layer porosity by setting

$$\phi_i = p\,\rho_i\,L_i\frac{d\eta}{dt} \quad . \quad (17)$$

Substituting for L_i from eq 2 and integrating the resulting expression yields, if $\eta = 0$ at time $t = 0$,

$$\eta = p^{-0.5}\,\alpha\left(\sum_{j=1}^{N_i} S_d\right)^{0.5} \quad . \quad (18)$$

A problem with using eq 18 for estimating ice growth through a porous layer of brash ice is that values of α would have to be different than those recommended for the growth of smooth monolithic ice covers. The geometry of jumbled brash ice would call into question the use of eq 2 and the assumptions behind it.

A shortcoming in the foregoing models is that they do not take into account the influences on ice growth of brash-ice displacement during transiting. For instance, except for Hamza's model, the models are based on the assumption that a full layer of brash ice develops immediately across a track transited by vessels. Furthermore, it is assumed for all models that all ice grown remains in vessel tracks. In accordance with the first assumption, β is held constant, either as zero or 0.25 (Ashton). Hamza, however, took β to depend only on number of transits. As a result of the second assumptions, none of the models enables prediction of ridge thickness. Although Sandkvist's empirical expression gives an equivalent thickness of the brash-ice layer, the other models give only the volume of solid ice produced. They do not allow the prediction of the bulked thickness of a layer that is brought about by icebreaking that converts a cover of solid ice to a porous brash-ice layer.

The models are presented as being capable of predicting ice growth in ice-covered channels generally. However, different hull forms and sizes may displace ice differently, result in different patterns of accumulation and thereby influence ice growth. Also, channel geometry, notably width and depth relative to the dimensions of transiting vessels, may influence ice formation, as may water currents.

FORMULATION OF A PREDICTIVE MODEL

It is likely that, at best, deterministic numerical models can simulated ice formation in frequently transited navigation channels only approximately. The nature of transiting, icebreaking and redistributing broken and brash ice entails stochastic processes that are difficult to predict and may vary from vessel to vessel and channel to channel. Nonetheless, a comparatively simple numerical model is formulated here as a means of evaluating the sensitivity of ice formation to transit frequency and number, air temperature, hull form and channel geometry. The model is an attempt to simulate ice formation more realistically than do the prior formulations, by taking into account the effects on ice growth of brash-ice redistribution during each transit of a vessel. Its formulation was guided in part by the observations of brash-ice accumulation and from insights and data gained from the ice-tank experiments.

The predictive model is designed to simulate ice formation, or cycles of ice regrowth and brash-ice accumulation, in a frequently transited navigation channel such as is illustrated in Figure 14. An assumption that is fundamental to the model is that transiting vessels displace brash ice only sideways and do not shove significant amounts of it along their tracks. Also, it is assumed that no fragments break from the ice sheet bordering the track. In accordance with these assumptions and Figure 14, ice formation can be described as fol-

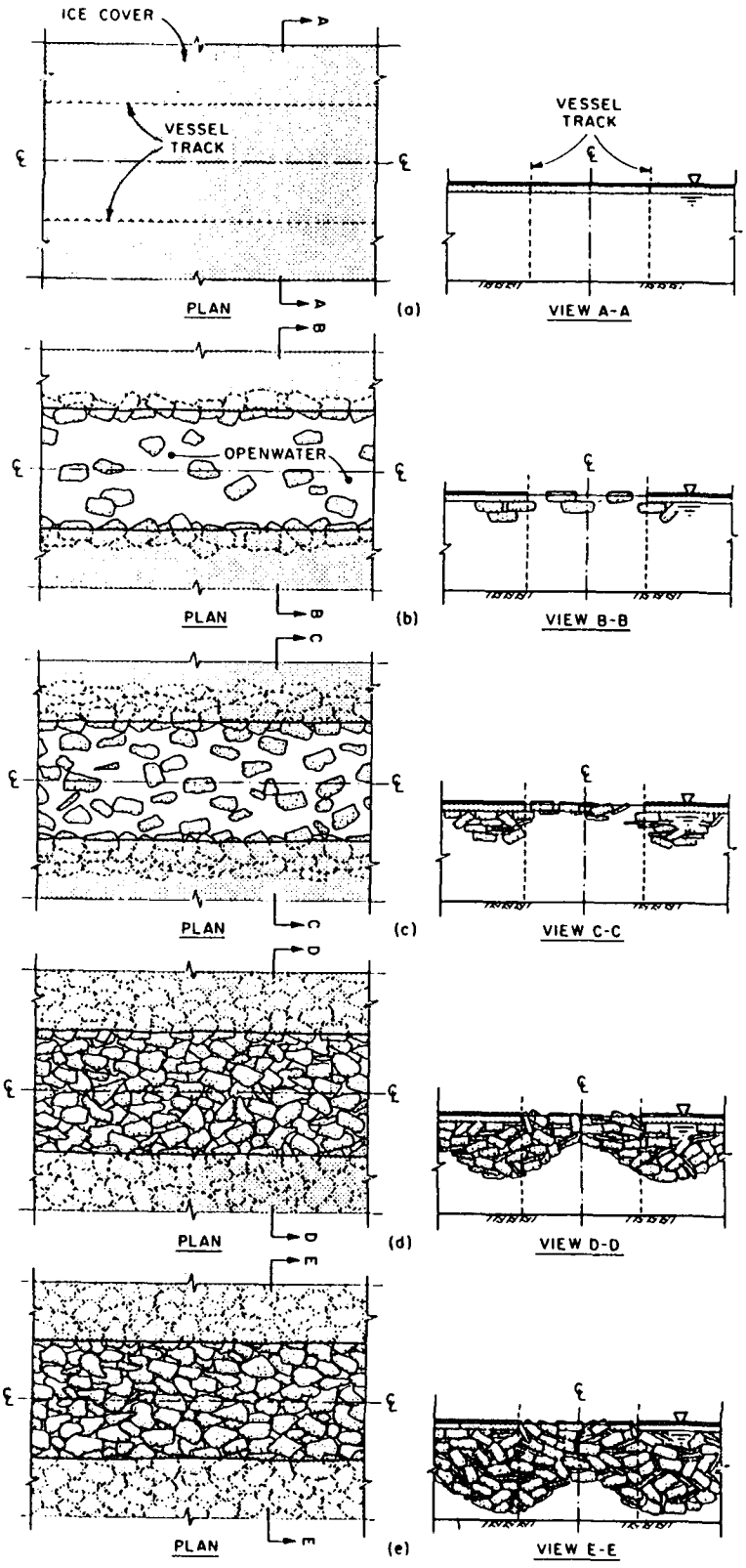

Figure 14. Ice formation in a frequently transited navigation channel (with no conveyance of ice along the channel).

lows. The first few transits of an ice-covered navigation channel leave an open layer of broken or brash ice uniformly spread over a track opened through it, with some ice being cast beneath the adjoining ice cover along each side of the track (Fig. 14b). With subsequent transits and periods of ice regrowth, more ice is broken, causing the track to become increasingly covered by a thickening layer of brash ice. Brash ice cast laterally collects as inverted ridges flanking the channel (Fig. 14c). Once the track is completely covered with a layer of brash ice, further transits cause the brash-ice layer to thicken uniformly but lagging behind the thickening of the ice ridges because brash ice is always displaced sideways to ridges beneath the ice cover bordering the track (Fig. 14d). Also, each transit causes the entire brash-ice layer to be disrupted and churned over such that refreezing commences again. However, some brief period of time is required for the water or the water and ice in the track to calm sufficiently for ice to regrow. In relatively shallow channels the ridges may eventually extend down to the channel bed (Fig. 14e), confining brash ice within the track.

The predictive model

Consider a section of vessel track filled with brash ice, as shown in Figure 15. *Conservation of* thermal energy flux between ice, water and frigid air enables the volume of ice in the track per unit area of track surface at any instant η_i to be expressed as

$$\eta_i = \eta_{i-1} + \beta_i \alpha \left[\sum_{j=1}^{N_i} \Delta T \left(P_t - t_p \right) \right]^{0.5} + (1-\beta_i) \left\langle \left[(1-p)^2 \eta_{bi-1}^2 + \alpha^2 \sum_{j=1}^{N_i} \Delta T \left(P_t - t_p \right) \right]^{0.5} - (1-p)\eta_{bi-1} \right\rangle \cdot \quad (19)$$

The first term is the value of η_i immediately prior to the i^{th} vessel transit; the second term is the average thickness of ice regrowth over open water; and the third term is the equivalent thickness of ice grown through and under accumulated brash ice occupying the track at areal concentration (1–ρ). In the second and third terms, the conventional cumulative degree-days of freezing

$$\sum_{j=1}^{N_i} S_d$$

is modified to allow for the time required for water in the track to become sufficiently calmed after a vessel transit such that ice regrowth can commence. In accordance with this condition,

$$\sum_{j=1}^{N_i} S_d$$

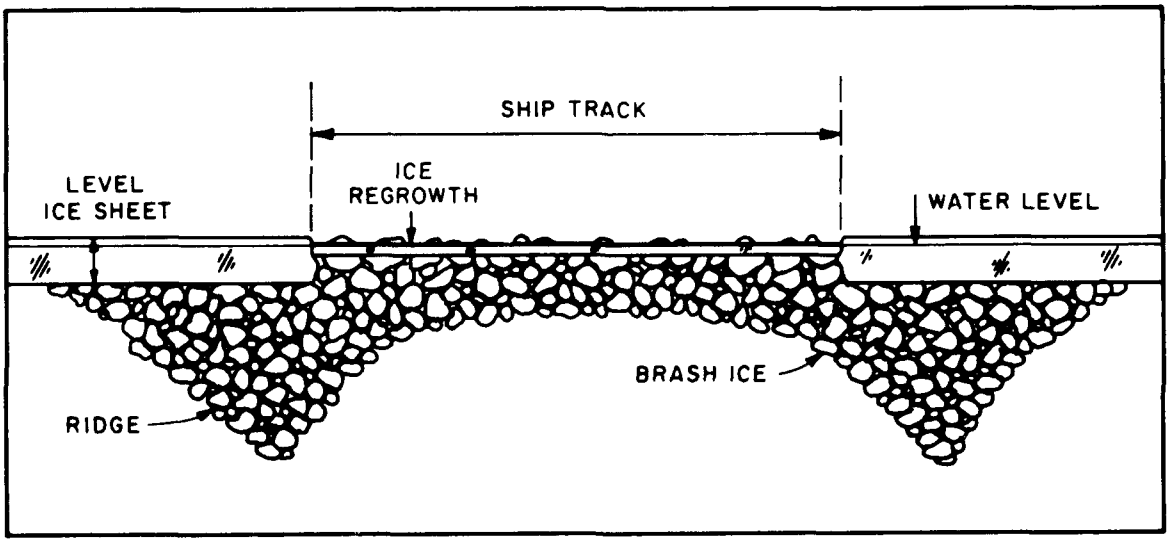

Figure 15. Modeled geometry of brash-ice accumulation across a vessel track.

is modified to

$$\sum_{j=1}^{N_i} \Delta T(P_t - t_p)$$

with $P_t = 1/f_t$ being the period between transits, and t_p is the time for the water or brash-ice layer to calm before regrowth commences after a transit. At very large frequencies of transiting, when $P_t - t_p$ approaches zero, little opportunity occurs for regrowth, and the effect of transiting is to maintain an open track. During each transit of the track, when it is fully covered by brash ice as depicted in Figure 14, the regrown ice cover is broken, mixed with existing brash ice, and bulked with water to form a layer of uniform thickness:

$$\bar{\eta}_{bi} = \frac{(1-\varepsilon_i)\left[\eta_{bi-1}(1-p)(1-\beta_i) + (\eta_i - \eta_{i-1})\right]}{(1-p)} \quad (20)$$

in which ε_i is the rate of brash or broken ice displacement from the track to the ridges flanking the track.

Evaluation of ice volumes grown within a porous accumulation of brash ice entails a calculation that agrees with many assumptions concerning the thermodynamics of ice growth within an assemblage of irregular cavities (namely, eq 11, which was proposed by Bérenger and Michel). Rather than becoming enmeshed in a net of tenuous assumptions and calculational complexities, such as ascertaining when growth through a layer reaches the layer underside and thermal thickening of layer commences, the present formulation invokes the following simple assumption: for the purpose of estimating ice growth associated with a layer of brash ice, it is assumed that, between transits, ice growth through and beneath a layer of thickness η_{bi} and porosity p can be reasonably represented by the growth of an equivalent monolithic ice cover of thickness $(1-p)\eta_{bi}$.

So far, no account has been made of brash ice that may have been displaced to ridges developing beneath the ice cover adjoining the track. A simple mass-conservation relationship can be formulated to account for brash ice that accumulates in the track and collects in the ridges flanking it. The volume of ice displaced per unit length of track surface, and supplied to each ridge, is

$$0.5\,\varepsilon_i\,\bar{\eta}_{bi}\,B_i/(1-\varepsilon_i).$$

Each ridge is assumed to thicken and broaden, as shown in Figure 14, in a manner similar to heaping a linear pile of granular material. If at any instant the ridge thickness is η_{ri}, and its shape is defined in terms of an angle of static repose of brash ice θ_r, the ridge volume is

$$V_{ri} = \eta_{ri-1}^2 \tan\phi_r + \frac{\varepsilon_i B_i \bar{\eta}_{bi}}{2(1-\varepsilon_i)} + \left\langle \left[(1-p)^2 \eta_{ri-1}^2 + \frac{\alpha^2}{p} S_d \right]^{0.5} - (1-p)\eta_{ri-1} \right\rangle \frac{W_{ri-1}}{2} \quad . \quad (21)$$

The first term is the volume of ice (per unit length of track) already included in a ridge; the second term is the volume of brash ice (per unit length of track) displaced from the track; and the last term is the volume of ice grown (per unit length of track) at each ridge. As the last quantity is negligible compared to the other two, it is discarded hereafter. The ridge thickness η_{ri} and width W_{ri} after the i^{th} transit can be expressed as

$$\eta_{ri} = \left(\frac{V_{ri}}{\tan\theta_r}\right)^{0.5} \quad (22)$$

and

$$W_{ri} = 2\,\eta_{ri} \tan\theta_r . \quad (23)$$

The maximum values of η_{ri} and η_i are, of course, limited by channel depth and water currents. Brash ice resting along a ridge may be entrained by water currents.

In the formulation of ice formation in transited channels, several quantities are difficult to know. These include the areal concentration of the open water along a track β, the porosity of the brash-ice layer p, the proportion of ice displaced from the layer to the ridges ε, the slope angle of the ridge accumulations θ_r, and the time required for ice regrowth to commence after a transit t_p. Among other things, β, ε, p, θ_r and t_p are influenced by the hull geometry, draft and speed, the number and frequency of transits, the channel geometry and water currents, and, in some cases, the relative sizes of ice fragments and vessel hull. The value of β diminishes with increasing number of vessel transits, becoming more-or-less constant once a track is completely covered by brash ice. The

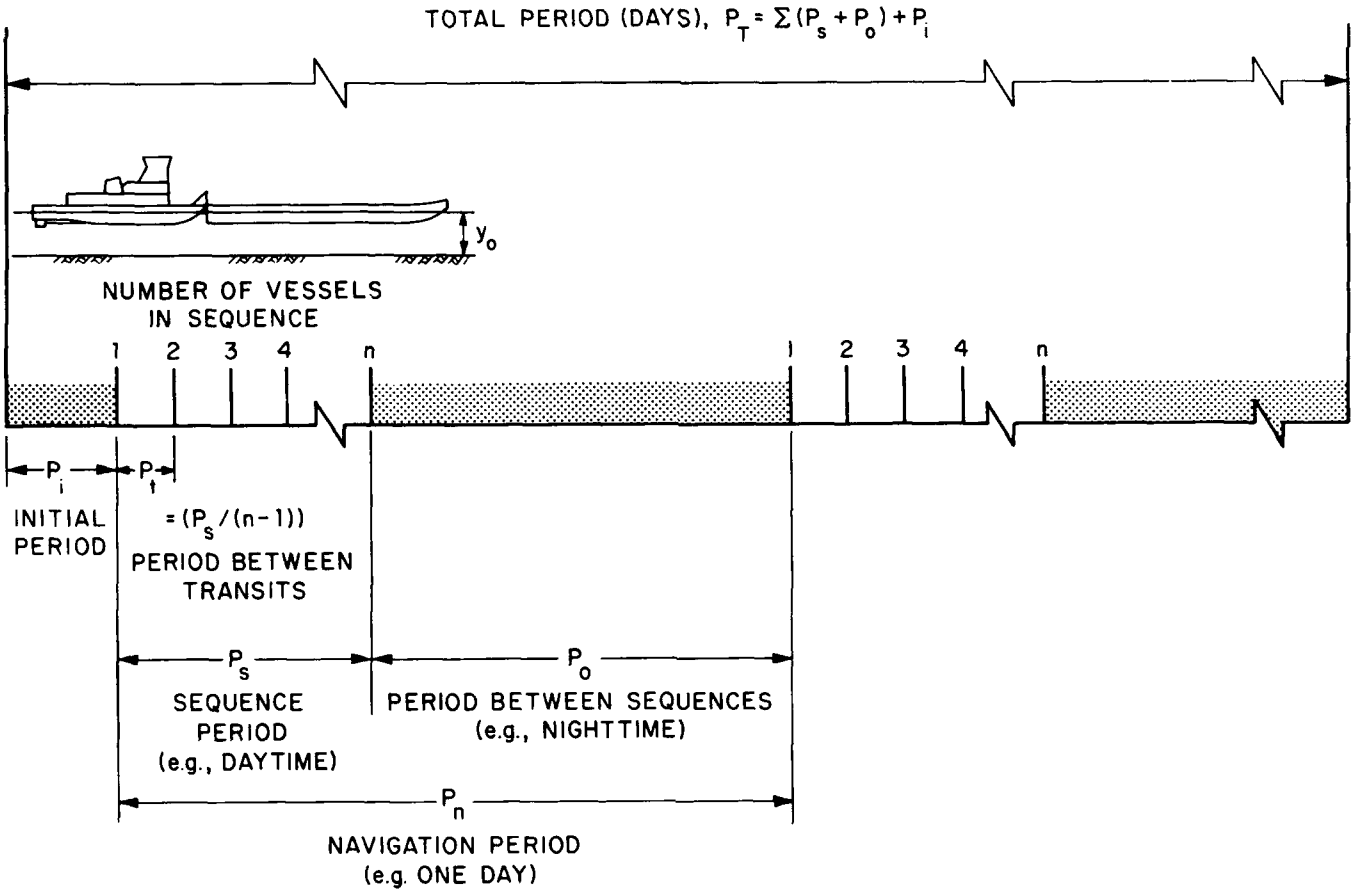

Figure 16. General transit schedule.

proportion of ice displacement ε, in addition to varying with hull geometry, draft and speed is influenced by the ratio of ridge thickness and channel thickness η_r/η_b. The larger η_r/η_b is, the less ice is displaced and accordingly the smaller is ε. In a sense, during a series of hull transits, η_r/η_b and ε are cyclic. A goal for the ice-tank experiments was to determine how β, ε, p, θ_r and t_p vary with some of these factors.

Transit frequencies

Vessels may transit channels at a single frequency. For example, a channel may be transited round-the-clock at hourly or multi-hourly frequencies. Typically, however, transits conform to some form of navigation schedule. The simplest are daily transits limited to daylight hours. Transits may also occur randomly.

Most schedules can be described in terms of a general schedule (Fig. 16). After an initial period of ice-cover formation P_i, a sequence ensues of n transits with a time interval P_t for a sequence period P_s. If $n = 1$, then $P_t = P_s/n$; if $n > 1$, then $P_t = P_a/(n-1)$. The sequences of transits may be intermittent, being separated by a period of no navigation P_o. A fairly simple schedule that can be defined in terms of three periods, P_t, P_n and P_o, gives rise to three transit frequencies:

- Frequency $f_t = 1/P_t$ defines the frequency of transits within a sequence of transits (e.g. one transit every two hours);
- Frequency $f_s = n/(P_s+P_o) = n/P_n$ defines the frequency of transits within a navigation period (e.g. six transits every day); and
- Frequency $f_n = 1/P_n = f_s/n$ defines the sequences within a navigation period (e.g. one sequence of transits daily).

For example, consider a transit schedule requiring 20 days of daily transits with five transits during eight hours of daylight. For this schedule, $n = 5$, $f_t = 1$ transit/(2 hours), $P_s = 8$ hours of daylight, $P_o = 16$ hours of darkness, $f_s = 5$/day, $P_n = 1$ day, and $f_n = 1$ sequence/day. Another schedule may entail continuous sequences of four vessels, 0.5-hour apart, with six hours between sequences; i.e. $n = 4$, $f = 2$ transits/hour, $P_s = 1.5$

hours, P_o = 6 hours, f_s = 4/(7.5 hours), and f_n = 1 sequence/(7.5 hours). Theoretically the general schedule shown in Figure 14 is part of a larger, self-similar array that can be described more formally in terms of fractal geometry. Typical frequencies of transiting on ice-covered rivers within the U.S. range from 1/(several days) to about 6/day.*

The predictive model is, after being calibrated against the laboratory results, exercised later with the aims of determining the effects of frequent vessel transit on river ice formation, and ascertaining if scheduling of vessel transits might be a feasible means for minimizing excessive ice growth in navigation channels. The exercises involve vessel transits during a range of meteorological conditions and channel geometries.

ICE-TANK EXPERIMENTS

The ice tank at the Iowa Institute of Hydraulic Research (IIHR) was used to simulate an ice-covered navigation channel during experiments aimed at determining and documenting the effects of frequent vessel transit on ice-cover formation. The ice tank, which is located in a refrigerated laboratory, enabled these effects to be examined under controlled conditions of air temperature, channel depth, hull geometry and transit frequency. The experiments entailed towing model-scale hulls through ice covers formed on still water (i.e. there was no water flow through the ice tank).

The program began with a brief set of preliminary experiments aimed at gaining an overview of the effects of tow transit on ice formation. These experiments used a 1:30-scale tow configuration comprising conventional barge and towboat hulls. The insights gained from these experiments were used in designing a subsequent set of experiments that was conducted using two larger (1:15-scale) but radically simplified hull forms. These experiments, which are here termed the main experiments, were conducted to obtain detailed information on the principal effects of frequent vessel transit of ice-covered channels.

In addition to the transit-frequency experiments described in this section, two other laboratory studies were conducted to examine significant features of tow transit that were brought to light during the preliminary experiments. One feature, which was related to the facility of tows to entrap and move broken ice beneath flat-bottomed hulls, was the subject of an extensive sideline study. Its objective was to ascertain the equilibrium characteristics and dimensions of ice accumulations formed beneath barges moving through ice-covered channels. This study involved experiments that used a 1:30-scale barge towed along a nonrefrigerated flume, as well as along the ice tank.

Another study was conducted to elucidate the general characteristics of tow transit through layers of brash ice. The interest here was on the manner by which tows move and displace brash ice, on the levels of resistance that they encounter when transiting layers of brash ice, and on the merits of convoying as a means of reducing problems produced by frequent transiting. This study entailed experiments using the ice tank. The layout, conduct and results of this study are presented in Appendix A.

The ice tank

IIHR's 21-m-long, 5-m-wide, 1.3-m-deep ice tank was used to simulate a length of ice-covered channel. The layout of the ice tank and the refrigerated laboratory housing it are shown schematically in Figure 17, which also indicates the alignment of the track along which the model-scale hulls were towed. The track width, for most of the experiments, was about 0.7–1.0 m. The model-scale hulls were towed by means of the tank's motorized towing carriage, which runs along rails on the tank's walls. The ice tank, its towing carriage and the refrigerated laboratory can be seen in several of the illustrations presented later.

The air in the refrigerated laboratory, which is 543 m^3 in volume, was chilled and circulated through a refrigeration system comprising four air-chillers and eight dispersion ducts running the length of the ice tank but located about 2.36 m above it. Chilled air was discharged along the ducts, which dispersed it approximately uniformly over the ice tank such that ice sheets grew uniformly to within 10% of the mean thickness. Air was recirculated into the chiller units after passing over the ice tank.

The ice tank was filled to depths of 1.07, 0.53 and 0.22 m with freshwater doped with urea at 1.0% concentration by weight. At a depth of 1.07 m, the ice tank can be considered as a deep channel, in relationship to the draft of the model hulls. At depths of 0.22 and 0.53 m, the ice tank represented a shallow channel and a channel of intermediate depth, respectively.

*Personal communications with lockmasters on the Mississippi and Ohio rivers and the Illinois Waterway.

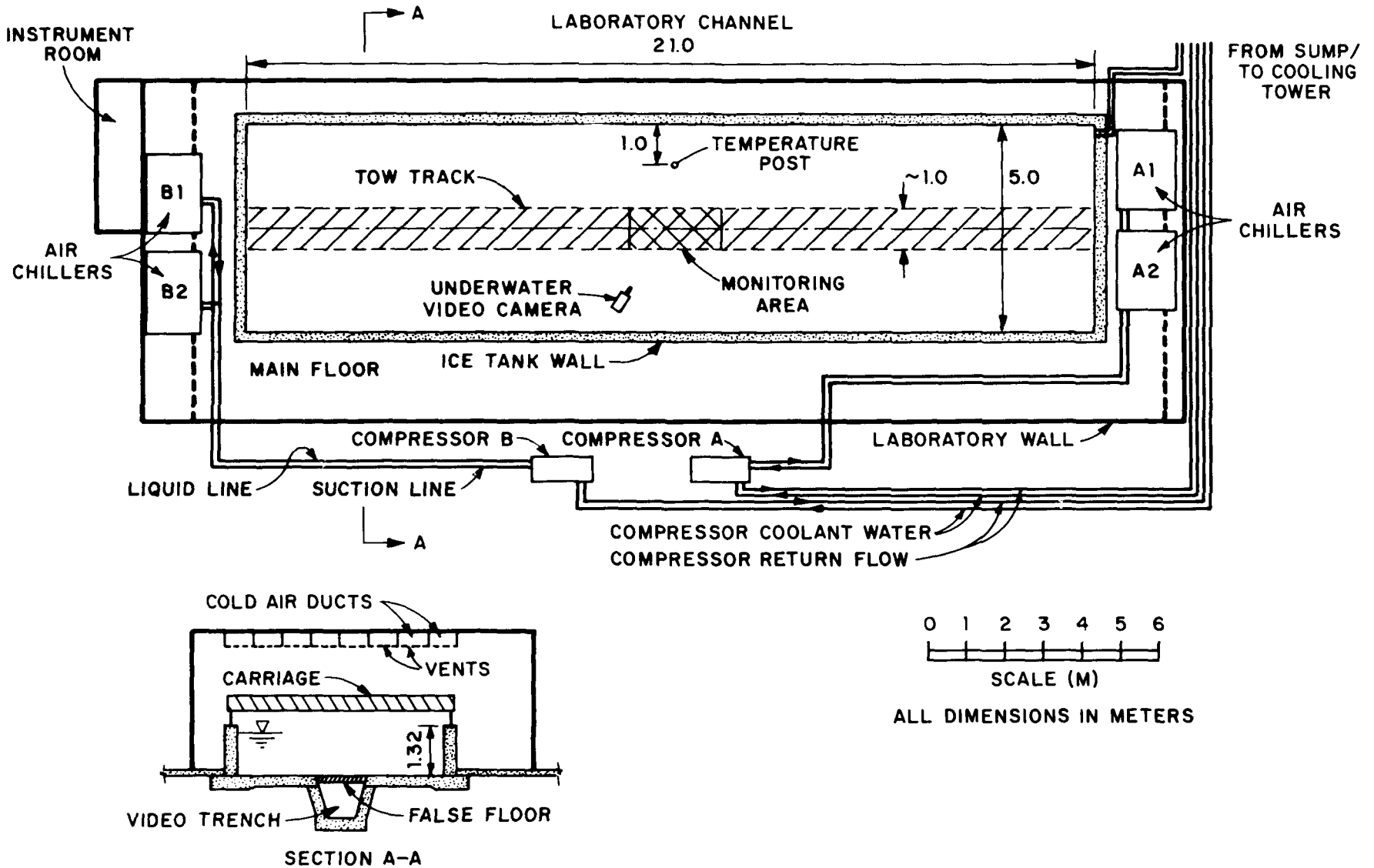

Figure 17. IIHR ice tank.

Model hulls

The experiments were conducted using model-scale hulls simulating several forms of vessel. The preliminary experiments, which provided an overview of transit-frequency effects, involved 1:30-scale hulls of a river towboat and two jumbo barges. These hulls were made of wood and had the dimensions and geometry shown in Figures 18 and 19; both model and full-scale dimensions are given. The hull forms of the models are identical to those of the full-scale towboat and barges used in the field study performed by Ashton et al. (1973). The towboat and barges were configured such that the towboat pushed the two barges in parallel configuration (Fig. 20). This configuration is termed the 1:30-scale tow. It was moved along the channel by means of a towing dynamometer mounted beneath the towing carriage. A guide pin fixed to the tow's bow and a guide bracket that extended from the carriage were used to ensure that the model held course along the centerline of the channel.

The main set of experiments used two simplified hull forms that are nominally 1:15-scale analogies of tows and ship-form hulls. One hull, which was flat-bottomed, is termed the 1:15-scale tow hull as it is intended to simulate a tow, albeit a shortened and greatly simplified one. Its dimensions and geometry are shown in Figure 21, and it is illustrated in Figure 22. The other hull was wedge-shaped and is termed the 1:15-scale wedge hull. It is intended to simulate a ship-form hull that does not entrap and shove broken ice. Alternatively it can be viewed as an idealized tow whose underside has developed a rounded accumulation of brash ice such that, when transiting an ice cover, it no longer accumulates and transports additional brash ice. The dimensions and geometry of the wedge hull are shown in Figure 23, and it is illustrated in Figure 24. The two hulls are considered to be 1:15 in scale because their drafts and beams are at 1:15 scale of the full-size towboat and barges depicted in Figures 18 and 19. The wedge hull has the same waterline beam as the tow hull. Both the tow and the wedge hulls were fabricated from 3-mm-thick, mild-steel plate so that they could withstand unscaled ice loads and ice abrasion when transiting the ice tank.

The tow hull was fitted with two 0.13-m-diameter propellers for secondary breaking of ice and for creating water currents around the rear of the hull. The propellers were driven by a 186-W electric motor, which is visible in Figure 22a. The propulsion system was not adequate to drive the hull through the ice, though it could propel the hull through open water. The tow hull was connected to the towing carriage by way of two rigid towing posts bolted to the towing carriage (Fig. 22a). Hinged joints between the hull and these posts enabled the hull to pitch but not to move in any other mode. The wedge hull was rigidly fitted to the towing carriage by way of a single steel post (Fig. 24). It could not pitch. The posts supporting both hulls were telescopic, so the hulls could be raised and lowered out of the channel and so that they could be towed at different depths. Between transits the hulls were hoisted from the channel to ensure that they did not become frozen into it. During each experiment, especially during periods when the hulls were suspended in frigid air, the hulls were kept warm with a 1.5-kW warm-air fan operating inside them. This was adequate for keeping ice from freezing to the two hulls.

Instrumentation

The air temperature and the temperature of the urea solution were measured using platinum resistance thermometers (RTDs) arrayed over and in the channel. Each probe was of 0.01°C precision. A post bearing four RTD probes was located halfway along the channel and close to the tracks cut through it, as indicated in Figure 17. Two probes for measuring the temperature of the urea solution were positioned on the post at 0.30 and 0.10 m (deep channel only) below the water level. The remaining two probes were positioned 0.05 and 0.20 m above the water level. Three additional RTD probes were placed 1.86 m above the water level in the ice tank. Temperature data from the temperature probes were automatically logged at quarter-hour intervals using IIHR's HP1000 computer.

The thicknesses of brash-ice accumulations, as a layer covering the track or as ridges flanking it, were measured over a 2-m-long area halfway along the channel. This area, designated in Figure 17 as the monitoring area, is adjacent to the temperature post in the tank. The thicknesses of the ice sheet η and the ice regrowth η_n were measured with a vernier caliper of 0.1-mm precision. Each measurement entailed cutting and removing a sample from the ice sheet or track.

At each time of measurement, the thicknesses of the layer η_b and ridge η_r were averaged from at least four measurements made at different sections in the monitoring area. The measurements were made using a specially developed, hook-shaped pointer fitted to a vernier scale that was

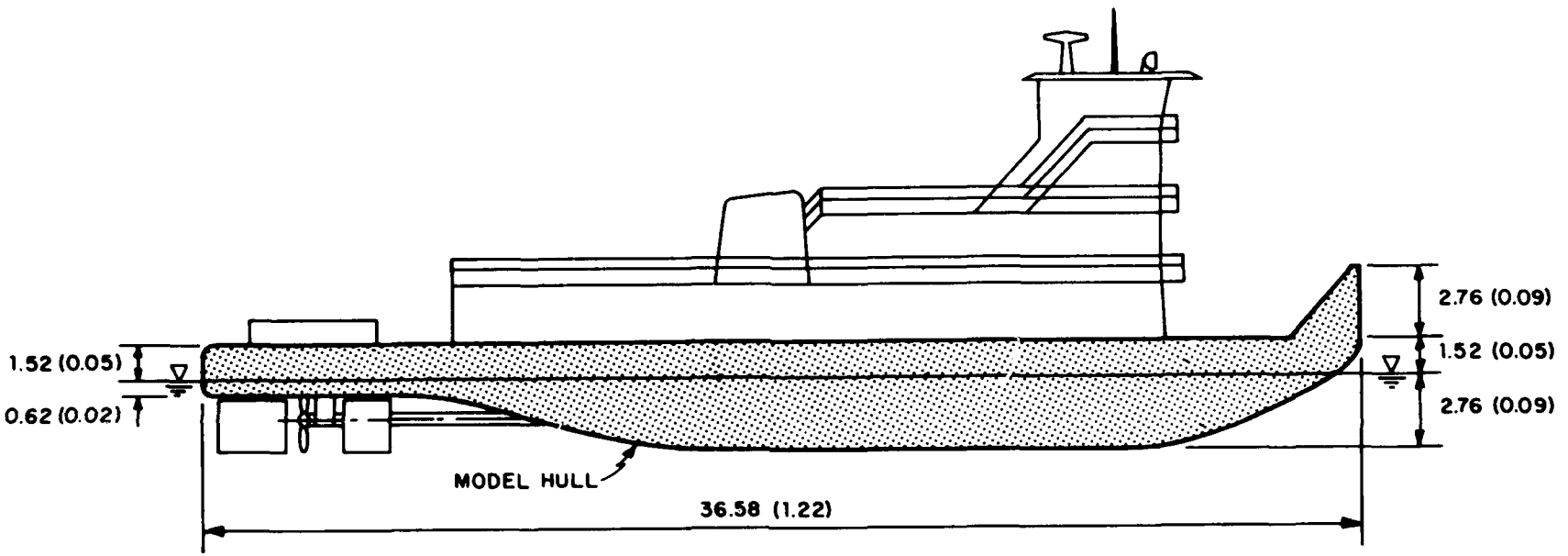

Figure 18. Dimensions and geometry of the 1:30-scale towboat. The shaded area indicates the model form; the propulsion system was not modeled. All dimensions are in meters.

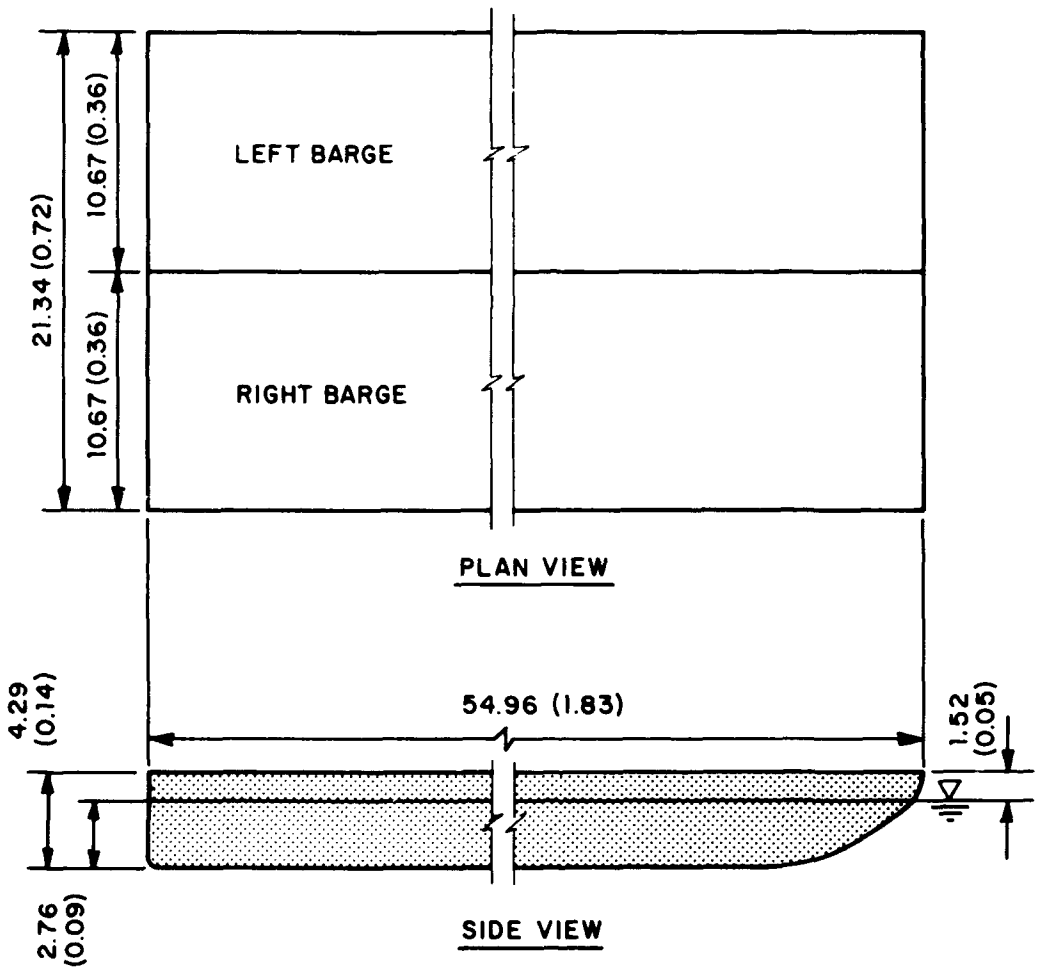

Figure 19. Dimensions and geometry of the 1:30-scale barges. All dimensions are in meters.

a. Transiting the ice tank.

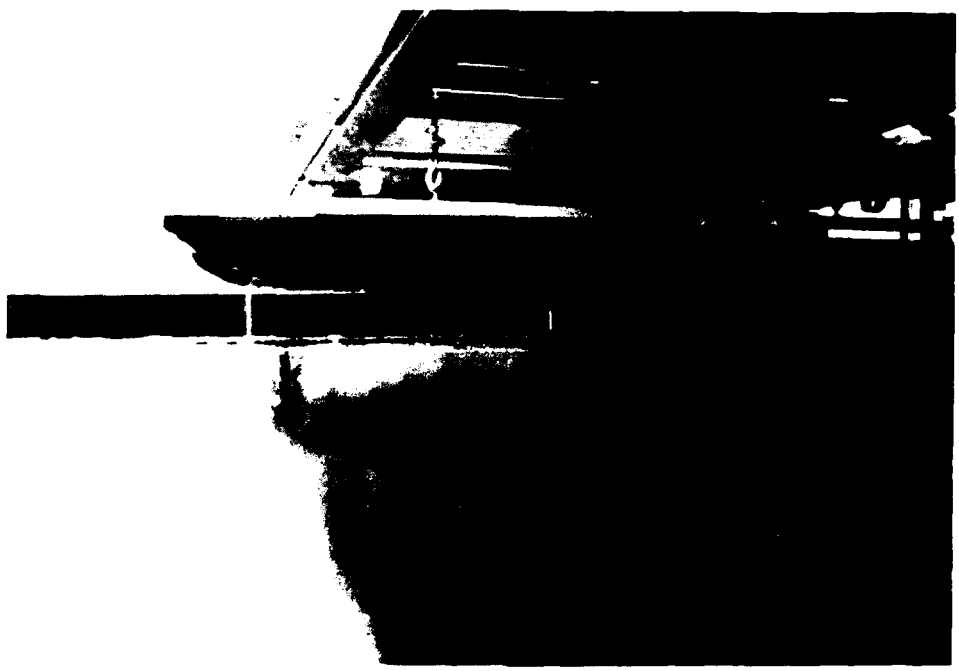

b. Stowed beneath the towing carriage.

Figure 20. 1:30-scale tow model.

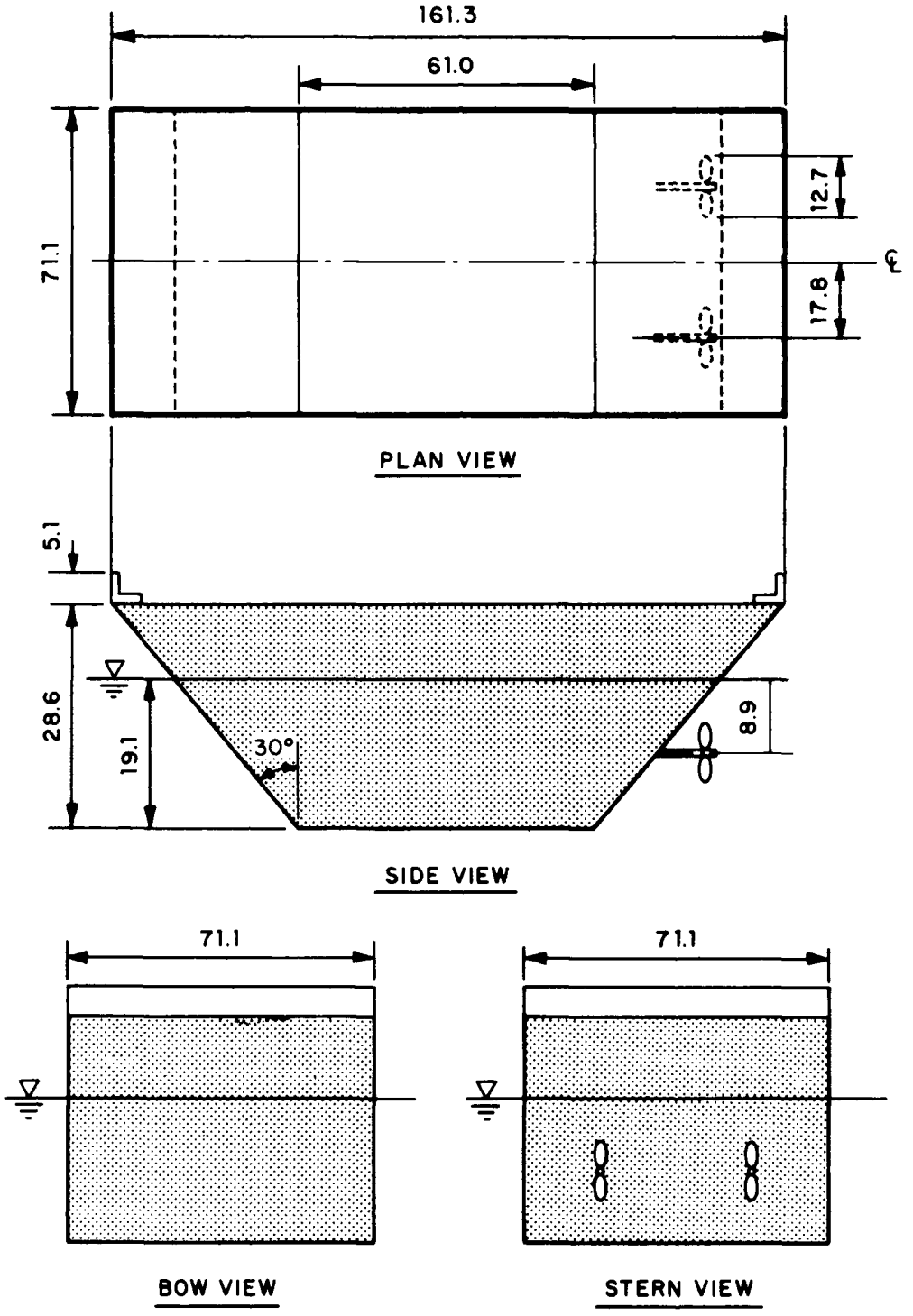

Figure 21. Dimensions and geometry of the 1:15-scale tow hull. All dimensions are in centimeters.

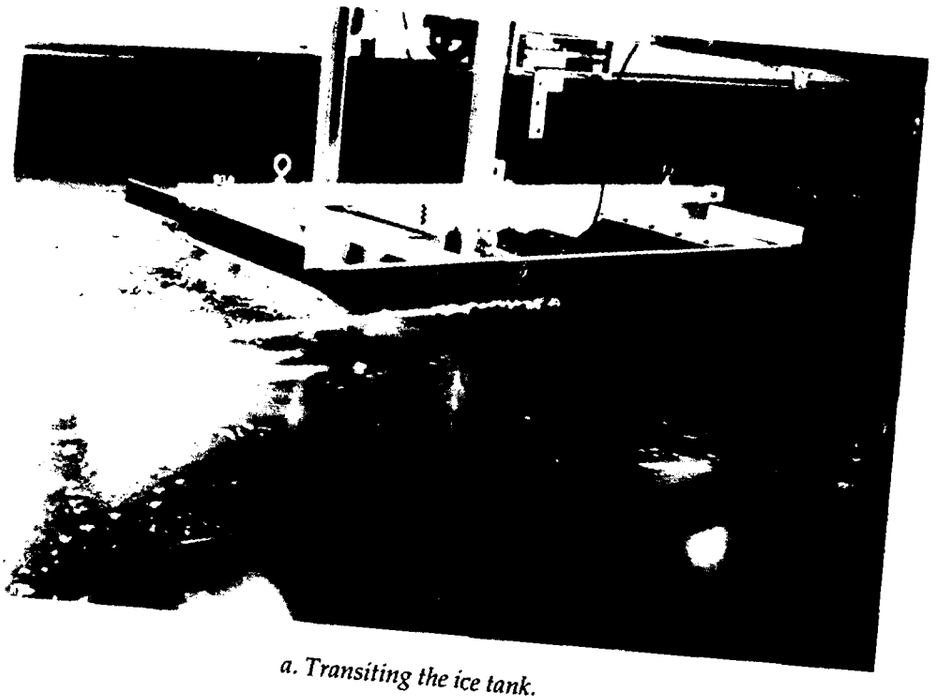

a. Transiting the ice tank.

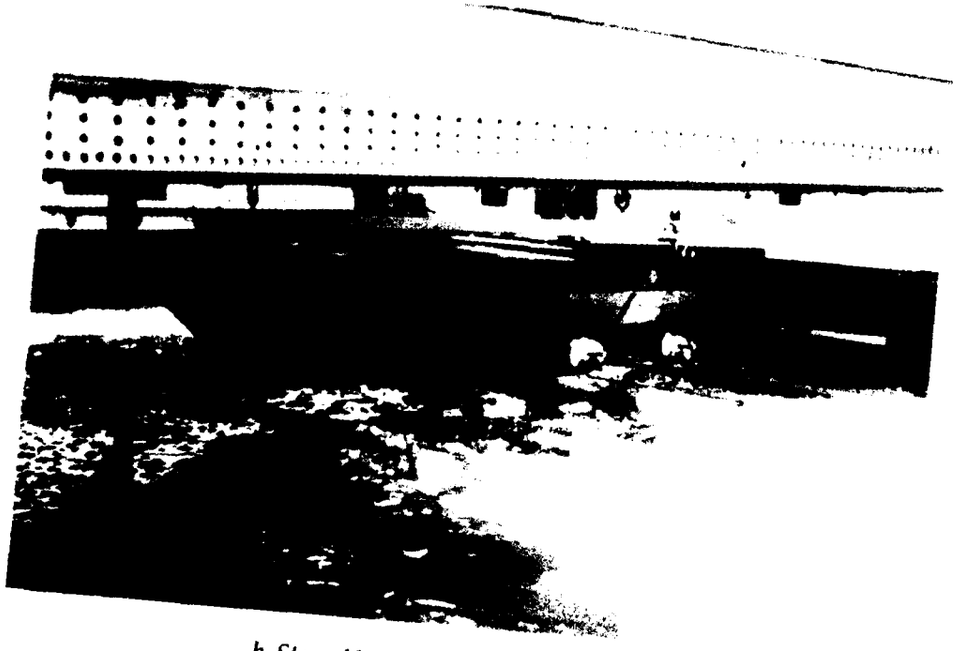

b. Stowed beneath the towing carriage.

Figure 22. 1:15-scale tow hull.

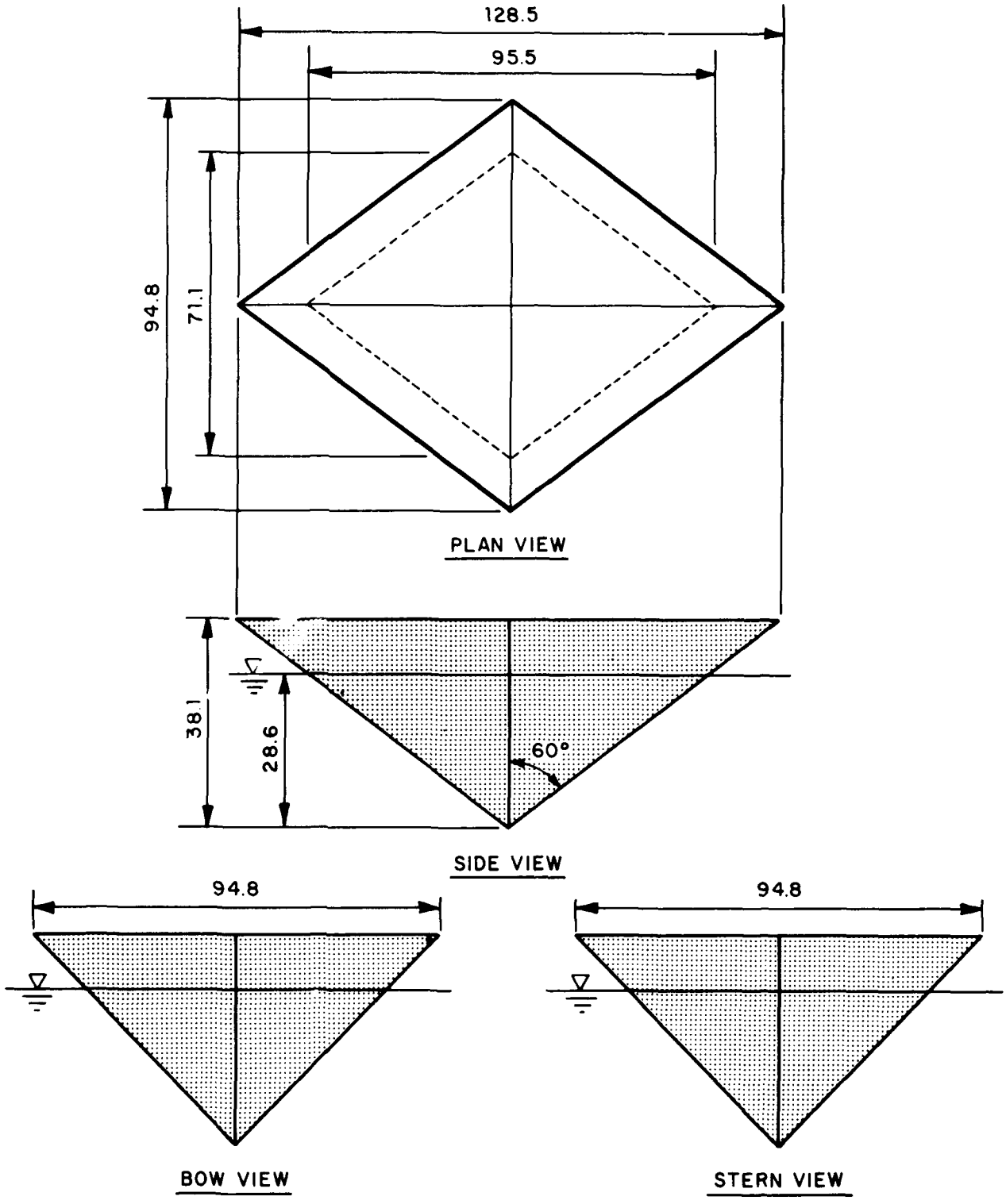

Figure 23. Dimensions and geometry of the 1:15-scale wedge hull. All dimensions are in centimeters.

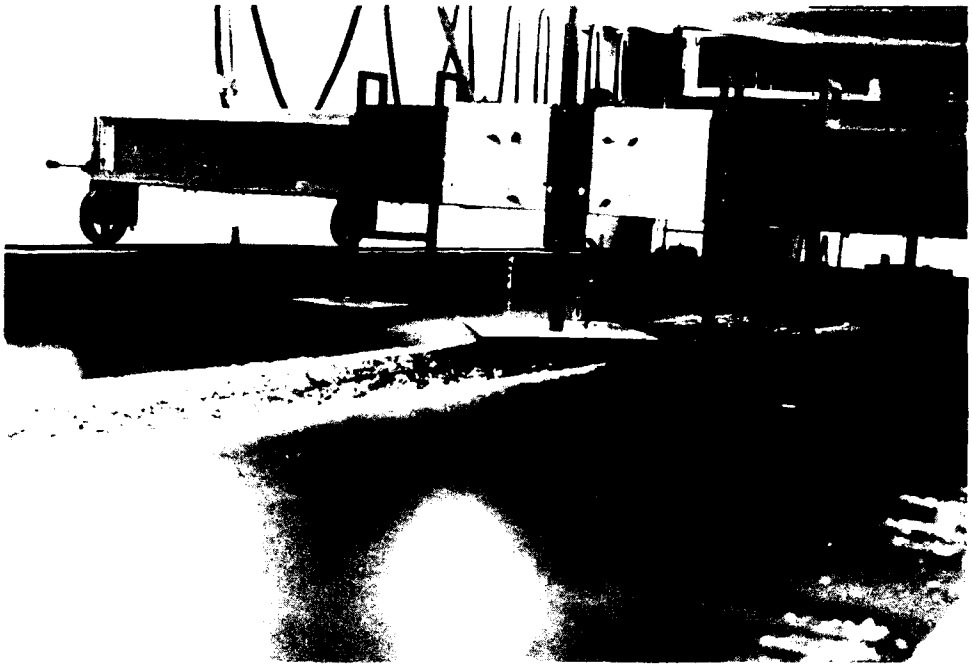

a. Transiting the ice tank.

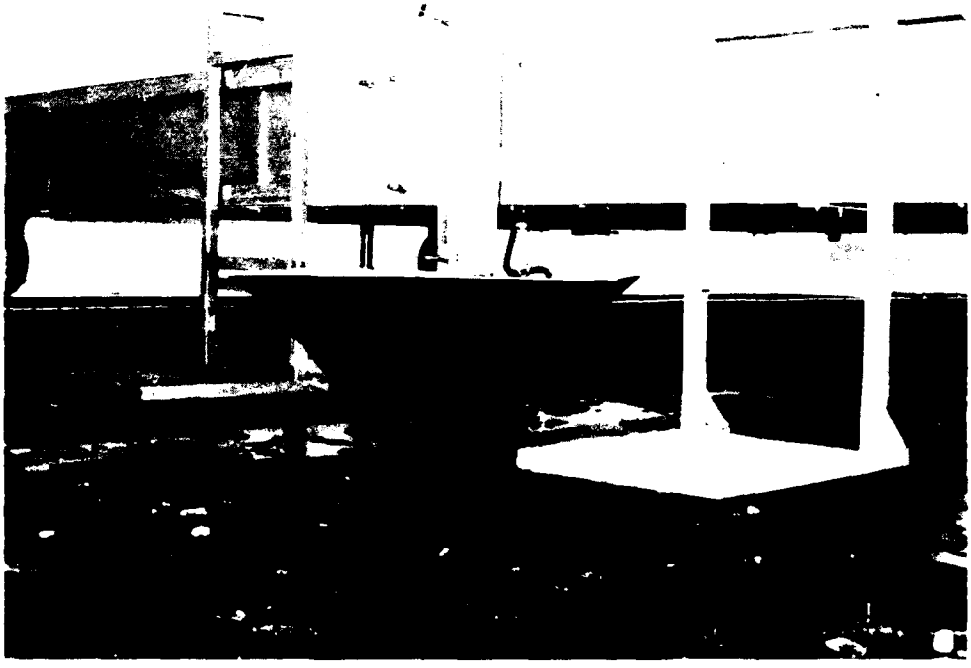

b. Stowed beneath the towing carriage.

Figure 24. 1:15-scale wedge hull.

mounted on a rigid cross beam. The precision of the vernier scale was 0.1 mm. For the deep-channel experiments, the beam was placed across two working platforms hung in front of the towing carriage. For the shallow-channel experiments, the beam was placed across concrete-block supports seated on the tank bottom.

During the preliminary experiments with the 1:30-scale tow, and subsequently with the 1:15-scale tow hull, brash ice collected in relatively thick accumulations at the ends of the channel. Such accumulations, here termed plugs, were found to be an important consequence of frequent transits as they eventually blocked, or plugged, tracks. The maximum thickness of plug η_p was measured using the hooked point gauge.

The porosity p of brash-ice accumulations was measured by removing a portion of each accumulation with a perforated 0.20-m-diameter canister of known volume and weight. The accuracy with which p could be determined varied with the size of individual pieces of brash ice relative to the 0.20-m-diameter opening of the canister; finer brash resulted in more accurate estimates.

The areal concentration of the open-water surface β over tracks formed by the hulls was determined after each transit by planimetry of photographs taken above the monitoring area.

The size distribution of brash ice in the track was determined at the end of each experiment. A 0.30-m-diameter bucket was used to obtain samples of brash ice, which were then visually sorted into several size classes and photographed. Appendix B contains photographs of brash-ice samples. The orthogonal dimensions (d_x, d_y and d_z) of ice pieces were measured so as to obtain an equivalent dimension:

$$d_e = \sqrt[3]{d_x d_y d_z} \tag{24}$$

for each class. Finally, each class was weighed such that a histogram and a cumulative-frequency curve of d_e values could be prepared. These were assessed for each experiment, in order to characterize the resulting brash ice in terms of a median dimension:

$$\bar{d}_e = \frac{1}{N} \sum_{n=1}^{N} d_e \tag{25}$$

and a geometric standard deviation:

$$\sigma_g = \left[\frac{d_{e84}}{d_{e16}} \right]^{0.5} \tag{26}$$

in which d_{e84} and d_{e16} are values of d_e for which 84% and 16%, respectively, of the brash-ice pieces are finer in size.

During and after several experiments (including all the preliminary ones), profiles of brash ice accumulated along the towing track were measured and recorded using an ultrasonic depth-sounder. The sonar head of the sounder was attached to an underwater towing carriage that ran along the video-camera trench indicated in Figure 17. The underwater carriage was connected to the towing carriage via a cable and pulley tow mechanism. Its use was eventually abandoned. Although the sounder enabled profiles to be determined with acceptable precision (to within 2 mm), it had to be towed slowly (14 mm/s). Furthermore, as transits by the tow hulls produced brash-ice accumulations that were of irregular thickness, the information yielded by the sounder proved to be of little use.

Model ice

As the primary focus of this study is on ice growth, or ice formation, the experiments were conducted using an aqueous model ice that can grow thermally in a similar manner as ice on rivers, lakes and seas. However, a major impediment to any laboratory or scale-model experiment involving ice growth as well as ship (or structure) interaction with ice is that both ice growth processes and structural interactions cannot be modeled simultaneously. In fact, there is no model ice that, with complete fidelity, can be used for model-scale simulations of either the growth or strength properties of ice.

To overcome this impediment, these experiments were conducted without strict adherence to similitude criteria for either ice growth or ice-vessel interaction. Instead, urea ice, which is a common model ice that can be grown in ice tanks, was used to replicate the major features of ice grown on rivers, lakes or seas. Urea acts as a brine included in ice sheets. Warming, or tempering, is a means of weakening ice sheets so that they can be used in scale models of vessel and structure interactions with ice sheets. A limitation for the present study, however, is that the ice could not be tempered prior to each transit of a model hull.

Scaling relationships

In accordance with the ice-growth and ice-vessel-interaction facets of the experiments, two time scales were required. One time scale is based on conventional Froude- and Cauchy-number scal-

ing of ice interactions with vessels or structures. The other scale is based on ice growth rates in the ice tank relative to typical rates of ice growth on rivers.

In accordance with the Froude- and Cauchy-number scaling criteria, the time scale associated with hull and ice-piece motion during vessel transit is

$$\lambda_t = \lambda_\ell^{0.5} \tag{27}$$

in which λ_ℓ is the geometric scale of the hull.

The time scale associated with ice growth in the ice tank can be evaluated using eq 4. Ice growth rate can be expressed as

$$\frac{d\eta}{dt} = \frac{1}{\rho_i L_i} \frac{\Delta T}{\frac{\eta}{k_i} + \frac{1}{h_{ia}}} \tag{28}$$

Integrating eq 28, and using the initial condition $\eta = 0$ at $t = 0$, as well as assuming that T is constant, leads to

$$\frac{\eta^2}{2k_i} + \frac{\eta}{h_{ia}} = \frac{\Delta T\, t}{\rho_i L_i} \tag{29}$$

Normalizing η with barge draft D or another appropriate vessel-related length, and rearranging eq 29, yields

$$\left(\frac{\eta}{D}\right)^2 + \frac{\eta\, 2k_i}{D^2 h_{ia}} = \frac{2k_i\, \Delta T\, t}{\rho_i L_i D^2} \tag{30}$$

From the first term, the scale of ice-sheet thickness, $\lambda_\eta = \lambda_D = \lambda_\ell$. From the first two terms, $\lambda_{ki} = \lambda_{hia} \lambda_D$. From all three terms, with $\lambda_{\rho i} = \lambda_{Li} = 1$, the time scale associated with ice growth is

$$\lambda_t = \frac{\lambda_\ell}{\lambda_{h_{ia}} \lambda_{\Delta t}} \tag{31}$$

The selection of an exact value for the time scale associated with ice growth clearly entails subjective assessment of the representative heat-flux conditions for channels in nature. If, to consider the simplest case, λ_{hia} and $\lambda_{\Delta T}$ are each taken to be unity, eq 31 implies that the time scale associated with ice growth is equivalent to the geometric scale. In other words, for geometric scales of $\lambda_\ell = 30$ and 15, one hour of ice growth in the laboratory channel is equivalent to 30 and 15 hours, respectively, at full scale.

In nature, h_{ia} and ΔT are unsteady, at least for periods in excess of one day, and they are difficult to assess. Shen (1985) estimated an h_{ia} value of about 20 W/m^2°C for the St. Lawrence River. Ashton (1986) recommended that heat fluxes from rivers under frigid conditions be assessed as 200 W/m^2. Values of heat flux from the laboratory channel were estimated by eq 5 to be about 70 W/m^2 when air in the refrigerated laboratory was maintained at –10°C. Therefore, if the product $\lambda_{hia} \lambda_{\Delta T}$ is taken as 200/70, λ_t would be about 10 and 5 for $\lambda_\ell = 30$ or 15, respectively.

Program of experiments

A two-part program of experiments was conducted. The first part comprised three preliminary experiments conducted with the 1:30-scale tow hulls. The second part, or main experiments, comprised thirteen experiments conducted with the 1:15-scale tow and wedge hulls. Details of the experiments are summarized in Table 1.

All but two experiments involved transits at a single frequency, such as one transit every two hours. The two experiments simulate a general schedule of transiting as depicted in Figure 16. For all experiments the air temperature above the ice tank was maintained at –10 ± 1.5°C, except for short designated periods (as explained later). The ±1.5°C variation in air temperature was caused by automatic defrosting of the chiller units, which took place at two-hour intervals.

The preliminary experiments were intended to gain an overview of the effects of tow transit on ice formation in a navigable channel. The results of these experiments guided the design and program of subsequent experiments. The first experiment involved 11 transits of the 1:30-scale tow at a transit frequency f_t of one every four hours. The second experiment was conducted with the tow moving alternately along two overlapping tracks, with f_t = 1/hour. The third experiment involved only the towboat.

The objective of the main set of experiments was to obtain detailed information on the effects of vessel transit on ice-cover formation for a range of transit frequencies and channel conditions. The principal variables were transit frequency f_t, hull shape and channel depth y_o. Values of f_t ranged from 1/(0.5 hour) to 1/(8 hours) at 1:15 model scale. Each experiment, except one, lasted about three to four days and ended when the ice sheet had attained a thickness of about 60–70 mm (0.90–1.05 m at full scale). A brief experiment lasting 4.2 hours was performed at the high transiting frequency of 1/(0.167 hours). Its purpose

Table 1. List of experiments on ice regrowth.

Experiment number	P_t^* (hour)	n	P_s (hour)	P_o (hour)	P_T (hour)	Σn	T_a (°C)	y_o (m)	α [mm/(°C-day)$^{0.5}$]	Note
Part 1. Preliminary Experiments with 1:30-Scale Hulls										
1	4.0	1	4.0	0	2.04	11	−9.27	1.07	10.0	Tow
2	1.0	1	1.0	0	1.07	12	−10.88	1.07	9.8	Alternate tracking of tow
3	2.0	1	2.0	0	1.44	13	−9.17	1.07	9.7	Towboat only
Part 2. Main Experiments with 1:15-Scale Hulls: Deep Channel										
1	2.0	1	2.0	0	4.34	29	−10.05	1.07	11.8	Tow
2	4.0	1	4.0	0	2.98	15	−10.38	1.07	13.0	"
3	0.5	4	1.5	6	2.33	32	−10.56	1.07	13.0	"
4	8.0	1	8.0	0	3.00	9	−10.82	1.07	12.5	"
8	4.0	1	4.0	0	3.67	18	−8.79	1.07	13.0	Wedge
9	2.0	1	2.0	0	4.00	30	−11.74	1.07	14.8	"
10	0.5	4	1.5	6	4.00	36	−12.78	1.07	13.0	"
11	8.0	1	8.0	0	3.10	9	−10.81	1.07	13.2	"
12	0.5	1	0.5	0	3.10	98	−10.88	1.07	13.0	"
13	0.17	1	0.17	0	0.18	25	−10.00	1.07	13.0	"
Part 3. Main Experiments with 1:15-Scale Hulls: Shallow Channel										
5	4.0	1	4.0	0	3.00	15	−9.41	0.22	13.6	Tow
6	4.0	1	4.0	0	2.94	14	−9.53	0.53	12.9	"
7	2.0	1	2.0	0	2.75	24	−11.02	0.22	12.7	"

* P_t = period between transits;
n = number of transits during navigation period;
P_s = period associated with a sequence of transits;
P_o = period between sequences of transits;
P_T = $P_i+\Sigma(P_s+P_o)$ = total period of navigation, or ice growth;
P_i = initial period of ice growth here set as P_t;
Σn = number of transits in the navigation period;
T_a = air temperature
y_o = water depth
α = Stefan coefficient.

was to determine how β varied with n at high values of f_t.

The effects of tow transits on ice formation were investigated for three channel depths: 1.07, 0.53 and 0.22 m. The 1.07-m-deep channel is considered to be deep because the channel bottom was distant from the underside of the tow hull. The 0.22-m-deep channel was used to simulate a shallow channel, with a minimum navigation depth of 3.05 m (10 ft). The water depth was not varied for experiments with the wedge hull because no ice passed beneath it, so the water depth would not significantly affect the movement of broken ice around its inclined sides.

Experimental procedure

At the beginning of each experiment, the air above the ice tank was chilled to an average temperature of −10°C. The urea solution in the tank simultaneously cooled to −0.1 ± 0.02°C. The surface of the tank was then wet-seeded by means of a fog of fine ice crystals. The nascent ice sheet was allowed to grow for an initial period P_i, the same as the interval between vessel transits P_t. Its thickness was measured immediately prior to each transit. The model hull for each experiment was launched from, and coupled to, the towing carriage at one end of the ice tank. At this stage the propellers of the 1:15-scale tow were set in motion.

Each hull was then accelerated and towed at a constant speed of 0.15 m/s (about 0.58 m/s, or about 2 ft/s, at full scale) along the simulated navigation channel. While each hull was being towed through the channel, the track behind it was wet-seeded so as to initiate regrowth of ice over the track. For several of the experiments, tow

transits and ice formation were videotaped.

On completion of a transit, each hull was winched from the channel and held beneath the towing carriage until the subsequent transit. The experiments were conducted continuously on a "round-the-clock" basis for about three to four days until the ice cover over the tank had grown to an equivalent prototype thickness of about 1 m (thicknesses greater than 1 m are extreme for most navigable channels, particularly those of the upper Mississippi River and its tributaries). Transiting was interrupted only for the period from approximately 0000 hours to 0500 hours, during which the air temperature was adjusted so as to give the same incremental value of ΣS_d as for the regular interval between transits.

Throughout each experiment the following quantities were measured:

- Thickness of the ice sheet η;
- Thickness of the ice regrowth over open water η_n;
- Average thickness of the ice accumulation in the navigation channel η_b;
- Average thickness of the ice accumulation as a ridge η_r;
- Thickness of plugs of brash ice η_p (for transits of the tow-hull);
- *Porosity p of brash ice accumulations;*
- Areal concentration of open water over the track β;
- Size distribution of brash ice (on completion of an experiment).

The first two measurements were made immediately prior to each transit, whereas the remainder were made after each transit. For a few experiments the variation of the average plan dimension of brash ice on the surface of the track was measured after each transit. Also measured occasionally were the ridge geometry and the time required for water and brash ice in the track to calm sufficiently so that ice regrowth could commence.

Experimental errors

One significant source of error arises because the experiments were performed without strict adherence to similarity criteria for modeling vessel transit through ice. These criteria had to be relaxed, as explained earlier, but the penalties of doing so have to be kept in mind. The following penalties, or scale effects, are perhaps the most important ones:

- Thermodynamic terms that are significant when describing thin ice (e.g. the thermal boundary layer) are not taken into account.
- Brash-ice fragments formed in the ice tank may, for several reasons, be larger than the equivalent brash ice formed at full scale. Incomplete scaling of ice strength and deformation characteristics may have resulted in the formation of initially larger sizes of broken ice and brash ice that may have been less readily broken during impact with the hull. Lack of direct control over the thermodynamics of ice growth at the crystal scale may have caused contacting ice fragments to fuse and form larger fragments.
- At the highest transit frequency [$f_t = 1/(0.167$ hour)], the resulting brash ice behaved cohesively, similarly to frazil ice. These ice fragments tended to bunch as flocs (akin to frazil ice) rather than to remain discrete ice fragments. Therefore, this ice may not replicate the behavior of full-scale ice, which would be less inclined to form flocs (an analogy here is the dissimilar behavior of clay and sand-size sediments). However, intensely transited channels may produce mush ice that can behave cohesively.
- Incomplete scaling of ice forces and hull motions may have affected brash ice displacement and distribution. (The ice resistance exerted against the rigid model hulls was strong enough for thick ice to scrape paint off them).

Despite concerns for the significant scale effects inherent in scale modeling of ice growth as well as ice interaction with vessels, the experiments do illuminate most of the more important features of ice formation in frequently transited ice-covered channels. In a simpler sense, one that sidesteps the nettlesome issue of scaling, the main experiments can also be viewed as a physical analogy of tow transit. In accordance with this view, the steel hulls are essentially greatly simplified tows, or tow-like hulls, that transit an element of ice-covered navigation channel.

Errors attributable to instrument precision are much smaller than errors resulting from the general design and conduct of the experiments. For example, the mechanical operation of the refrigeration plant caused the air temperature above the ice tank to fluctuate within a tolerance of 1.5°C, which exceeded the 0.01°C precision of the RTD temperature probes. However, a major source of error resulted from the nonuniform distribution of brash ice accumulated in, or next to, the tracks formed by the hulls. This error was because, for some of the experiments, the size of individual

pieces of brash ice in the accumulations comprised up to 50% of accumulation thickness. Therefore, the accuracy of accumulation thicknesses reported herein is typically of the order of the mean dimension of brash-ice fragments.

ICE-TANK OBSERVATIONS AND DATA

Frequent transits of the ice tank by both the 1:30- and 1:15-scale tow hulls revealed a pattern of ice formation that is markedly different from that portrayed in Figure 14 and that assumed in the development of prior predictive models. Ice formation in channels transited by the tow hulls was dominated by the propensity of these hulls to entrap, shove and drag ice along the tracks that they opened. The result was the formation of localized thick accumulations of brash ice, here termed ice plugs. Frequent transits of the ice tank by the wedge hull, which did not move brash ice along its track, resulted in essentially the same sequence of ice formation portrayed in Figure 14. The experiments demonstrated that, among other factors, hull shape significantly affects ice formation in frequently transited ice-covered channels. The experiments also demonstrated that accumulations of brash ice become especially troublesome when shallow ice-covered channels are transited.

Overview of ice formation in channels transited by tows

When the tow hulls first transited the channel covered by a thin, newly formed ice sheet (Fig. 25a), most of the resulting brash ice was displaced from the track opened by the tow. Some of it was cast beneath the edges of the adjoining ice sheet, forming inverted ridges that flanked both sides of the track. Much of it became entrapped and dragged along by the tow until it was deposited at some location along the tow's track (Fig. 25b). Only a relatively small proportion of the initial ice cover remained as brash ice strewn over the track, some of it having been drawn back into the track by propeller wash. At the end of the track (in actual channels, the equivalent locations could be bars, submerged rock outcrops, bends or channel constrictions such as are evident in Figure 3), broken ice was sloughed from beneath the tow and deposited as a plug lodged in the track.

Further transits, following periods of ice regrowth over the track, displaced additional ice sideways to the ridges or caused it to be dragged and shoved to the plugs formed in the track. The areal concentration of brash ice spread over the track usually remained small, and the track itself remained straight-edged, while the channel was covered by a thin ice sheet. The experiments suggest that, when the ice sheet is less than about 0.30 m thick at full scale, its edges become reamed by the sides of the tow.

The ice sheet continued to thicken and strengthen and encroached laterally inwards (as a form of border ice growth) along the track. Near the track, thickening of the ice sheet was augmented by freezing of water washed over it during transits. The edges of the track thickened and strengthened such that, when impacted by the tow's bow, comparatively large cuspate pieces of ice broke flexurally from the ice sheet. These pieces drifted into the track (Fig. 25c). Their comparatively large size caused them to pass less readily beneath the tows. Instead, they were either displaced beneath the edges of the ice sheet, becoming part of the ridge, or were shoved to plugs formed in the track. Although the amount of ice in the track initially increased with the entry of broken sheet ice, it was reduced by subsequent transits, which cleared it from the track (compare Fig. 25c and d). Regrowth of ice, together with the freezing of wave-generated wash from subsequent transits, smoothed serrated edges and sealed cracks in the ice sheet (Fig. 25e) at some locations. At others, fresh breaks occurred.

Fed with brash and broken ice during successive tow transits, the plugs thickened and extended along the track (Fig. 25f). In the ice tank, plugs grew as ice was dislodged and then deposited when the tow hulls overrode them. In river channels with substantial water current, brash ice may be conveyed along a track and collected at plug sites. Eventually, after numerous transits, and depending on plug spacing, the track becomes filled with broken ice. In a sense the ice formation processes illustrated in Figure 25f represent a pattern of lateral accumulation of brash and broken ice along a track, as opposed to the pattern of vertical accumulation, or thickening, occurring simultaneously along a track (Fig. 14).

The experiments revealed that transport of brash ice and plug formation are features that may dominate tow transits of ice-covered channels. However, a concern arises as to whether this finding is merely a quirk of the experiments or whether it also holds at full scale. Brash-ice accumulations beneath tows that have traveled long distances may have attained an equilibrium such that they no longer entrap and transport significant quanti-

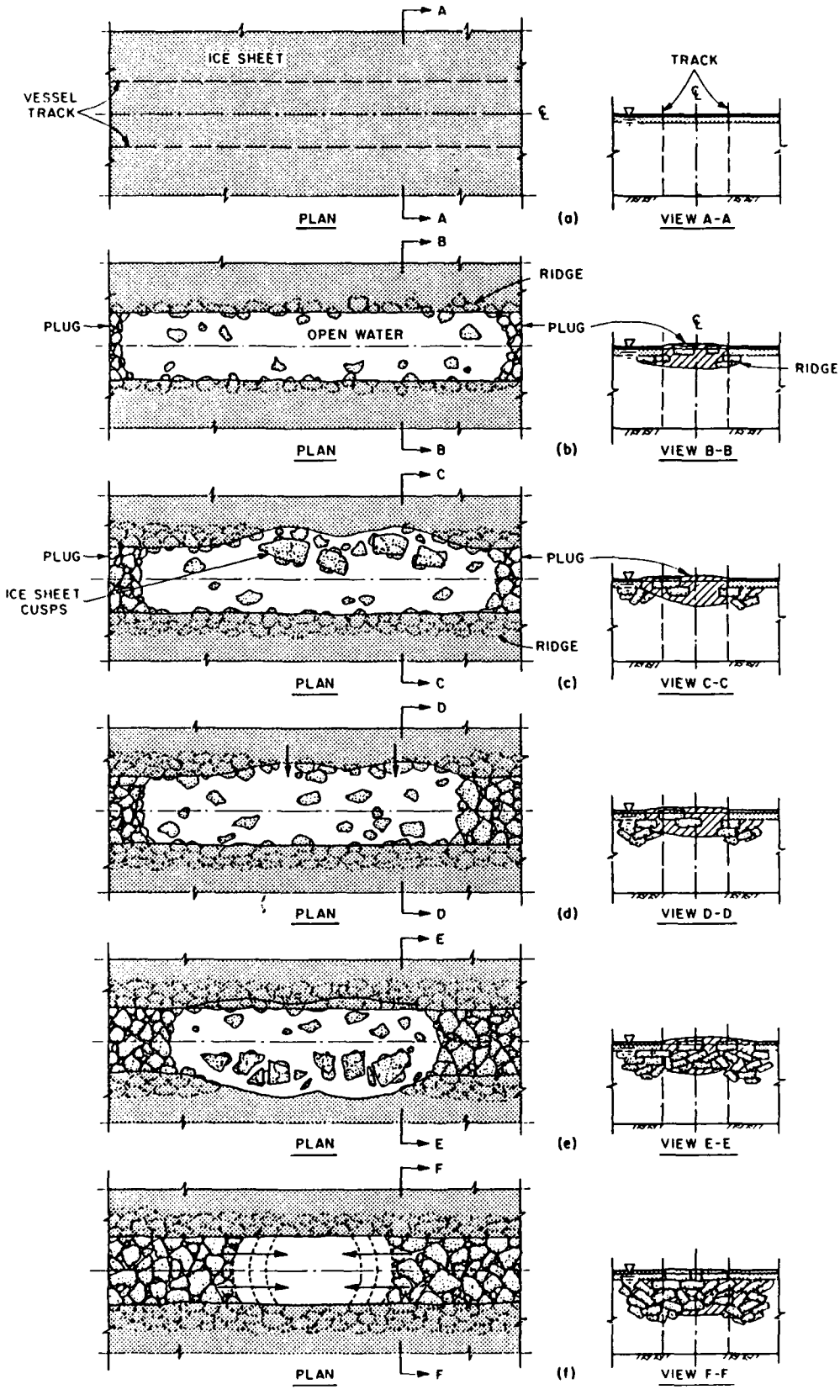

Figure 25. Ice formation in channels transited by tows that move ice along tracks.

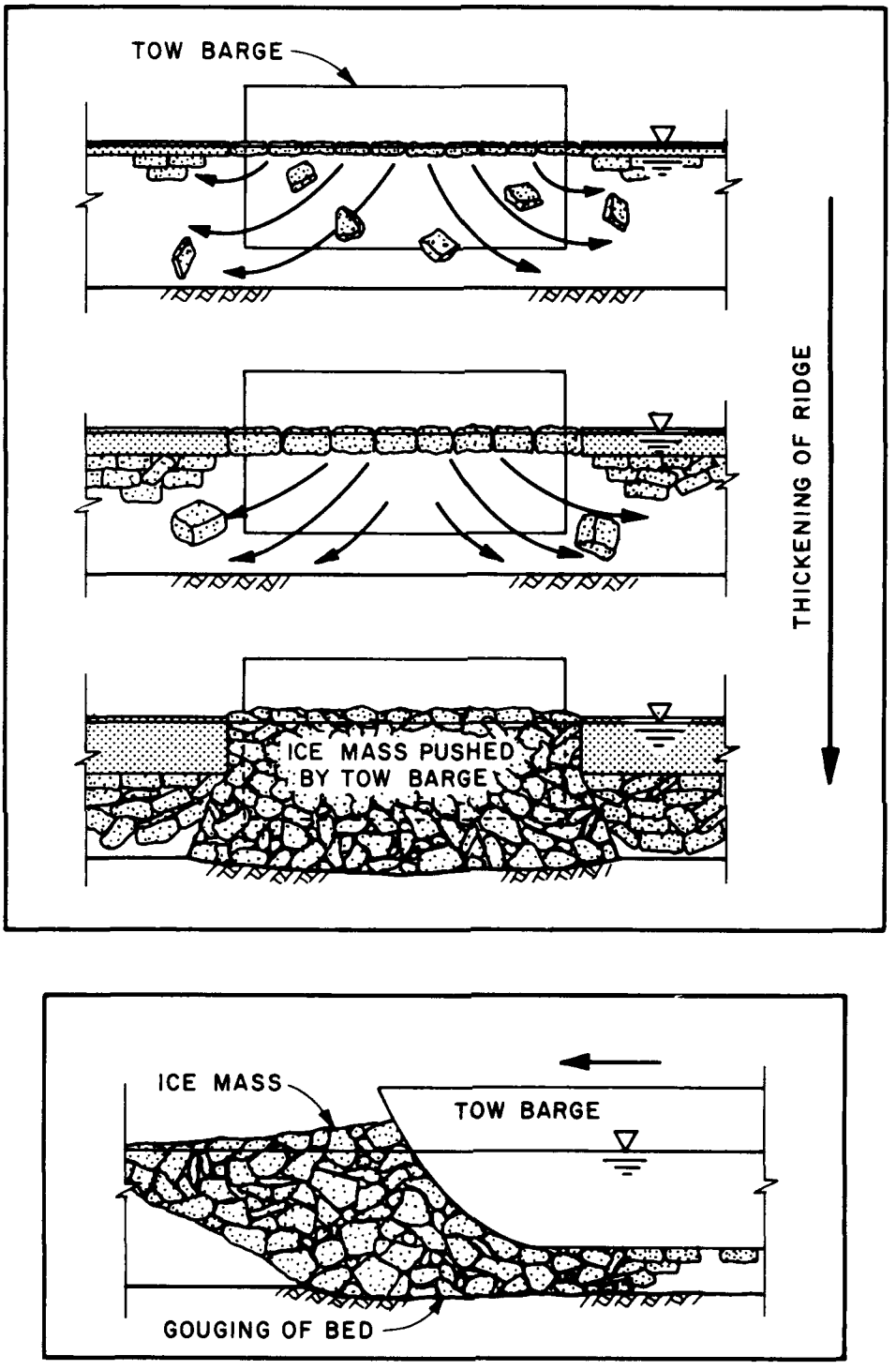

Figure 26. Ice accumulation and displacement in shallow channels transited by tows.

ties of brash ice. The ice-tank experiments, however, were conducted with an initially ice-free tow transiting a relatively short channel; it was only 10 tow-lengths long (nominally 600 m of channel) at 1:30 scale, or 20 tow-lengths long (nominally 1200 m of channel), if the 1:15-scale tow hull is assumed to simulate a 60-m-long tow.

To address this concern, experiments were conducted using the wedge hull. This hull was intended to simulate a hull form that does not entrap or shove ice. It could be viewed as being either a tow that is enveloped by an equilibrium accumulation of broken ice or more simply as a ship-form hull. Transits of the laboratory channel by the wedge hull resulted in practically the same sequence of ice formation illustrated in Figure 14, and they could be simulated by the numerical model presented earlier. In accordance with this sequence, most of the ice broken during transits by the wedge hull was passed beneath the hull and remained in the track, or it was displaced to ridges formed beneath the adjoining edges of the ice sheet. The wedge hull did not shove significant quantities of brash ice along the channel.

Though frequent transits of the ice tank by the tow and wedge hulls generally resulted in increased volume of ice growth, the increase was never strikingly large. At most, transiting resulted in a doubling of the volume of solid ice. For both hulls, ridges formed along the tracks were about three times the ice-cover thickness, whereas the 1:30-scale tow model formed ridges that were about five times the ice-cover thickness. The tracks formed by the tow hulls usually contained negligible amounts of brash ice, most of it having been pushed to the plugs that developed at the ends of the tracks. The plug thickness can be on the order of ten (or more) times the ice sheet thickness.

Plug and ridge formation pose problems in ice-covered channels because they are resistant to transit. They may also be troublesome when ice covers break up if they precipitate ice jamming. The problems associated with ridge and plug formation are exacerbated in shallow channels that provide little clearance beneath vessels. In such channels, ridges and plugs develop more rapidly than in deep channels, and they may extend over the full channel depth. The sketches in Figure 26 illustrate how the lack of clearance beneath a tow causes brash ice to be displaced sideways to ridges that flank the track, or to be accumulated as a jumbled ice mass shoved ahead of the tow. Under these conditions, a tow may become grounded on brash ice lodged against the channel bottom. Obviously the most difficult channels for tows to transit are those that are maintained to the COE minimum navigation depth of 3.05 m (10 ft).

Preliminary experiments

The photographs in Figure 27 show a track opened by the 1:30-scale tow transiting the ice tank at a frequency of $f_t = 1/(4 \text{ hours})$. The results show how little ice remained in the track opened by the model tow and how rapidly a brash-ice plug formed at the end of the channel.

After the first two transits, a negligible amount of brash ice remained in the track (Fig. 27a). Most of it had been entrapped beneath the tow, dragged along by it, and deposited as a plug at the end of the channel (the plug is evident in the foreground of Figure 27a) or cast sideways beneath the edges of the ice sheet bordering the track. There, inverted linear piles of brash ice accumulated as ridges. The tows transported brash ice by entrapping it along the tow's flat-bottomed underside, beneath its relatively bluff bow, and in small wakes immediately behind the barges comprising the tow. The amount of brash ice remaining in the channel after four transits was also negligible (Fig. 27b). Even after ten transits, little brash ice had accumulated in the channel, although by then the plug extended back along the channel for about one third of its length (Fig. 27c). The experiment was halted after 11 transits, as negligible amounts of brash ice had accumulated in the track.

The thicknesses of the ice sheet η and the accumulation as ridges η_r and the thickest plug η_p are presented in Figure 28 vs cumulative cooling time ΣS_d. At the monitoring area, $\eta_b/\eta = 0$. Although the ridges were by no means uniformly thick (being instead jagged), the average ridge thickness normalized with ice sheet thickness η_r/η was about 1.3. As plug formation was unforeseen, its thickness was not measured until the end of the experiment, when it was found that η_p/η was about 8.

The second experiment conducted with the 1:30-scale tow resulted in essentially the same channel condition as illustrated in Figure 27. For this experiment, $f_t = 1/\text{hour}$, but the tow model was transited alternately along two overlapping tracks as indicated in Figure 29 (the overlap being one barge width). The tracks overlapped to replicate the more realistic transit situation whereby tows move along several overlapping or adjoining tracks rather than along a single track. However, this experiment had essentially the same outcome as the first one. As indicated in Figure 30, negligible

a. n = 1.

b. n = 4.

c. n = 10.

Figure 27. Ice formation in the ice tank transited by the 1:30-scale tow; f_t *= 1/(4 hours).*

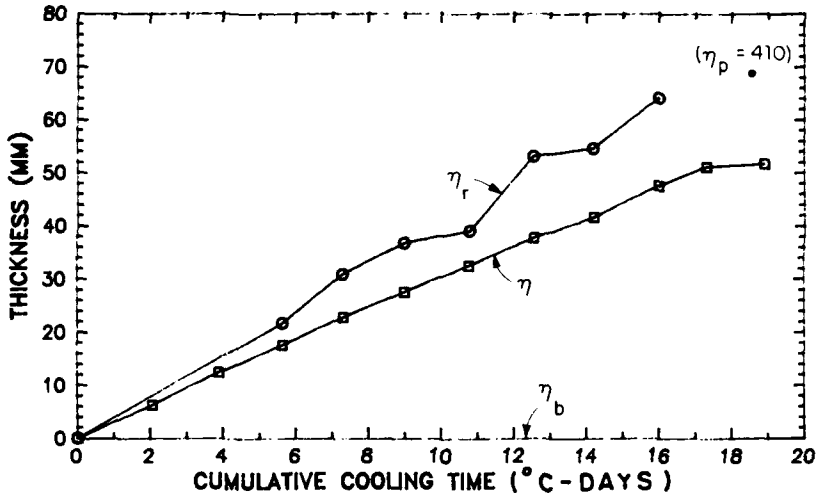

Figure 28. Ice thickness vs cumulative cooling time; 1:30-scale tow; f_t = 1/(4 hours).

Figure 29. Ice formation in the ice tank transited by the 1:30-scale tow along overlapping tracks; f_t = 1/ hour.

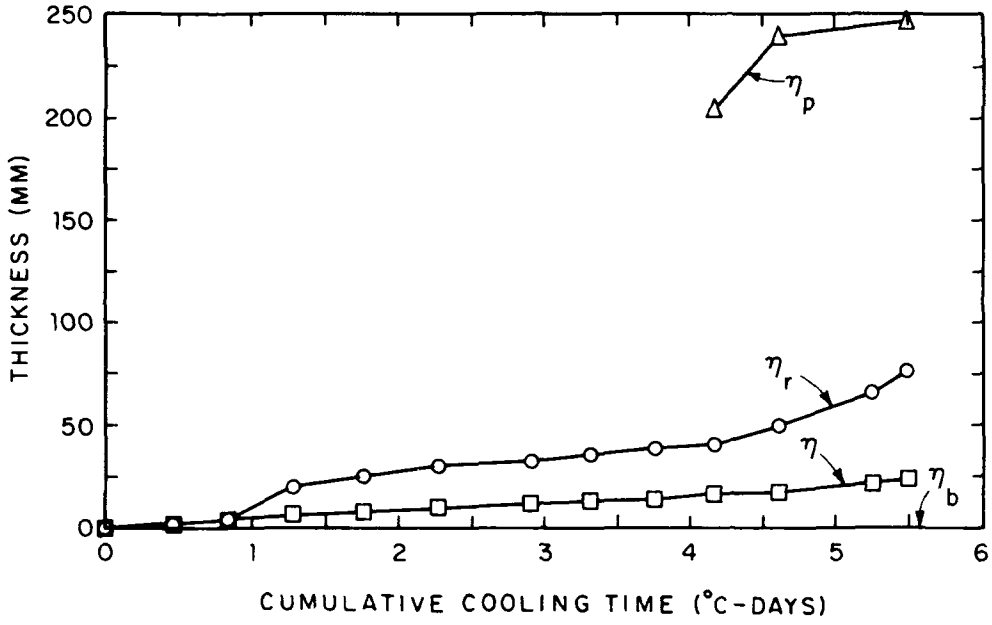

Figure 30. Ice thickness vs cumulative cooling time; 1:30-scale tow; f_t = 1/ hour.

brash ice accumulated in the track, $\eta_b/\eta = 0$, $\eta_r/\eta \cong 3$, and $\eta_p/\eta \cong 10$.

The third experiment was conducted using only the 1:30-scale towboat (its dimensions are given in Figure 18), which was transited through the channel at $f_t \cong 1/(2$ hours). The intent of this experiment was to indicate the effects of tow length on ice formation. The relative shortness and the rounded form of the towboat hull shoved and dragged considerably less brash ice than did the tow hull. However, the towboat left more brash ice in its track and produced a smaller plug, as can be seen by comparing Figures 31 and 27, or by comparing the data in Figures 32 and 28. This finding is likely identical to that observed at full scale by Ashton et al. (1973).

Although the preliminary experiments with the 1:30-scale tow and towboat hulls were useful in delineating the general features of tow transit through ice-covered channels, further experiments with larger hulls fitted with propellers were required to produce more detailed and quantitative information. For example, a drawback of the 1:30-scale towboat was that, without propellers, its rounded, flat-bottomed hull produced a track filled with dubiously long strips of broken ice, as is evident in Figure 31.

a. n = 2.

Figure 31. Ice formation in the ice tank transited by the 1:30-scale towboat; f_t = 1/(2 hours).

Deep-channel experiments

Presented here are observations and data from the experiments conducted with the 1:15-scale tow

b. n = 6. *c.* n = 12.

Figure 31 (Continued). Ice formation in the ice tank transited by the 1:30-scale towboat; f_t = 1/(2 hours).

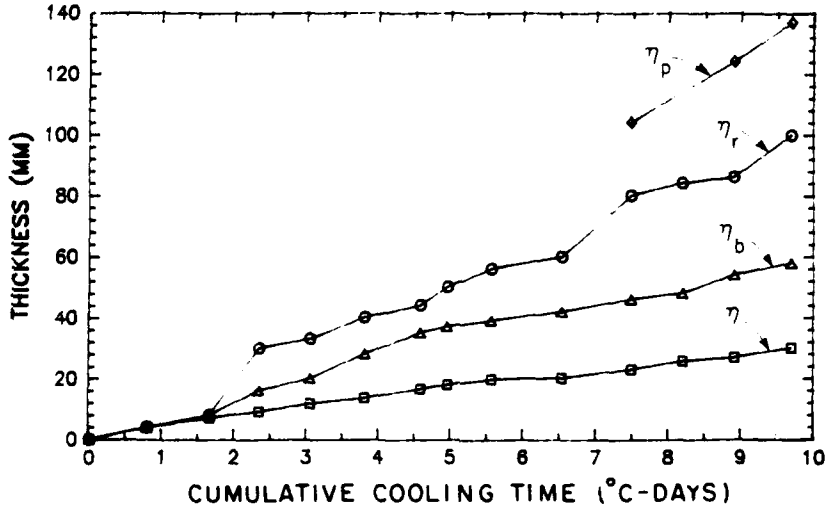

Figure 32. Ice thickness vs cumulative cooling time; 1:30-scale towboat; f_t = 1/(2 hours).

and wedge hulls transiting the ice tank at the deep-channel condition; the ratios of water depth to vessel draft y_o/D were 5.62 and 3.75 for the tow and wedge hulls, respectively. As listed in Table 1 the transit frequencies investigated with both the tow and wedge hulls were $f_t = 1/(2 \text{ hours})$, $1/(4 \text{ hours})$ and $1/(8 \text{ hours})$. An additional set of experiments was conducted with transits scheduled at $f_t = 1/(0.5 \text{ hour})$ and $f_n = 1/(7.5 \text{ hours})$. The wedge was used for two further experiments at $f_t = 1/(0.5 \text{ hour})$ and $1/(0.17 \text{ hour})$. The latter experiment was performed for a short duration in order to assess the variation of β with the number of transits. Full-scale equivalent frequencies can be assessed using eq 31. Included in the results presented for each experiment are the following:

- A brief illustrated description of the salient features of ice formation;
- The effect of ΣS_d on the thicknesses of the brash-ice layer over the track η_b, the ridge η_r, the plug (for the tow hull) η_p and the ice sheet η;
- The effect of ΣS_d and number of transits n on the areal concentration of open water β and the porosity p of brash-ice accumulations; and
- The size distribution of brash ice in the channel.

Each data point in plots of η_b, η_r and η vs ΣS_d represents a transit. The brash-ice sizes, given in terms of d_e and σ_g, are summarized in Table 2. Photographs of brash-ice samples taken at the end of each experiment are presented in Appendix B. The volumes of ice grown along each track transited by the wedge hull, and the thickness of brash-ice accumulation in each track, both normalized with η, are presented in Appendix C.

Transits at $f_t = 1/(0.5 \text{ hours})$

Figure 33 illustrates the formation of an ice-filled track along the laboratory channel transited at 0.5-hour intervals by the wedge hull. Ice formed along the track in approximately the same sequence as illustrated in Figure 14. The first few transits left brash ice strewn along the track at high areal concentrations. Most of the ice was cast sideways beneath the ice sheet, and no ice plug formed at either end of the channel. Further transits by the wedge hull led to increased coverage of the track with brash ice, and eventually the track became fully covered by a brash-ice layer that thickened more or less continuously with subsequent transits. Values of η_b, η_r and η increased monotonically, though somewhat erratically, with increasing ΣS_d and n (Fig. 34), reflecting the nonuniformity of the accumulations. Also, as shown in Figure 33d, the layer of brash ice accumulated in the track was occasionally marked by a furrow [similarly the ice thickness is much less at the center of the profile measured by Kannari (Fig. 9)]. The rate at which the track became covered with brash ice can be determined from Figure 35, which shows that the

Table 2. Summary of brash-ice dimensions.

Hull form	P_t *(hours)*	y_o *(m)*	d_c *(mm)*	σ_g
Wedge	0.5	1.07	15	2.3
	2.0	1.07	93	2.5
	4.0	1.07	135	1.5
	8.0	1.07	124	2.4
Tow	2.0	1.07	76	3.7
	4.0	1.07	179	1.5
	8.0	1.07	149	1.7
	4.0	0.53	69	1.9
	2.0	0.22	24	3.8
	4.0	0.22	36	4.5
Wedge	*	1.07	66	3.9
Tow	*	1.07	48	5.9

* Multifrequency transits [$n = 4$, $f_t = 1/(0.5 \text{ hour})$, $f_n = 1/(7.5 \text{ hours})$]

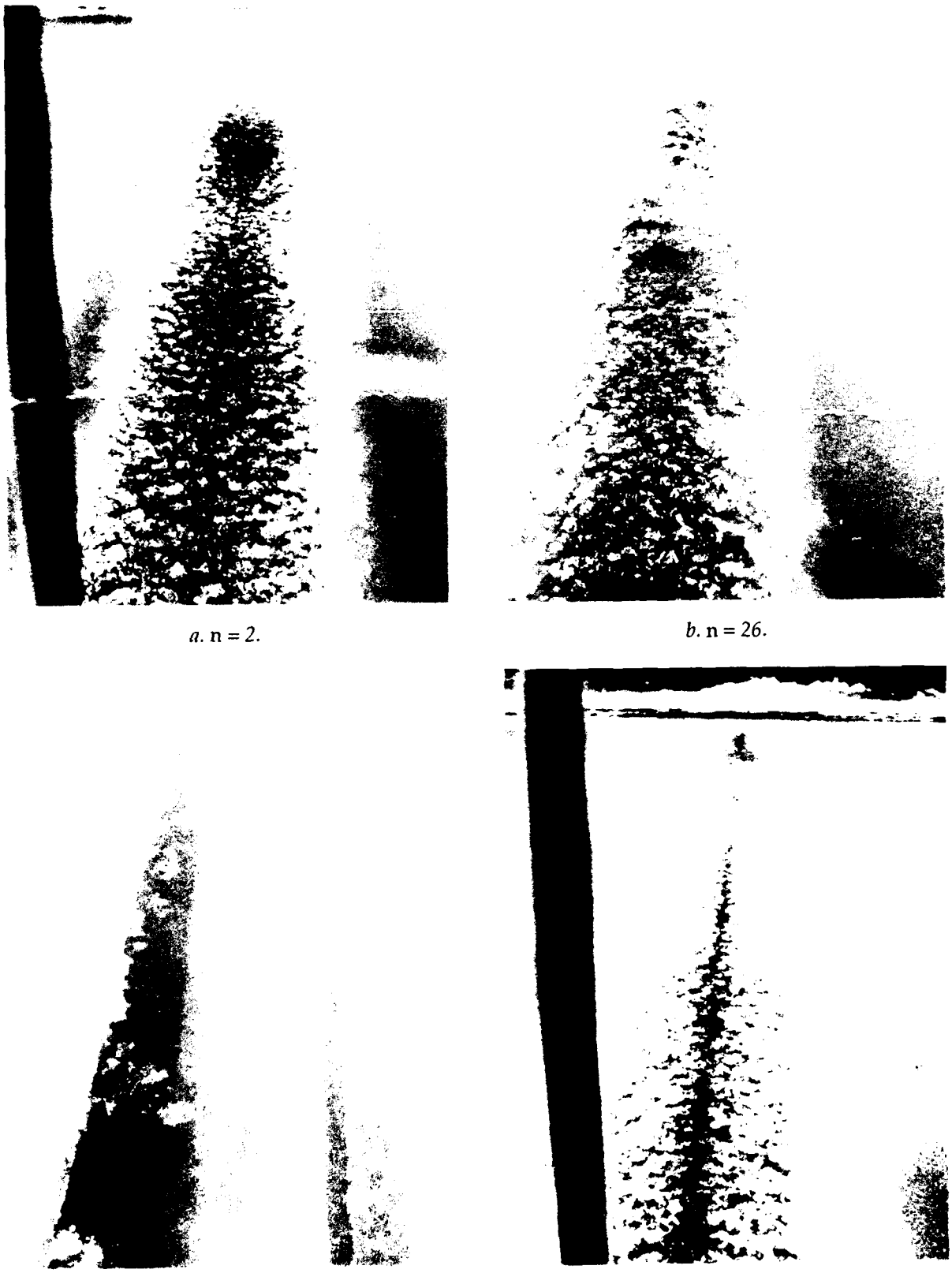

a. n = 2. *b.* n = 26. *c.* n = 51. *d.* n = 98.

Figure 33. Ice formation in the ice tank transited by the 1:15-scale wedge hull; f_t *= 1/(0.5 hour).*

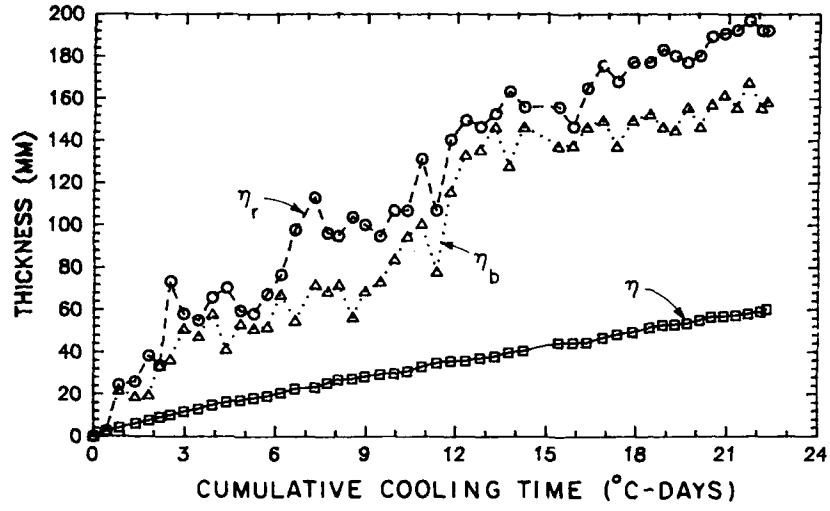

Figure 34. Ice thickness vs cumulative cooling time; 1:15-scale wedge hull, f_t = 1/(0.5 hour); the total number of transits is 98.

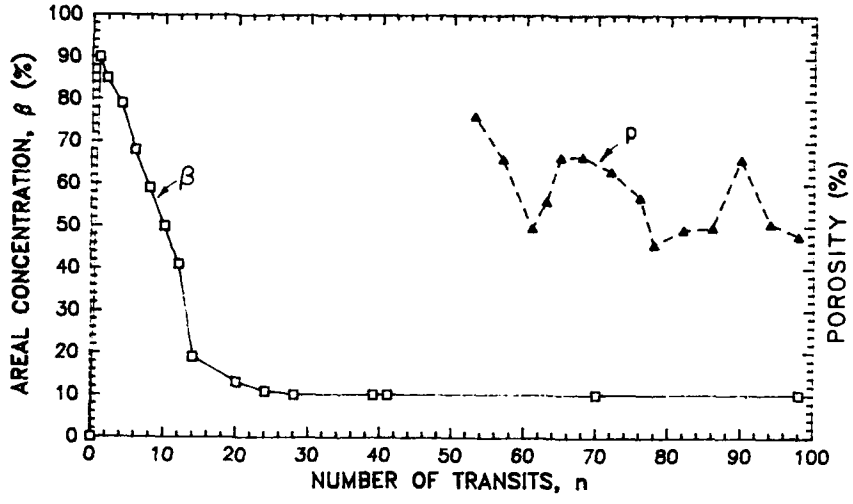

Figure 35. Variation of areal concentration of open water and porosity p with number of transits n; 1:15-scale wedge hull; f_t = 1/(0.5 hour).

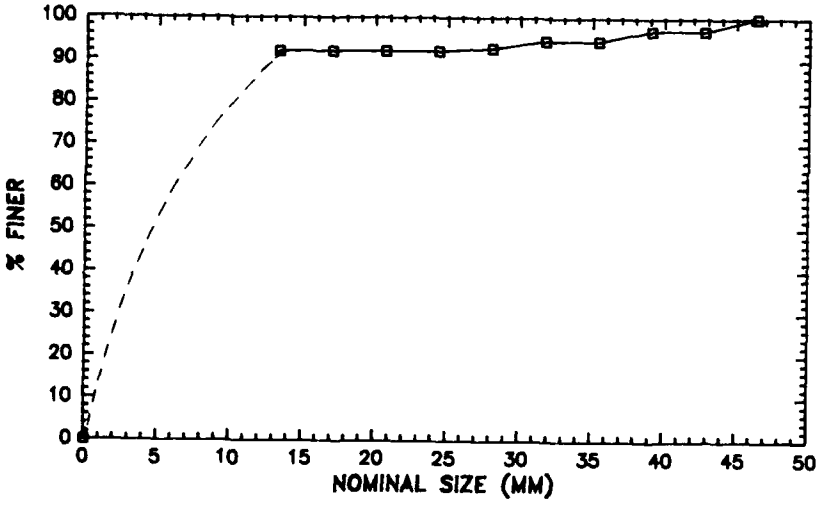

Figure 36. Size distribution of brash ice; 1:15-scale wedge hull; f_t = 1/(0.5 hour).

areal concentration of open water β steeply declined with increasing number of transits n. Throughout this and the other experiments, approximately 10% of the track remained open water. As shown in Figure 35, the layer was very porous, with values of porosity p generally ranging from about 65 to 45%.

On completion of the experiment, when $\eta = 60$ mm (0.9 m at full scale) and $n = 98$, the brash-ice layer had an average thickness such that $\eta_b/\eta \cong 2.5$ to 3 (App. C). The ridges adjoining the track attained an average thickness such that $\eta_r/\eta \cong 3.5$. The estimates (in Appendix C) of the volume of ice grown per unit area of the track, or the equivalent to ice thickness expressed as η_i/η, was about 2.

The transits produced comparatively small ice pieces that resulted from broken regrowth ice and from ice that was crushed or sheared from the ice-sheet edges. Figure 36 shows that at least 90% of the brash ice in the layer consisted of fine ice pieces with d_e less than 10 mm (0.150 m at full scale). The remaining 10% of the brash ice comprised pieces with d_e up to 65 mm (about 1 m at full scale, for $\lambda_\ell = 15$). These larger sizes were formed from smaller pieces that had fused together and grown during periods of regrowth. During this experiment no large pieces of the ice sheet were broken and drawn into the channel.

Transits at $f_t = 1/(2$ hours)

Figures 37 and 38 illustrate ice formation in the channel when transited every two hours by the wedge and tow hulls, respectively. Figure 39 gives values of η_b and η_r for thickness vs ΣS_d.

Frequent transits of the channel by the wedge hull resulted in practically the same pattern of ice formation as portrayed in Figure 14 and as described for $f_t = 1/(0.5$ hour). A layer of brash ice covered the track, then thickened, as did the adjoining ridges, with increasing number of transits. At the end of the experiment, η_b/η and η_r/η were both approximately 1.7 to 2.3, with $\eta_i/\eta \cong 1.5$ to 1.7 (Fig. 39a, App. C).

Figure 40 shows the decline of β with increasing number of transits, and it shows that, once formed, the layer of ice pieces was comparatively porous, with values of p of about 30–65%. A notable difference, made evident by comparing Figures 37 and 33, is that transits at $f_t = 1/(2$ hours) produced larger ice pieces than did transits at 0.5-hour intervals. Because individual ice pieces were larger, correspondingly larger variations occurred in η_b and η_r (Fig. 39a). For $f_t = 1/(2$ hours), $d_e \cong 93$ mm (1.40 m at full scale), with $\sigma_g = 2.5$. The ice pieces

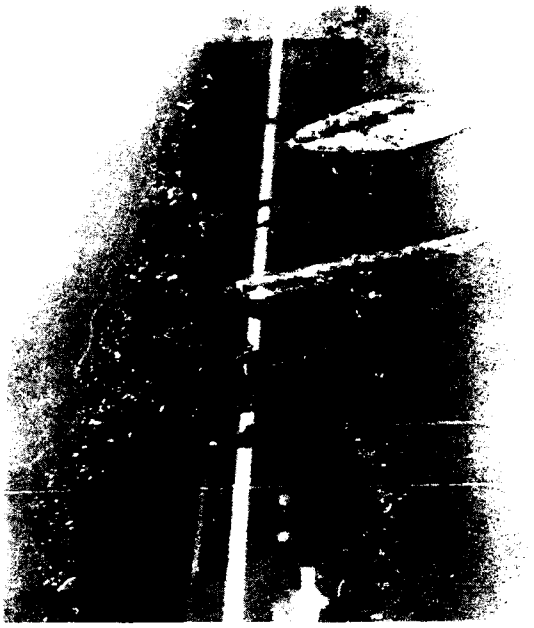

a. n = *1*

b. n = 4.

Figure 37. Ice formation in the ice tank transited by the 1:15-scale wedge hull; $f_t = 1/(2$ hours).

c. n = *11.*

d. n = *17.*

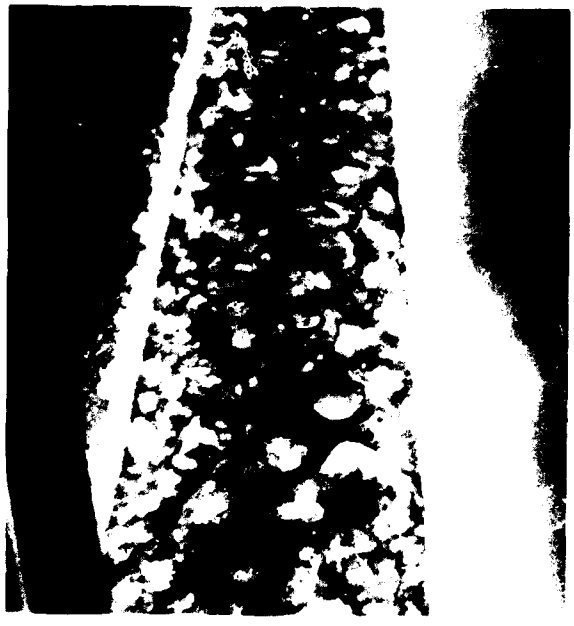

e. n = *21.*

f. n = *30.*

Figure 37 (Continued). Ice formation in the ice tank transited by the 1:15-scale wedge hull; f_t = *1/(2 hours).*

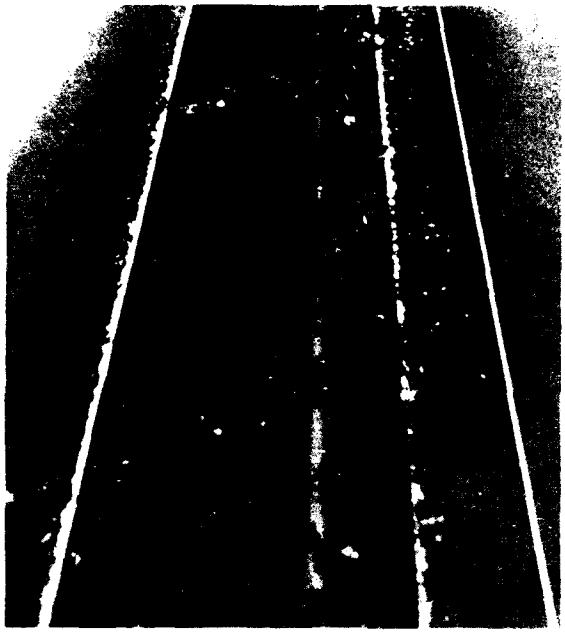

a. n = 4.

b. n = 11.

c. n = 16.

d. n = 20.

Figure 38. Ice formation in the ice tank transited by the 1:15-scale tow hull: f_t = 1/(2 hours).

e. n = 24.

f. n = 29.

Figure 38. Continued.

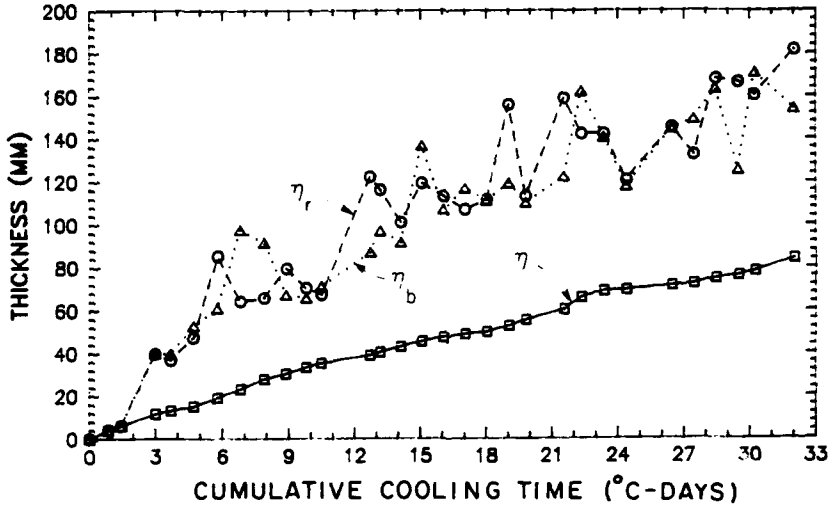

a. 1:15-scale wedge hull.

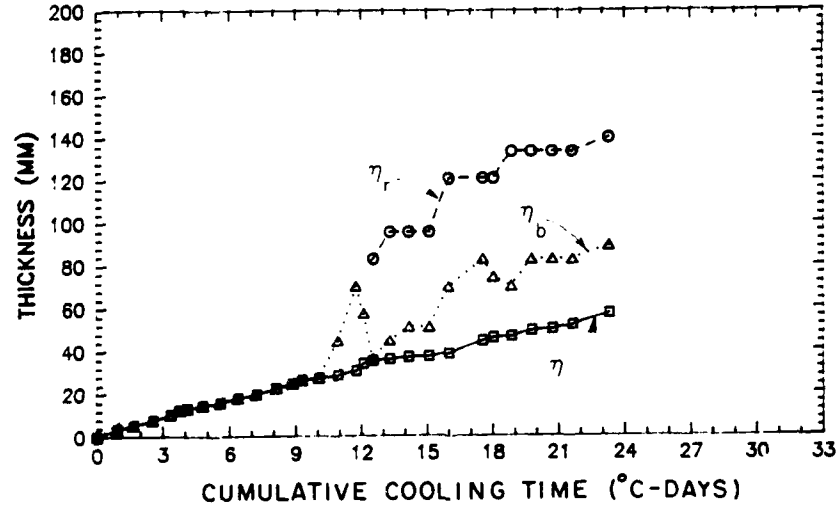

b. 1:15-scale tow hull.

Figure 39. Ice thickness vs cumulative cooling time; f_t = 1/(2 hours).

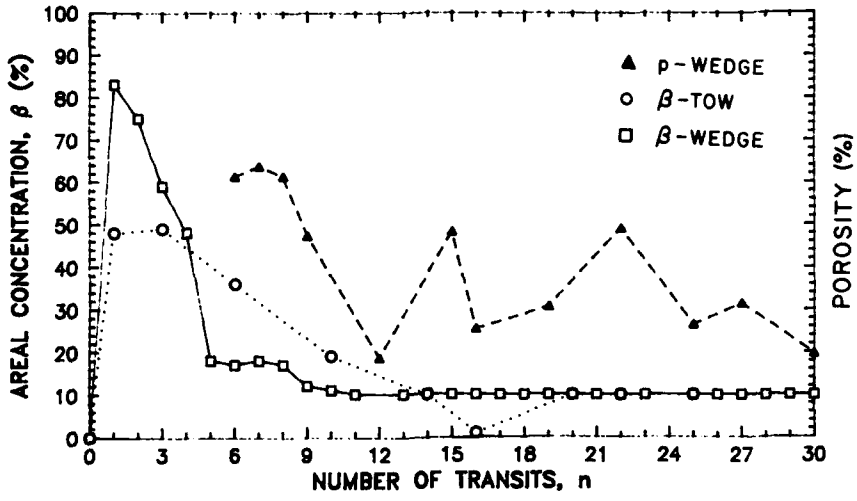

Figure 40. Variation of areal concentration of open water β and porosity p with number of transits n; f_t = 1/(2 hours).

were typically formed of broken, platy pieces of regrowth ice fused together.

Frequent transits of the channel by the tow hull resulted in the same manner of ice formation indicated in Figure 25. During the first six to ten transits, the tow broke and reamed a straight-edged track (Fig. 38a,b) that retained small pieces of regrowth ice at high areal concentrations. Most of the brash ice was either conveyed to a plug that formed at one of the channel, or it was displaced sideways beneath the adjoining ice sheet. During later transits the tow hull rode against and broke sections of the ice sheet bordering the track, causing relatively large pieces of ice sheet, and portions of the ridge, to enter the track (Fig. 38c). After several more transits the major portion of the ice in the track was cleared and shoved to the plug (Fig. 38d) or displaced beneath the ice sheet. The broken section of ice edge became smoothed and re-reamed during further periods of regrowth and transit (Fig. 38d,e). However, other portions of ice sheet were broken and resulted in more broken ice bursting into the track (Fig. 38e). Still further periods of regrowth and transit enabled the edges of the track to become smoothed (Fig. 38f). Conceivably a track could experience several cycles of this process of sheet breaking and self-healing, until the edge, reinforced by its ridge, could not be flexurally broken by a tow; then tows would be unable to transit the channel.

The fluctuations in η_b and η_r shown in Figure 39b coincide with periods when pieces of ice sheet and segments of ridge entered the channel and were eventually cleared from it. The wedge hull produced a single population of brash-ice sizes in its track, but the tow hull, by mixing regrowth ice and pieces of broken ice sheet, produced at least two populations of brash-ice size. The mixture of the two populations led to a nonuniform distribution of brash-ice sizes, as shown in Figure 41; d_e = 76 mm (1.14 m at full scale) and σ_g = 3.7.

Transits at f_t = 1/(4 hours)

Ice formation and tracks formed by the wedge hull and the tow hull transiting the laboratory channel at a frequency of f_t = 1/(4 hours) are shown in Figure 42. Figure 43 presents values of η_b and η_r for wedge and tow transits at 4-hour intervals. Figure 44 presents values of β and *p*.

For the wedge hull the reduction in transit frequency from 1/(0.5 hour) to 1/(4 hours) led to a mild decrease in the thickness of the brash-ice layer formed over the track and accumulated as ridges next to it. A reduction in the volume of ice formed is expected in accordance with the formulation presented earlier. However, the comparatively slight decrease in regrowth with decreasing frequency (by a factor of 16) is somewhat unexpected, especially in light of what current literature might lead one to expect (e.g. Greisman 1981). Transits of the wedge hull resulted in a brash ice layer for which $\eta_b/\eta \cong 2.0$ to 2.5 and $\eta_i/\eta \cong 1.5$ to 1.7 (App. C). The ridge thickness was such that $\eta_b/\eta \cong 2.3$ to 2.6.

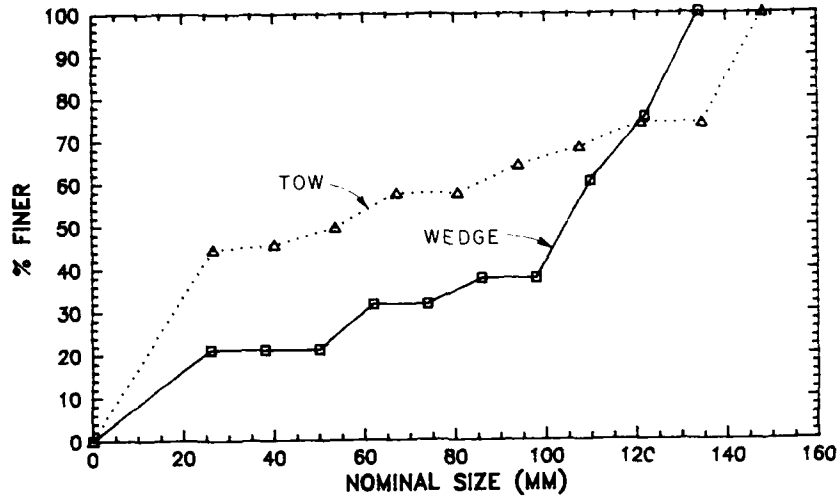

Figure 41. Size distribution of brash ice; f_t = 1/(2 hours).

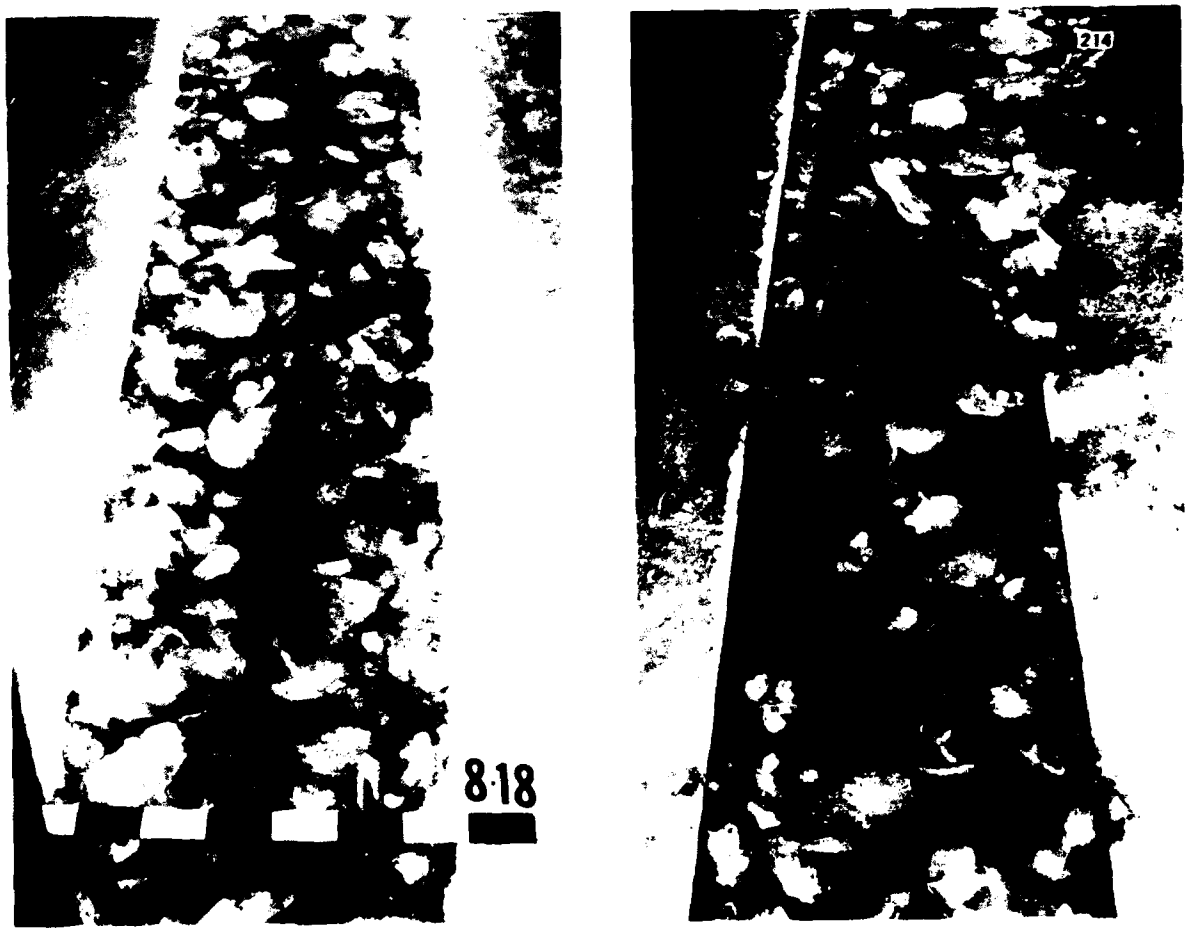

a. 1:15-scale wedge hull (n = 18).

b. 1:15-scale tow hull (n = 14).

Figure 42. Ice formation in the ice tank transited at f_t = 1/(4 hours).

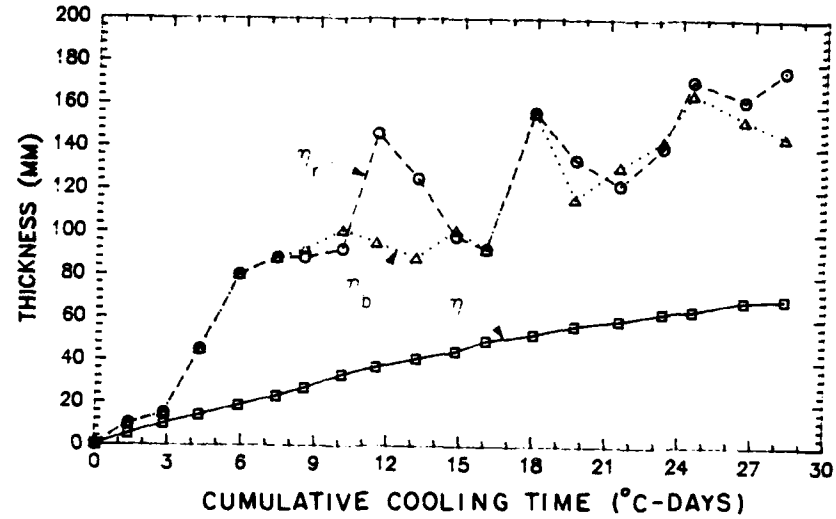

a. 1:15-scale wedge hull.

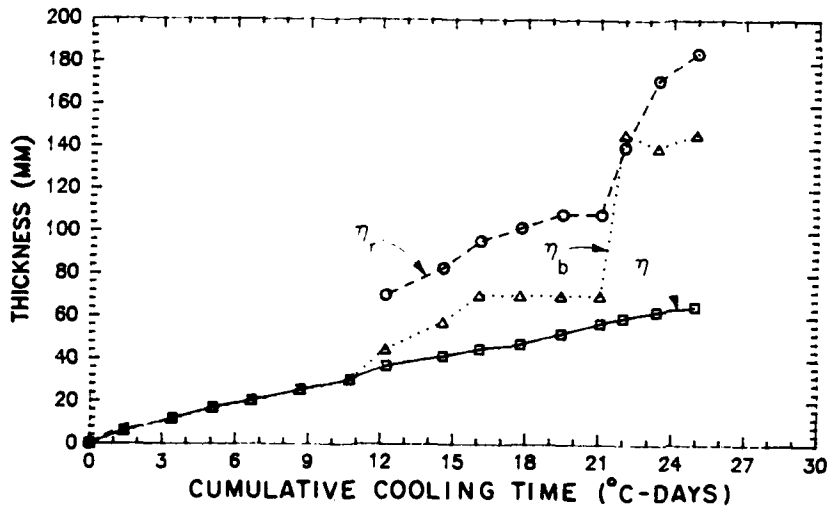

b. 1:15-scale tow hull (n = 14).

Figure 43. Ice thickness vs cumulative cooling time; f_t *= 1/(4 hours).*

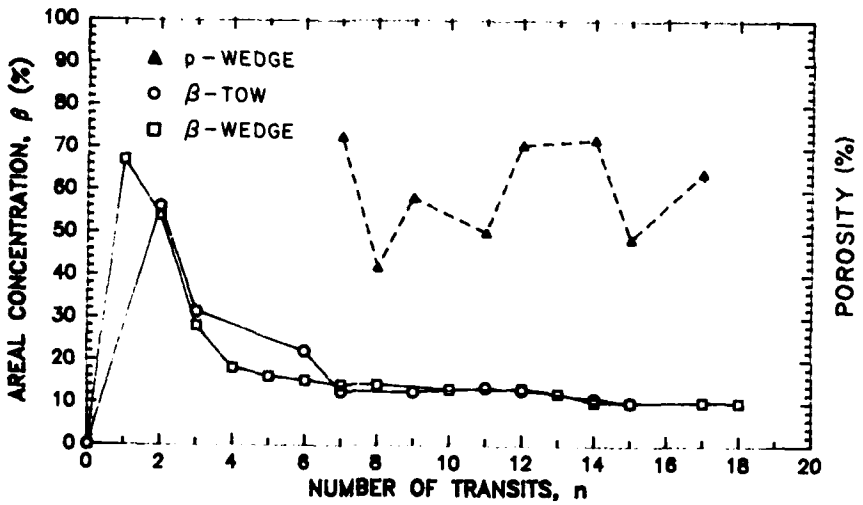

Figure 44. Variation of areal concentration of open water β *and porosity* p *with number of transits* n; f_t *= 1/(4 hours).*

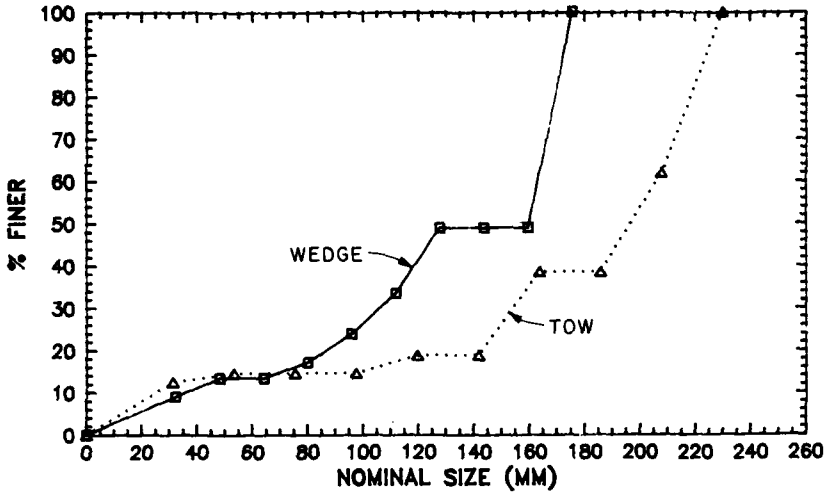

Figure 45. Size distribution of brash ice; f_t = 1/(4 hours).

Reductions in the frequency of tow transit from 1/(2 hours) to 1/(4 hours) resulted in only slight changes to the manner by which ice formed in the tow's track, and they did not result in dramatic variations in the thickness of ice accumulated as a layer in its track or in ridges flanking the tracks. The accumulations, however, were less uniform in thickness for the lesser transit frequency. At the end of the tow-hull experiment, $\eta_b/\eta \cong 2.3$ (at the monitoring area, but elsewhere $\eta_b/\eta \cong 1.5$) and $\eta_r/\eta \cong 3.0$. For these two patterns, ice formation was dominated by the facility of the tow to move ice along the channel. However, less frequent transits led to less movement of ice along the channel, proportionately less plug development, and larger pieces of brash ice in the track. Fewer occasions to clear ice and therefore longer periods of regrowth produced thicker, more rounded (by regrowth) ice pieces (compare Fig. 38 and 42) that were less easily shoved by the tow; they more readily rolled around and beneath it. Comparison of Figures 45 and 41 shows that, for tow transits at a frequency of 1/(4 hours), $d_e \cong 179$ mm, which is about two to three times the value of d_e resulting from a transit frequency of 1/(2 hours). Also, the lesser transit frequency resulted in more uniform brash ice.

Transits at f_t = 1/(8 hours)

The condition of the channels transited by the wedge and tow hulls at a frequency of 1/(8 hours) is shown in Figure 46. Figure 47 presents values of η, η_b and η_r vs ΣS_d. Transits by the wedge and tow hulls at a frequency of 1/(8 hours) had about the same effect on ice formation as at a frequency of 1/(4 hours). Figures 48 and 49 present values of β, p and d_e for these experiments. At the end of the experiment, η_b/η and $\eta_i/\eta \cong 1.8$ to 2.0 and $\eta_i/\eta \cong 1.2$ to 1.3.

Transits at f_t = 1/(0.5 hour) and f_n = 1/(7.5 hours)

Figures 50 and 51 show the main features of ice formation in the channel when transited by the tow and wedge hulls in a multifrequency transit schedule involving sequences of four transits at f_t = 1/(0.5 hour), with the sequences having a frequency f_n = 1/(7.5 hours). (At full scale, one could envision four transits every 8 hours with 3–4 day lapses between transits.) Values of η_b, η_r and η vs ΣS_d are presented in Figure 52 for the wedge and tow hulls.

These experiments show that when a schedule of transits involves sequences of transits at relatively high frequency, then displacement, movement and clearance of brash ice are important. For transits by the wedge hull, ice was displaced sideways beneath the bordering ice sheet, giving the track a furrowed appearance as shown in Figure 50. For transits by the tow hull, ice was shoved and dragged toward plugs formed at either end of the track. Figure 51 illustrates the clearance of ice during three consecutive transits by the tow hull.

Displacement of ice from the tracks formed by the wedge hull caused cyclic fluctuations in the recorded values of η_b and η_r, as shown in Figure 52. Typically the first transit of a series reopened the track and displaced broken ice sideways to the ridge beneath the ice sheet. Some of the displaced ice was drawn back into the track. Subsequent

a. 1:15-scale wedge hull.

b. 1:15-scale tow hull.

Figure 46. Ice formation in the ice tank transited at $f_t = 1/(8\ hours)$.

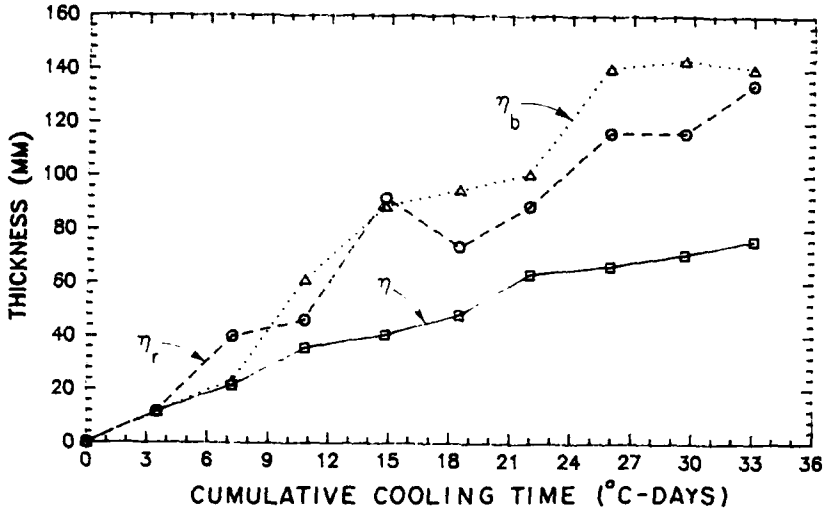

a. 1:15-scale wedge hull.

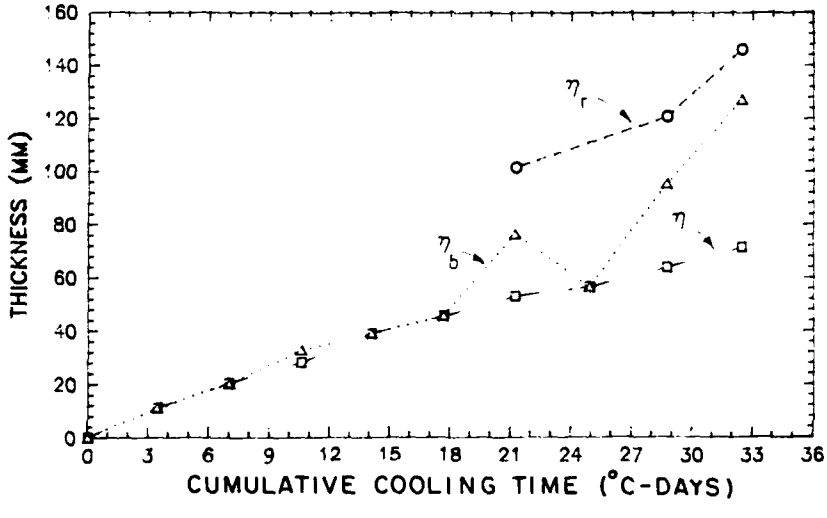

b. 1:15-scale tow hull.

Figure 47. Ice thickness vs cumulative cooling time; $f_t = 1/(8\ hours)$.

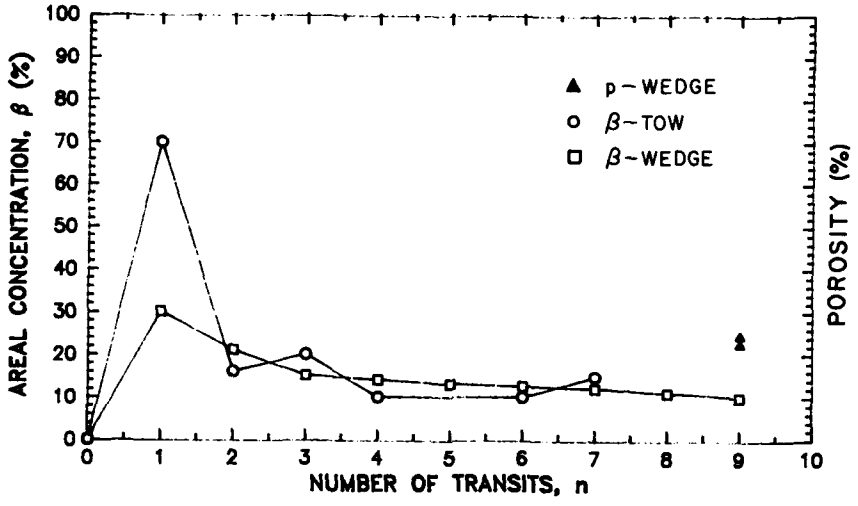

Figure 48. Variation of areal concentration of open water β and porosity p with number of transits n; f_t = 1(8 hours).

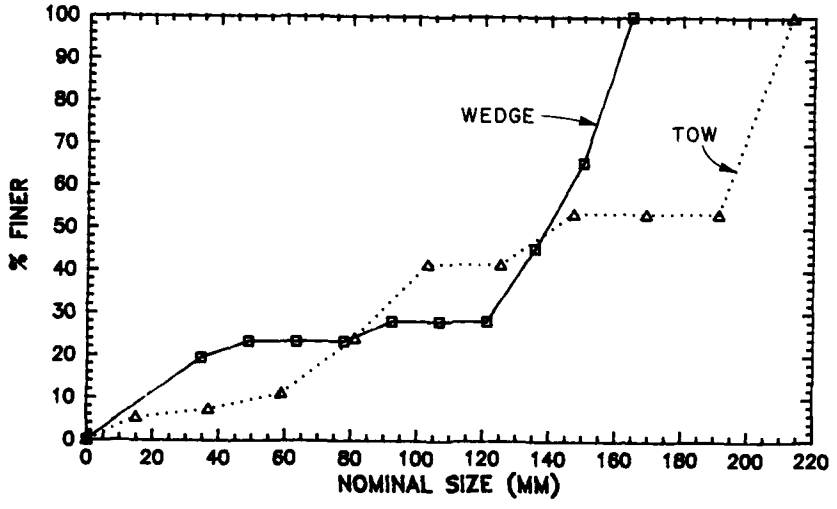

Figure 49. Size distribution of brash ice; f_t = 1/(8 hours).

a. n = 34.

b. n = 35.

c. n = 36.

Figure 50. Ice formation in the ice tank transited by the 1:15-scale tow hull; f_t = 1/(0.5 hour) and f_n = 1/(7.5 hours),

a. n = 25.

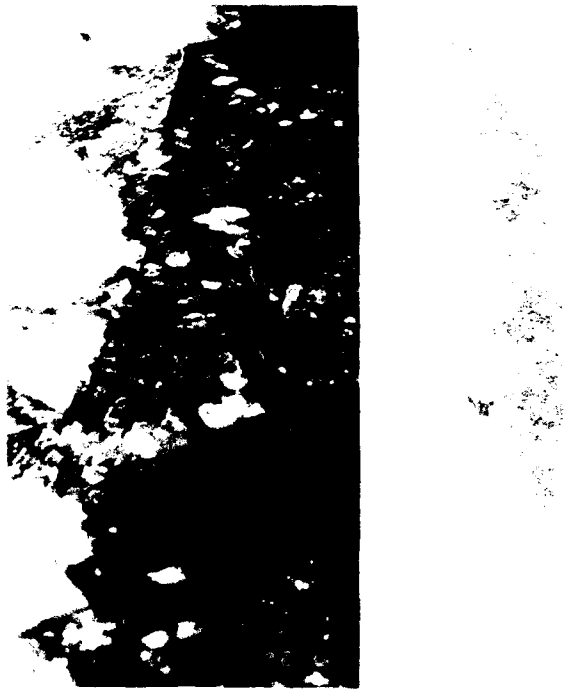

c. n = 27.

b. n = 26.

Figure 51. Ice formation in the ice tank transited by the 1:15-scale tow hull; f_t = 1/(0.5 hour) and f_n = 1/(7.5 hours).

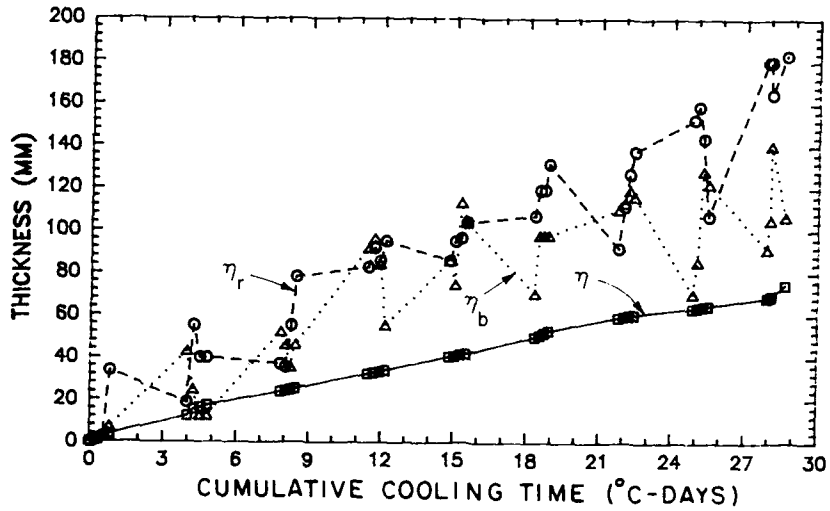

a. 1:15-scale wedge hull.

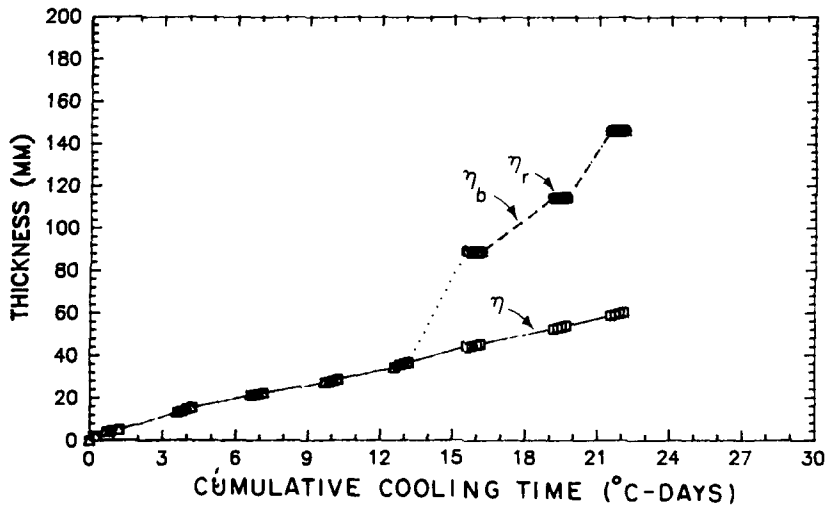

b. 1:15-scale tow hull.

Figure 52. Ice thickness vs cumulative cooling time; f_t = 1/(0.5 hour) and f_n = 1/(7.5 hours).

transits in quick succession, and without much opportunity for regrowth, displaced more broken ice to the ridges, causing them to enlarge and thinning the layer in the track as well as creating a furrow along its center line. This process is evident in Figure 52a for transit sequences until $\Sigma S_d \cong$ 12°C-days. Thereafter, it is obscured in the data because of poor accuracy of measurement; the thickness of individual ice pieces was a significant proportion of the overall thickness. Throughout the experiment the track filled with brash ice such that, on average, $\eta_b/\eta \cong 2$. The series of three transits at f_t = 1/(0.5 hour) depicted in Figure 51 is representative. The first transit following a 6-hour interval between transits (Fig. 51a) left the track strewn with broken ice. The two subsequent transits at 0.5-hour intervals (Fig. 51b,c) cleared much of the broken ice from the channel, shoving it into the plug or displacing it to the ridges. Data on β, p and d_e are presented in Figures 53 and 54.

Shallow-channel experiments

The three experiments conducted with the tow hull transiting shallow, ice-covered channels (y_o/D = 1.16 and 2.78) indicate that ridges and plugs develop more rapidly than they do during frequent transits of deep channels. The experiments also demonstrated that ridge and plug formation

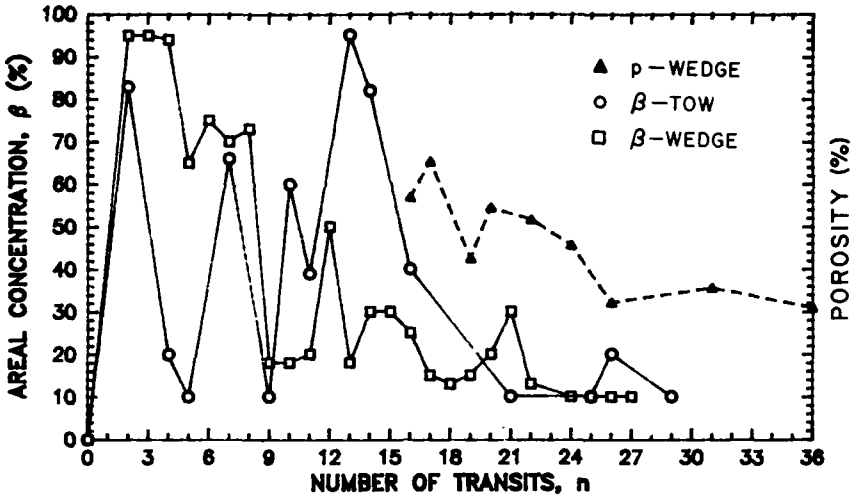

Figure 53. Variation of areal concentration of open water β and porosity p with number of transits n; f_t = 1/(0.5 hour) and f_n = 1/(7.5 hours).

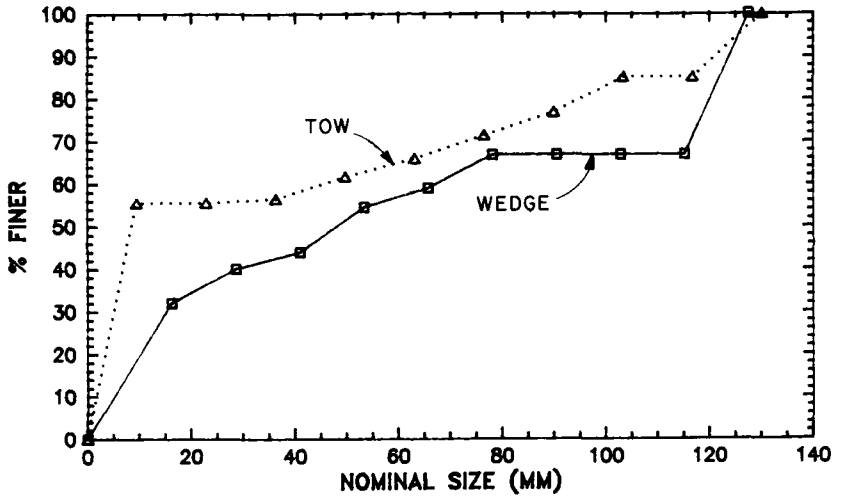

Figure 54. Size distribution of brash ice; f_t = 1/(0.5 hour) and f_n = 1/(7.5 hours).

pose potentially severe problems for navigation of ice-covered shallow channels because they may extend over the full depth of the channel, as illustrated in Figure 26.

Transits at f_t = 1/(2 hours) and 1/(4 hours)

Figures 55 and 56 show the shallow channel (0.22 m deep) after being transited by the tow hull at f_t = 1/(2 hours) and 1/(4 hours), respectively. It is apparent from these figures that little ice accumulated in the tracks opened during transiting. Figure 57, which shows η_b, η_r and η vs ΣS_d, shows that little brash ice remained in the track. The constricted clearance (only 0.03 m) between the tow and the channel bottom forced ice to be displaced sideways to the ridges or shoved along the track. Figure 57 indicates the resulting rapid growth of the ridges, especially when compared with the rates of ridge growth indicated in Figures 39b and 43b. As the ridges approached the channel bottom, less ice could be displaced sideways and more was confined in a jumbled mass shoved ahead of the tow hull, as shown in Figure 58. The mass grew as the tow moved along the track, collecting additional ice. The ice mass was shoved to plugs at either end of the track. While shoving ice, the tow overrode and frequently grounded on ice. The frequency of grounded increasing as the ridges neared the channel bottom.

An obvious consequence of increasing confine-

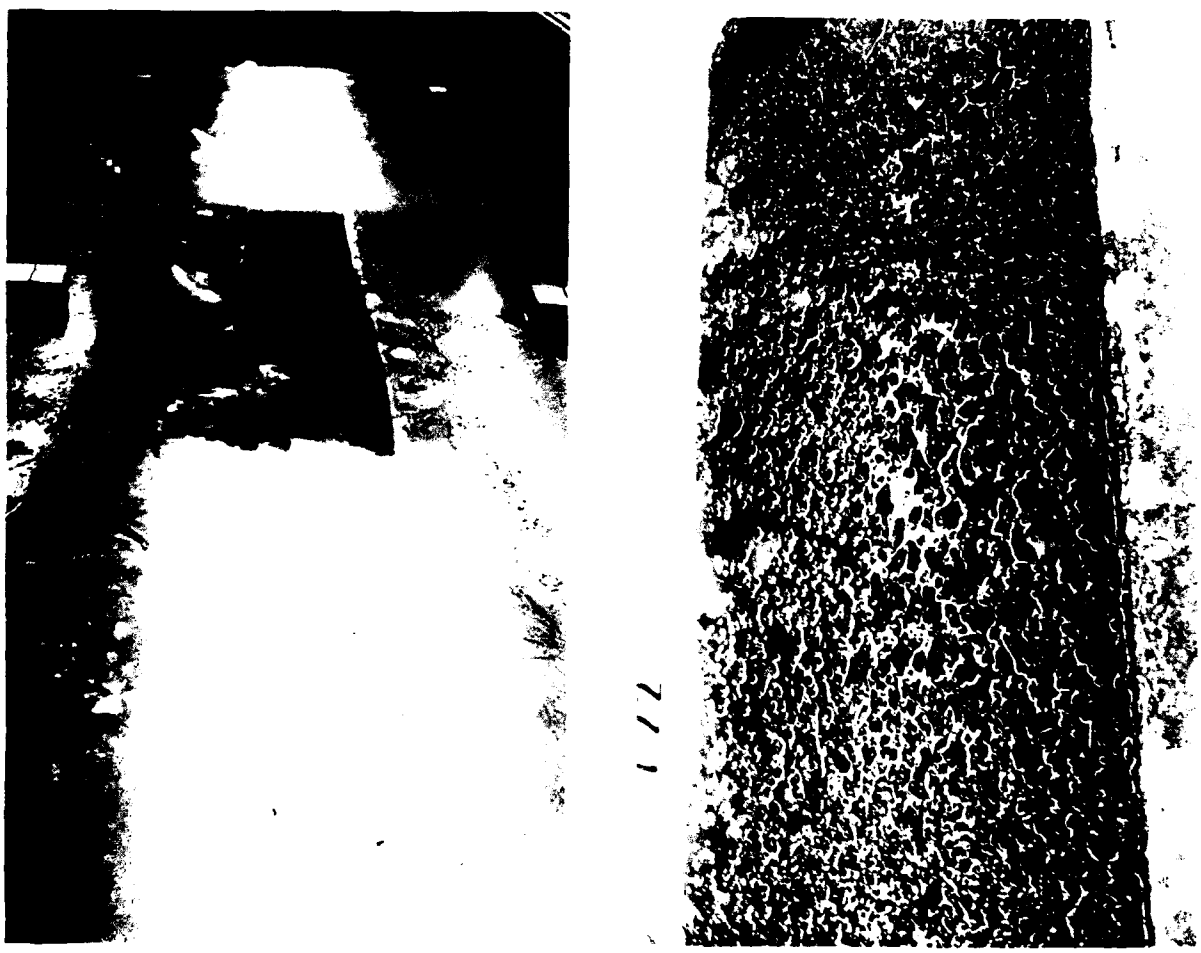

a. n = *18.* *b.* n = 22.

Figure 55. Ice formation in the ice tank transited by the 1:15-scale tow hull; f_t = *1/(2 hours),* y_o/D = *1.16.*

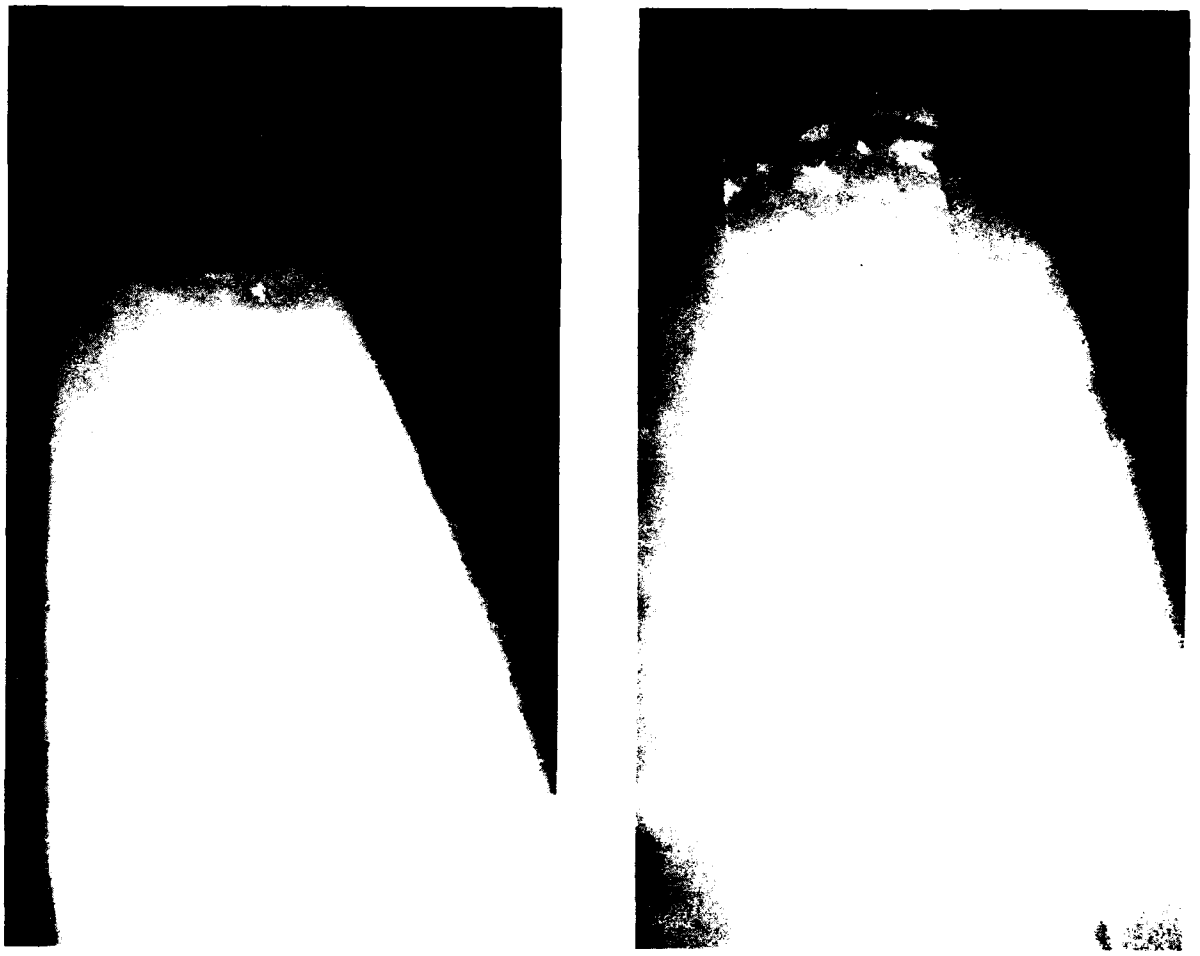

a. n = *1.* *b.* n = *3.*

Figure 56. Ice formation in the ice tank transited by the 1:15-scale tow hull; f_t *= 1/(4 hours);* $y_o/D = 1.16$.

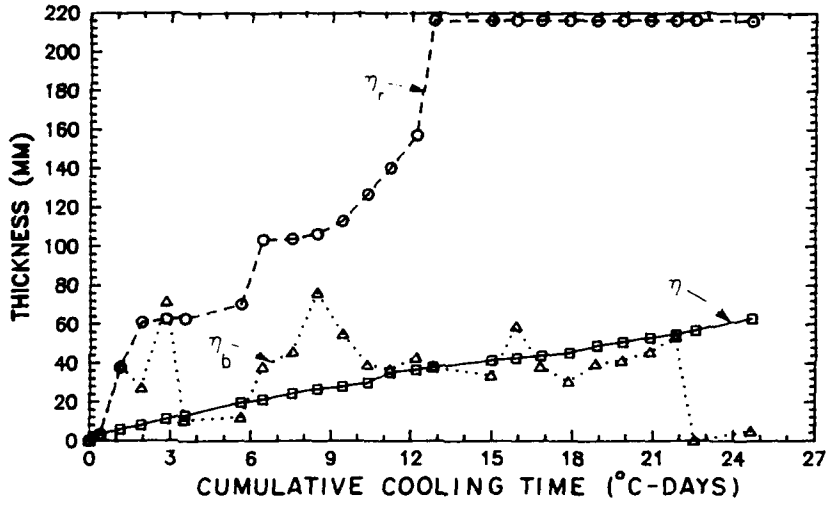

a. $f_t = 1/(2\ hours)$.

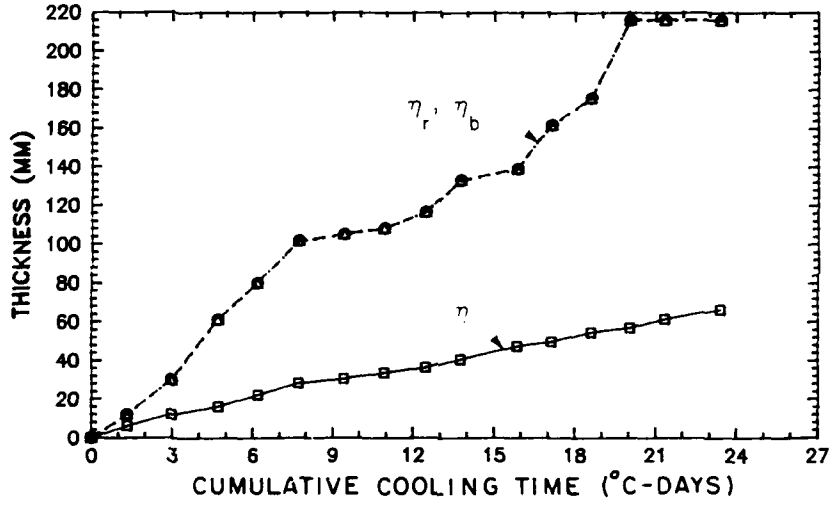

b. $f_t = 1/(4\ hours)$.

Figure 57. Ice thickness vs cumulative cooling time; $y_o/D = 1.16$.

ment of ice to the track was increasing the resistance encountered by the tow hull. Although the resistance was not measured, the levels of resistance were obvious from the vibrations of the towing arms and the noise generated during breaking and shoving of ice. The resistance increased noticeably when the ridges extended about three-quarters of channel depth and when the ice sheet thickness was of similar magnitude to the clearance beneath the tow. From then on, ice was increasingly confined and shoved ahead of the tow or forced sideways to the ridges, which thickened rapidly until they reached the channel bottom or were overridden by the tow. During such transits the tow exerted considerable force against the bordering ice sheet, occasionally breaking large cusps (underpinned by ridge), as shown in Figure 55a. Further, when the tow and the ice beneath it occasionally ground against the channel bottom, it would bend the aluminum false floor that was used to simulate part of the channel bed. At full scale this grounding would gouge the channel bed and possibly damage the tow. The level of resistance was such that, after about a dozen transits (at

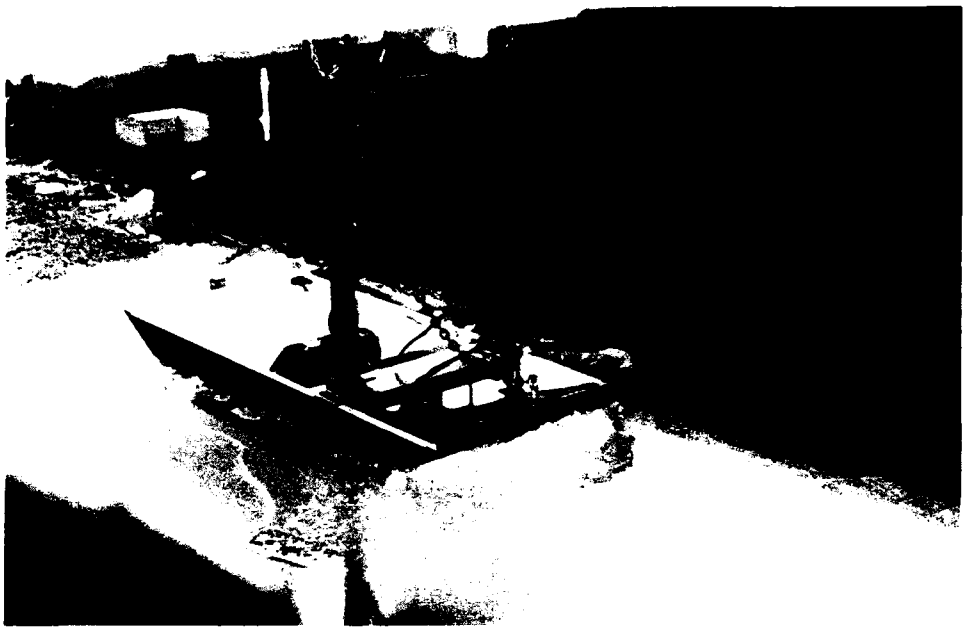

Figure 58. 1:15-scale tow hull shoving confined broken ice while transiting the shallow channel; $y_o/D = 1.16$.

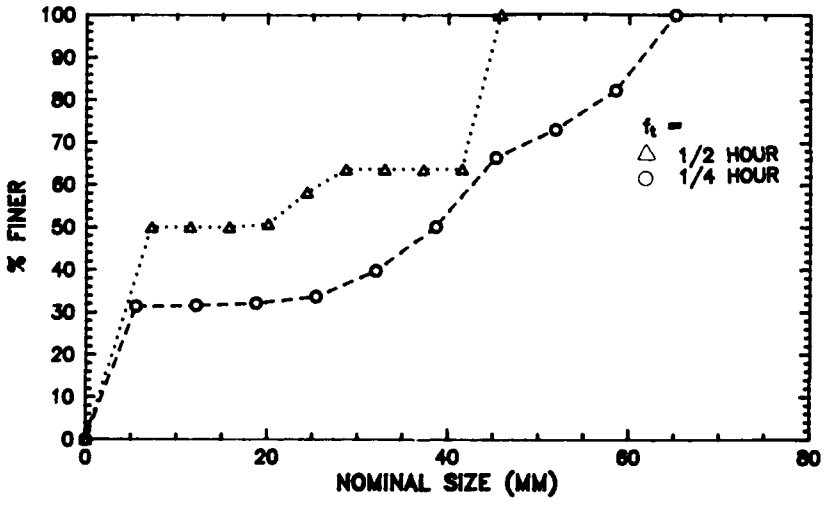

Figure 59. Size distribution of brash ice; $y_o/D = 1.16$.

either frequency), a full-scale tow would find the channel unnavigable.

Brash ice remaining in the shallow tracks was considerably finer in size than the brash ice in tracks through the deep channel, as can be seen by comparing values of d_e in Figures 59 and 41 and Table 2. The average sizes of brash ice in the shallow channel were about 20–30% of those in the deep channel. Confined clearance between the tow underside and the channel bottom screened large ice from passing beneath the hull. Additionally, ice in the shallow channel underwent much more abrasion and breaking than did ice in the deep channel.

Analysis of results

The major value of the ice-tank experiments is that they enabled detailed observation and description of ice-formation processes in a frequently transited, ice-covered channel. Before now, many of these processes were either unknown or inadequately understood and documented. Quantitative evaluation of the data, notably in the accurate evaluation of volumes and rates of ice growth, was complicated by substantial variations in the way that brash and broken ice accumulated in tracks cut through the channel, especially those created during transits by the 1:30- and the 1:15-scale tow hulls. Consequently the numerical model could only be calibrated with, and tested against, the results obtained from experiments conducted with the wedge hull. Those experiments, however, were also fraught with variations in the pattern of ice formation, though not to the same extent as for the tow hull. The results of the ice-tank experiments suggest that precise simulation of ice formation in frequently transited channels is complicated by the occasionally irregular, or stochastic, manners by which brash ice forms and is redistributed in vessel tracks. For example, large fragments of sheet ice bordering a track may drift into it and temporarily alter the local pattern of ice regrowth and brash-ice accumulation.

The experiments confirm the conclusion tentatively drawn earlier that hull characteristics, especially bow form and hull length, significantly influence ice formation in navigation channels, and that they do so by affecting the patterns of brash-ice accumulation. The disparate patterns of ice formation produced by ships and ice-entrapping tows, two very different hull forms, are summarized in Figures 14 and 25, respectively. The essential feature of transiting that causes the dissimilar patterns is the propensity of tows to entrap and move brash ice along the tracks that they open. As a consequence, ice plugs form as thick local accumulations of brash ice. The two patterns would be more similar if the tow hull form were modified by ice accumulation so as to become rounded and entrap less, or no additional, ice.

In the ensuing discussion the influences of transit frequency f_t on ice formation are evaluated first. The influences of water depth on ice formation are then appraised. Finally, an attempt is made to

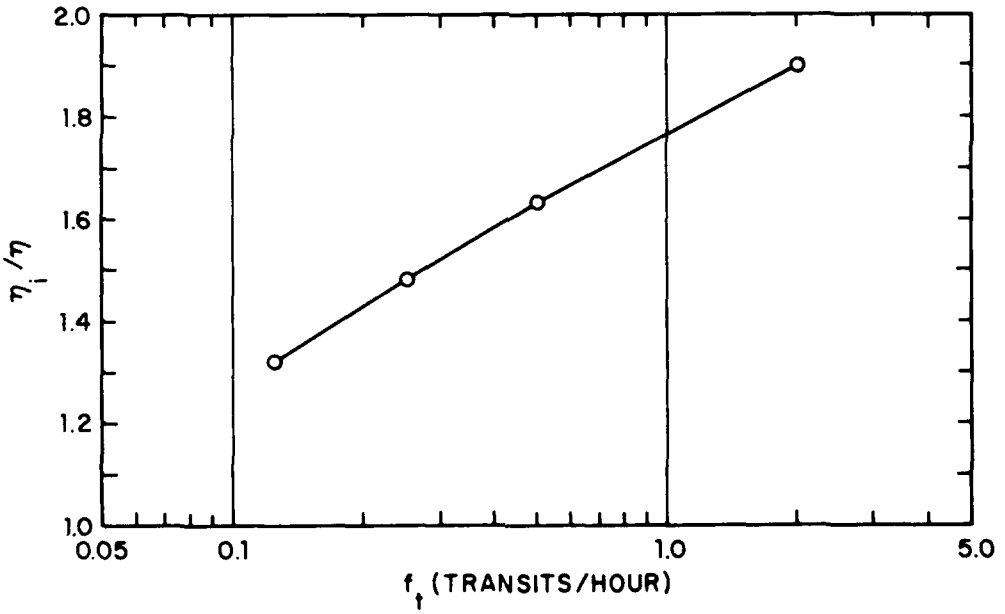

Figure 60. Variation of η_i/η with f_t for the wedge hull.

relate the areal concentration of open water β to the number of transits and the transit frequency. Also assessed is the variation of ice-displacement proportion as a brash-ice layer forms.

Influence of transit frequency

For the range of frequencies examined, increasing transit frequency f_t led to increased volume of brash-ice growth in the ice tank. The equivalent thickness of solid ice grown in tracks transited by the wedge hull, normalized with ice sheet thickness, η_i/η, is shown in Figure 60 vs f_t; η_i is the volume of brash ice per unit surface area of track, with the track width taken as being equivalent to the hull beam. Each value of η_i/η is estimated using an average cross-sectional profile and an average value of porosity of accumulated brash ice. The maximum value of η_r/η attained in the ice tank is about 2. For the wedge hull the thickness of brash-ice layers and ridges, expressed as η_b/η and η_r/η, increased mildly with increasing f_t, as shown in Figure 61a. The propensity of the tow hull to clear ice from its track resulted in somewhat different trends, as shown in Figure 61b. The ratio η_b/η did

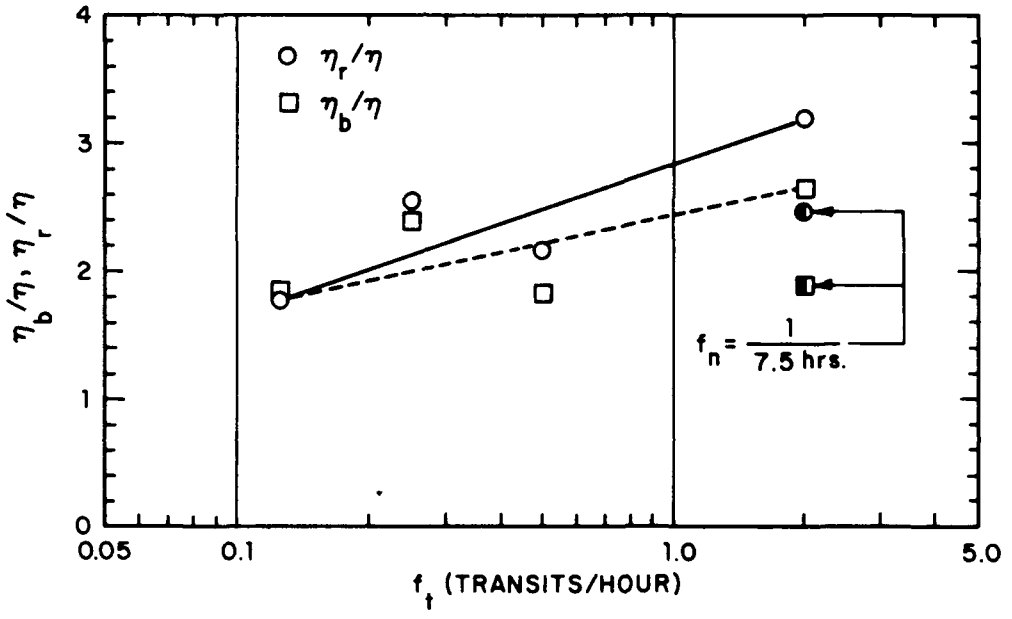

a. 1:15-scale wedge hull.

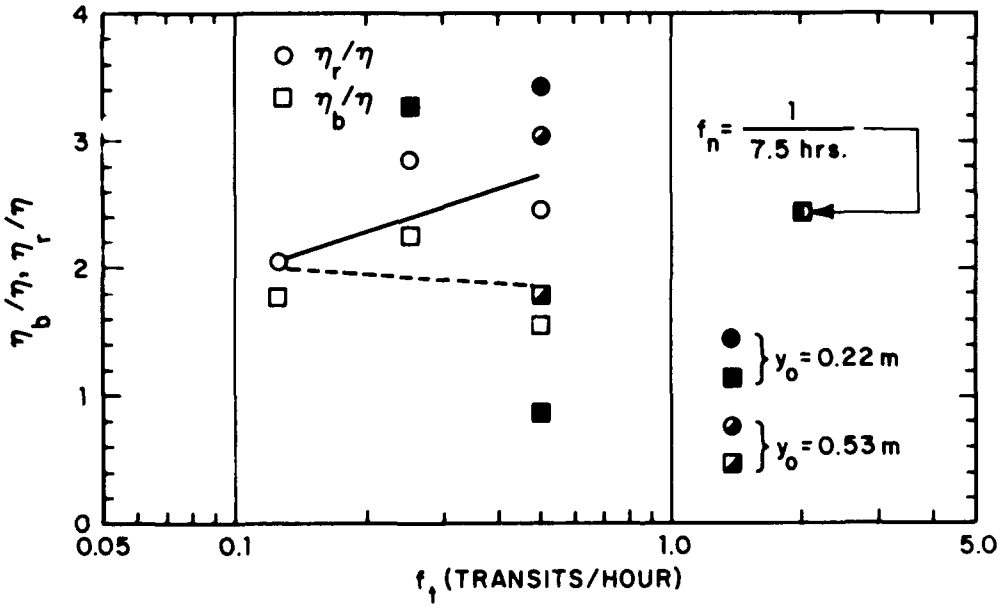

b. 1:15-scale tow hull.

Figure 61. Variation of η_b/η and η_r/η with f_t.

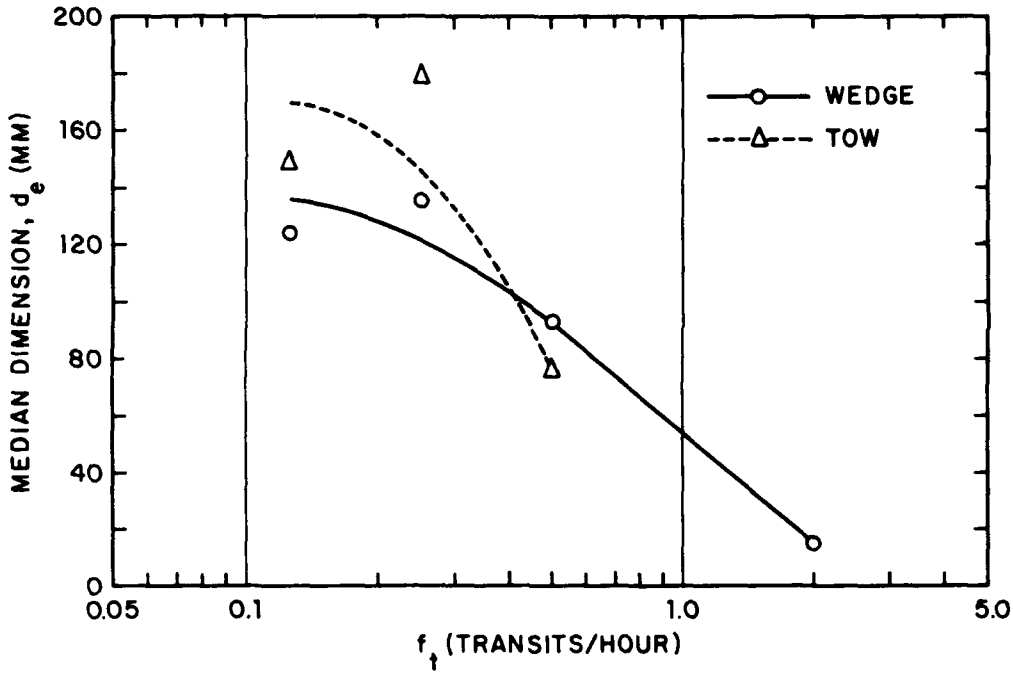

Figure 62. Variation of median dimension of brash ice with f_t.

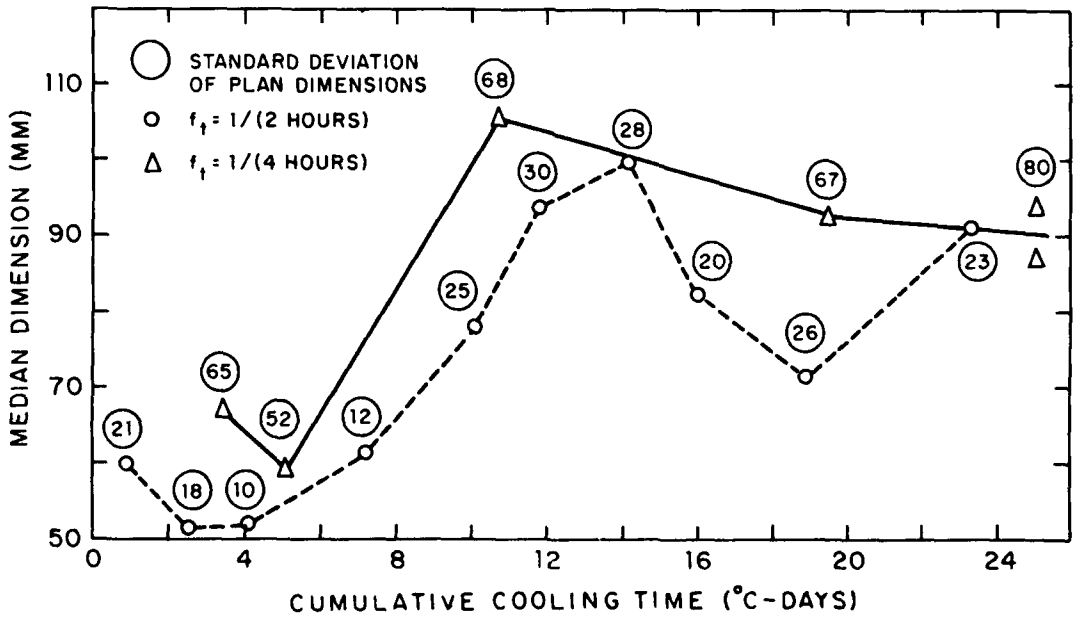

Figure 63. Variation of median plan dimensions of brash ice with cumulative cooling time.

not vary significantly with f_t for the tow hull. If anything, η_b/η decreased slightly with increasing f_t. However, for the tow hull, η_b/η did increase with increasing f_t. For both hulls the error margin in measuring η_b/η and η_r/η is on the order of the mean size of brash-ice pieces comprising layers or ridges. For both hulls the ridges thickened more rapidly with increasing f_t than did the layers because more ice was displaced from the channel.

Transit frequency influenced the mean size of the brash ice formed during transits by either the wedge and the tow hulls. For f_t greater than about 1/(4 hours), Figure 62 and Table 2 show that d_e decreased almost linearly with increasing f, at least for the range of f_t used in the experiments. The few data corresponding to f_t less than about 1/(4 hours) suggest that d_e is likely to be independent of f_t. The mean plan dimensions of brash and broken ice were measured and recorded versus ΣS_d during two experiments with the tow hull, those for which f_t = 1/(2 hours) and 1/(4 hours). The data, presented in Figure 63, show that the mean plan size of brash ice decreased initially but thereafter attained more-or-less constant values with increasing ΣS_d. This result is similar to that reported by Sandkvist (1980) for the variation of brash-ice thickness with number of transits (Fig. 11).

Influence of channel depth

Figures 25 and 57 show that, for transits of shallow channels, ridges and plugs develop more rapidly for smaller values of y_o/D. Also, as is evident in Table 2 and Figure 64, finer brash ice accumulated in the shallower channels. The relationship between d_e and y_o/D is almost linear for the data shown. Only smaller ice pieces could pass through the diminished clearance between the hull and the channel bottom. Larger ice pieces were either displaced to ridges along the track or were shoved to plugs in the track. Additionally, transit of shallower channels resulted in considerably more abrasion and grinding of ice pieces than for the deeper channels, thereby contributing to the greater amount of fine ice in the track.

Variations of β *and* ε

To use the numerical model outlined earlier, mathematical expressions must be developed for the variations of β and ε throughout a navigation period. This task, however, is made complicated by the diverse variables that may influence β and ε, e.g. hull dimensions and shape, hull speed, ice-sheet thickness, and thickness of brash ice accumulated in a vessel track and ridges flanking it, as well as the element of randomness that pervades ice formation in frequently transited channels. Nonetheless, an attempt is ventured here to establish sets of curves for the variations of the ice-tank data from the experiments with the wedge hull. Note that terms β and ε are not necessarily in direct relationship to one another, because ice cleared from the surface of the track may not only be

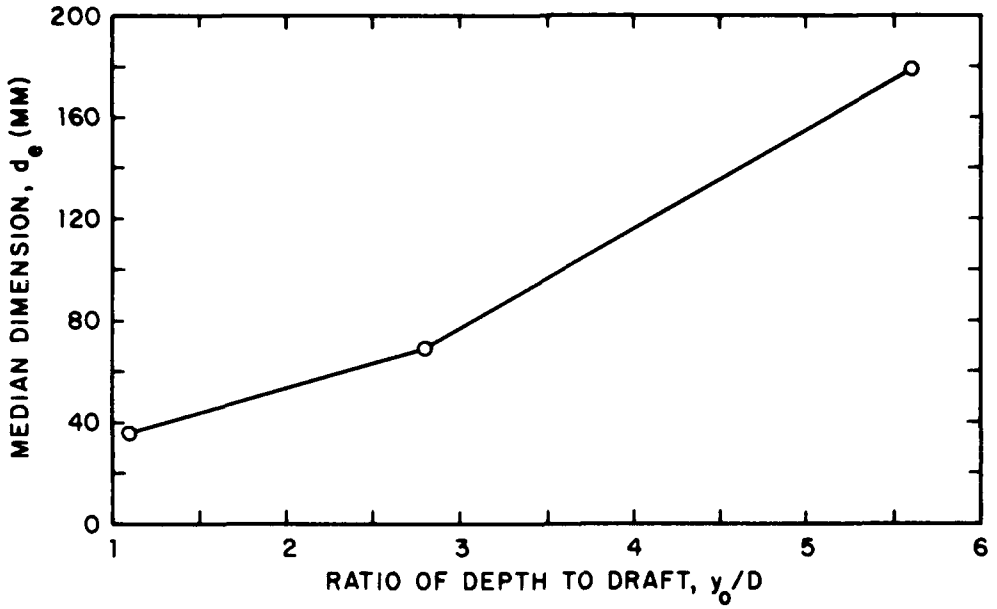

Figure 64. Variation of d_e *with* y_o/D *at* f_t = 1/(4 hours).

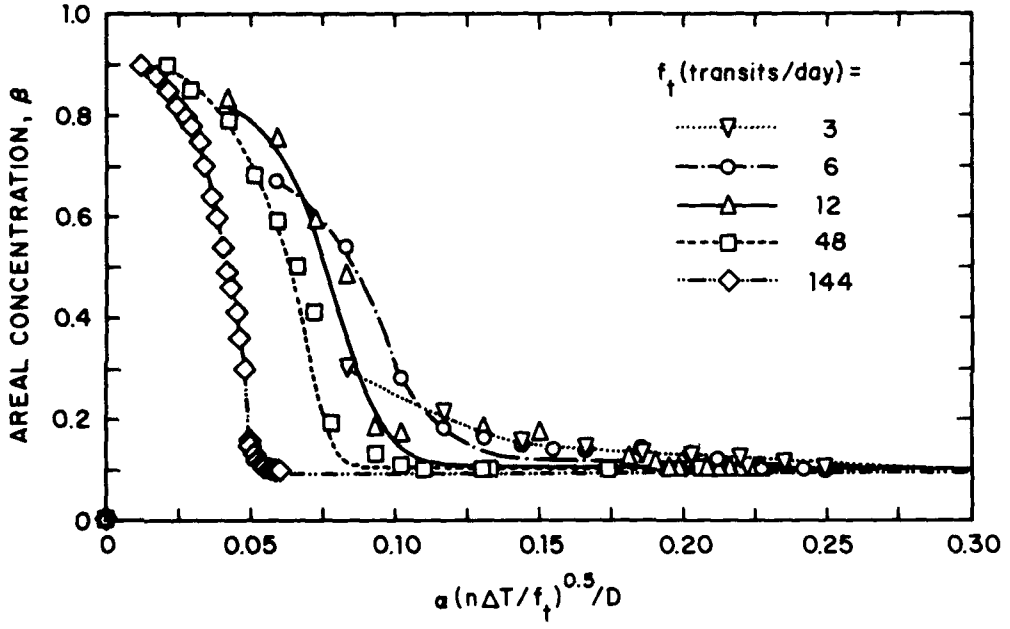

Figure 65. Variation of β *with* α ($n\Delta T/f_t)^{0.5}$ /D *and* f_t.

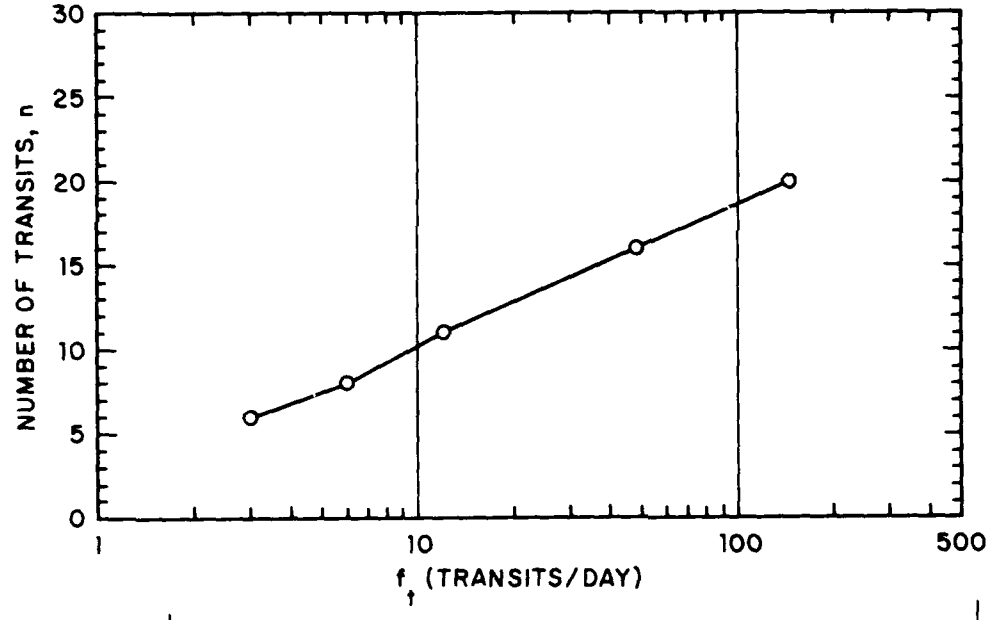

Figure 66. Variation of n *required for a virtually full cover with* f_t.

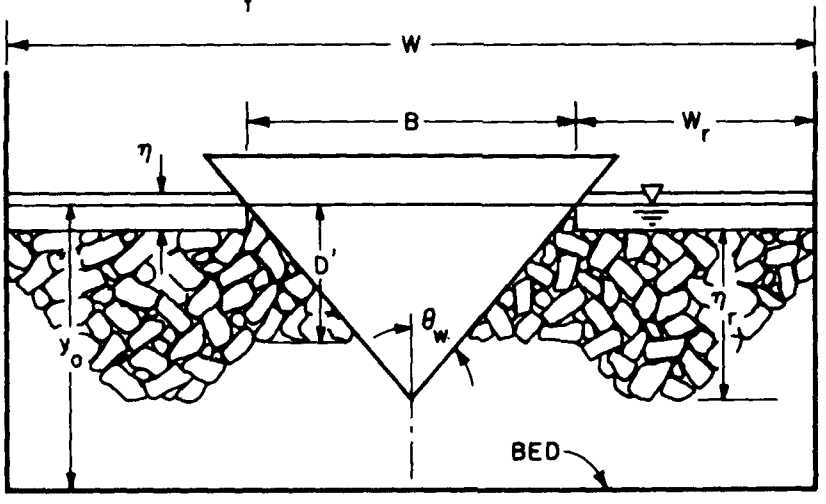

Figure 67. Displacement of brash ice around a transiting hull.

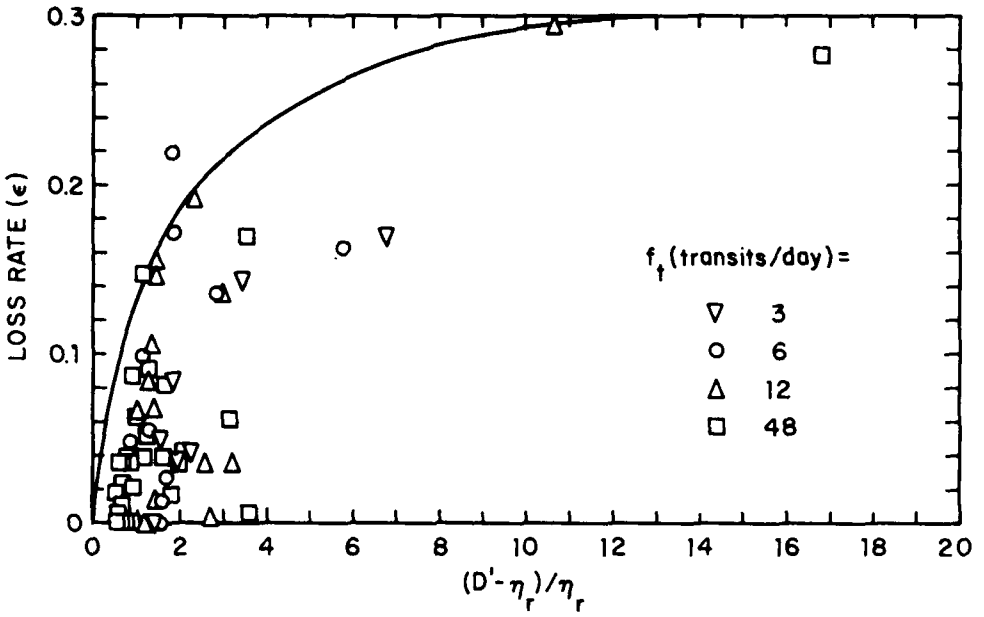

Figure 68. Variation of ε with $(D'-\eta_r)/\eta_r$.

displaced to the ridges, but it may collect as multilayer clusters within the track (Fig. 14).

Figures 35, 40, 44 and 48 show that β varied fairly consistently with the number and frequency of transits by the wedge hull. Generally, lesser values of f_t resulted in initially lower values of β and required fewer transits before the track became fully covered by a layer of brash ice. This trend becomes more apparent when values of β are related to the nondimensional parameter $\alpha(n\Delta T/f_t)^{0.5}/D$, as shown in Figure 65. This parameter is significant because it reflects the effect of relative magnitudes of ice-cover thickness as well as hull draft and shape on β_o, the initial value of β after the first transit of a vessel. Transits of thicker ice covers left more ice in the track. A family of curves can be defined in accordance with values of β_o and the decline of β with increasing n. It was found, as shown in Figure 66, that the number of transits required for a virtually full cover to develop over the track was linearly proportional to log (f). Actually, throughout the experiments, coverage was never full. There always seemed to be about 10% of the track that was open water.

Variation of the ice-displacement parameter ε during each experiment with the wedge hull was estimated as $2\Delta V_r[(1-p/(\eta_i B)]$ and related to the parameter $(D'-\eta_r)/\eta_r$, in which $D' = [\eta_i B/(\{1-p\}\tan\theta_w)]^{0.5}$, with $\theta_w = 53°$ (Fig. 67). As indicated in Figure 68, the latter expression is intended to take into account the relative elevations of the brash-ice layer when it is passed around the hull and the ridge thicknesses. Similar expressions can be devised, provided they reflect the influences on ε of the relative thicknesses of the ridge and the layer, as well as the layer thickness relative to the hull form and draft. Generally, ε increased as η_r/η_b decreased and as the layers thickened. Ridges acted to partially contain such ice in the tracks. The considerable scatter in the plot of ε versus $(D'-\eta_r)/\eta_r$ can be related to the irregular, and noncontinuous, manner by which layers and ridges actually thickened. As can be seen from Figure 34, for example, η_b and η_r did not increase smoothly with either time or number of transits. No influence of f_t or n was evident in the data.

On the whole, values of ε are quite small, being typically on the order of 0.1 or less. The curve fitted as an envelope to the data is used for selecting values of ε used in exercising the numerical model.

NUMERICAL PREDICTIONS

The numerical model is exercised here to extend the insights obtained from the ice-tank experiments and to obtain a broader understanding of ice formation in frequently transited channels. The model is used first to determine volumes and distributions of brash ice produced in a deep, wide channel transited at a single, sample frequency of

f_t = 6 transits/day under a range of air temperatures. The resulting predictions illustrate the information that the model yields. The effects of transit frequency and scheduling on the volume of ice grown and the distribution of brash ice are considered subsequently. Investigated finally are the influences of channel geometry, notably channel width and depth, on ice formation. This section finishes with some reflections on the validity of the numerical predictions.

Ice formation is simulated for a representative channel that is transited in frigid air for a navigation period of 30 days, which is long enough so that the calculations would illustrate the salient features of ice formation. It is assumed, somewhat conservatively, that no snow falls during this period. The channel is initially taken to be deep and wide so as to exclude the influences of channel geometry on ice formation. All predictions are based on an ice-growth coefficient of α = 24 mm/(°C-day). This value is suggested from estimates made for ice growth on the Mississippi River (Ashton 1974) and on the St. Marys River (Vance 1980). Furthermore it is comparable to the value of 28 mm/(°C-day) recommended by Michel (1971) for ice growth over snow-free lakes. A wide river, such as the Mississippi River, without a snow cover can be likened to a small lake.

As stated earlier the model simulates transits by vessels that do not shove or move significant amounts of ice along channels. Therefore, it simulates transits by tows, or other bluff-bowed flat-bottomed vessels, only if they do not move ice along the tracks. This assumption may be reasonable for tows that either have attained equilibrium under-hull accumulations of ice or are moving fairly rapidly so as not to entrap much ice. The ice-tank experiments revealed that numerical simulation of ice formation is useless if tows accumulate and transport ice while transiting a track.

Values for the parameters β and ε are obtained from curves fitted to the experimental data contained in Figures 65 and 67, respectively. When using Figure 65 to estimate β values, experiment-scale values of transit frequency f_t are related to full-scale values through the geometric scale λ_l = 15, in line with the reasons explained earlier. In accordance with this relationship, $f_t \approx 1/(0.5 \text{ hour})$, or 48/day, at the ice tank is taken here to be equivalent to (48/15)/day ≅ 3/day at full scale. All predictions are calculated with p = 0.5, which is obtained from experimental data. As channel size (relative to vessel size) primarily affects the space available for brash ice to be displaced from tracks opened by vessels or to accumulate as ridges flanking tracks, an attempt is made to account for these influences on ice formation by modifying the relationships for ridge geometry. In the ice tank, approximately one minute was required for water and brash ice to calm sufficiently after a transit such that ice could begin to regrow. If a factor of 15 is used for the time scale, one minute translates to 0.25 hour at full scale. This value, which is used here for t_p, agrees well with observed times for ice regrowth to commence after vessel transit.* A value of θ_r = 30° obtained from experimental data is used for estimating ridge proportions.

Influences of air temperature on ice formation

The influences of air temperature on ice formation in frequently transited channels are examined here by estimating ice formation under three temperatures of frigid air: T_a = –5, –10 and –20°C. As noted above, all predictions are based on an assumed value of $\alpha \approx 24$ mm/(°C-day). The temperature at which water freezes is taken as 0°C. Transits at a sample frequency of f_s = 6/day are considered, with the initial ice growth period $P_i = P_t$ (Fig. 16), and navigation period P_n = 30 days.

The volumes of ice grown, the layer thicknesses and the ridge thicknesses predicted for simulated transits of the representative channel are presented in Figure 69 vs time, with T_a as the third parameter. The ice-cover thickness η is shown only for T_a = –10°C. The corresponding ice-cover thicknesses for T_a = –5 and –20°C can be determined by using eq 9 with appropriate factors. For these figures the ice volumes are calculated as ice volume per unit area of track opened by transiting vessels η_i; the unit area of track is taken as the unit length of track times the track width, which here is taken to be equal to the vessel beam B. Figure 69 reveals that, after 30 days of transiting at f_t = 6/day with T_a = –10°C, the ice cover thickness η is about 415 mm, $\eta_i \cong 900$ mm, $\eta_r \cong 1000$ mm and $\eta_r \cong 1100$ mm. It is also evident that, if normalized with η, values η_i, η_b and η_r are not fully independent of T_a. The model predicts that values of η_i, η_b and η_r are of nearly comparable magnitude during the first four days of transiting when T_a = –5 and –10°C. This somewhat surprising prediction is a consequence of the relationship adopted for β, the proportion of the track covered by open water during transiting. From Figure 65, it follows that fewer transits are required to establish a full layer of brash ice over a track transited in colder air, because thicker and

*Personal communication with J. Sandkvist.

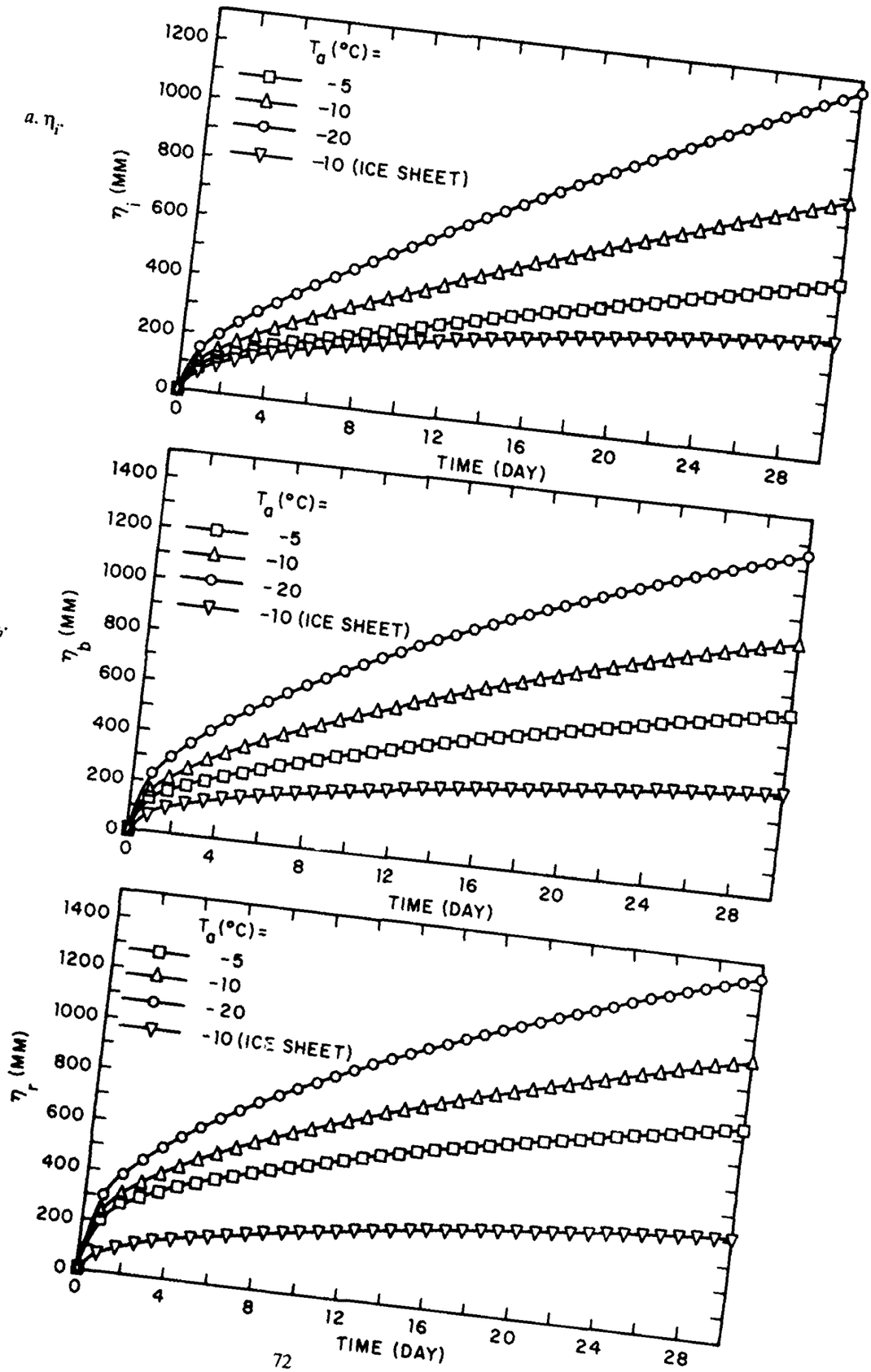

Figure 69. Variation of ice formation variables with time and T_a.

larger ice fragments result during transiting. As larger ice fragments are less readily displaced beneath the bordering ice sheet, a rapid decrease in β, or smaller values of β, result and less ice is produced. The example presented in Figure 69 reflects the sensitivity of the predictions to values of β.

Transit frequency effects

Consider now the predicted effects of transit frequency f_t on ice formation under a single value of T_a. Figure 70, which generalizes the trends presented in Figure 69, shows the effects of f_t on volume of ice grown, normalized as η_i/η, and on the thicknesses of brash ice accumulated as layers and ridges in the representative channel, normalized as η_b/η and η_r/η, respectively. Values of η_i/η, η_b/η and η_r/η are determined for a navigation period P_n = 30 days under steady conditions of constant T_a = –10°C, with α = 24 mm/(°C-day). The transit frequency f_t ranges from 8/day through 1/(15 days) to zero.

Though the volume of ice produced during frequent transits of a navigation channel increases with increasing duration of navigation period and with increasing f_t, values of η_i/η, η_b/η and η_r/η follow slightly more complex trends. For each value of f_t, η_i/η generally increases with increasing time or number of transits (Fig. 70a). Values of η_i/η increase very rapidly during initial transits at large values of f_t because of the initially large values of β for larger values of f_t (as indicated in Fig. 65). Once β values have decreased to constant values and the track is virtually covered by a layer of brash ice, values of η_i/η increase mildly with increasing time or n. Larger values of f_t lead to larger values of η_i/η at any instant, but they also cause greater rates of increase of η_b/η. The variation of η_b/η with duration of navigation period (Fig. 70b) is similar to that between η_i/η and time or number of transits. Values of η_b/η initially increase rapidly with time as a full layer develops across the track, and the rate of increase is larger for larger values of f_t. Once a virtually full layer has developed across a track, η_b/η increases only mildly with increasing time or n. Values of η_r/η (Fig. 70c) begin at their maximum values and then gradually diminish. The trends for η_i/η and η_b/η are very similar to those from the experiments conducted with the ice tank (the pertinent trends are presented as Appendix C).

The relationship between the volumes of ice produced, normalized as η_i/η, and the transit frequency f_t after 30 days of transiting under air temperatures of –5, –10 and –20°C reveal that η_i/η increases with increasing f_t until attaining a maximum value, as shown in Figure 71. That a maximum value for η_i/η should occur with variation of f_t is evident from eq 19; although η_i/η increases with f_i initially, when $1/f_t$ decreases to t_p, the actual time of ice regrowth is decreased such that, eventually, there is insufficient time for ice to regrow. Here, as t_p is taken to be 0.25 hours, no regrowth occurs when f_t = 96 transits/day. This frequency is an order of magnitude above the frequencies at which channels are likely to be transited. Therefore, for practical purposes, it can be stated that increased frequency of transiting generally leads to increased volume of ice regrowth. Figure 71 indicates that η_i/η attains a maximum value of about 3, which occurs when f_t = 30–50 transits/day. At values of f_t exceeding $1/t$, transiting vessels are essentially in convoy (if f_t relates to transits of different vessels, rather than a single vessel, such as a harbor tugboat, repeatedly transiting a track). Transits in close convoy prevent or greatly limit regrowth of ice over a track, with the possible result that channel water may supercool and spawn frazil ice. The likely effect is channels through shallow rivers. The present model does not handle frazil-ice growth.

Values of η_i/η do not form a single curve for the three values of T_a used in the calculations. By and large, lower values of T_a show negligibly larger values of η_i/η. This result is attributable to the larger initial values of β that result when using Figure 65 and smaller values of T_a.

Effects of scheduled transits

Vessels may transit navigation channels in complex sequences involving several transit frequencies, not just a single frequency such as once or a dozen times daily. A general schedule is outlined in Figure 16. It may, for example, consist of daily transits that are limited to daylight hours, during which transits occur at some constant frequency. Transits also may occur randomly. A practical motivation for examining scheduled transiting is to determine whether there are any significant advantages in scheduling transits so as to minimize ice growth due to transiting.

The numerical model was exercised to ascertain the effects on ice formation of scheduled transits involving the two frequencies f_s and f_1 as defined earlier. For a total period P_T = 30 days, the transit-series frequency $f_s = n$/day was varied, with n = 2, 4 and 6 transits. Transits are taken to occur in a navigation period $P_n = (n-1)\,P_t$, with the transit

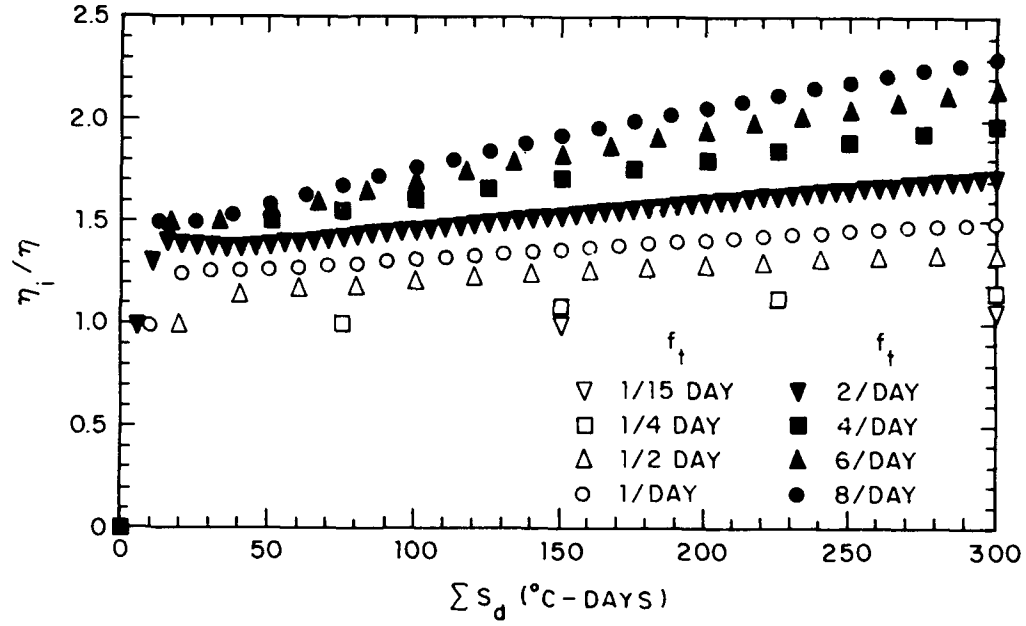

a. η_i/η.

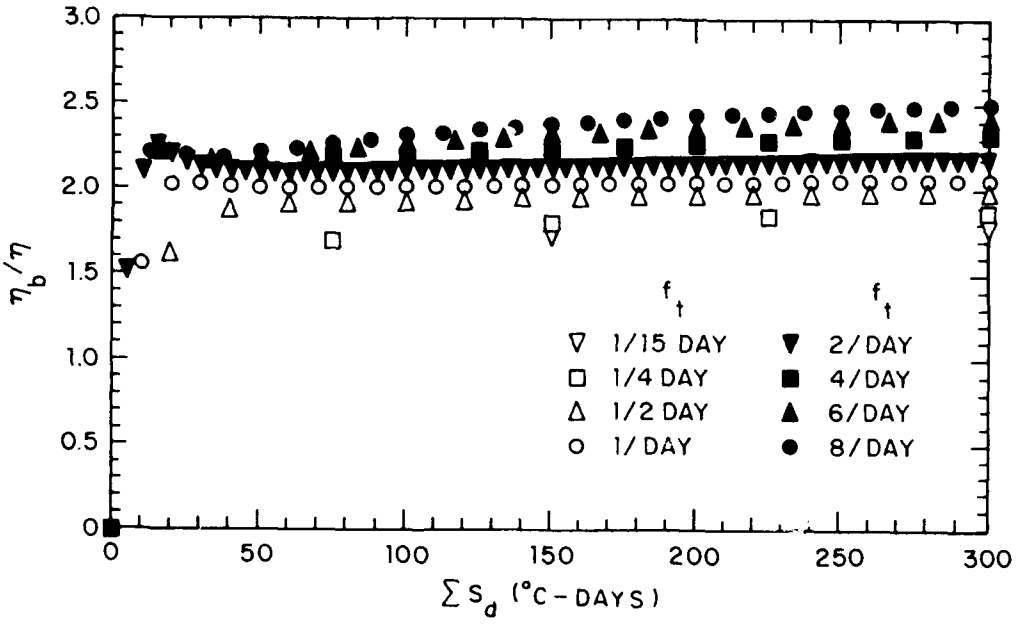

b. η_b/η.

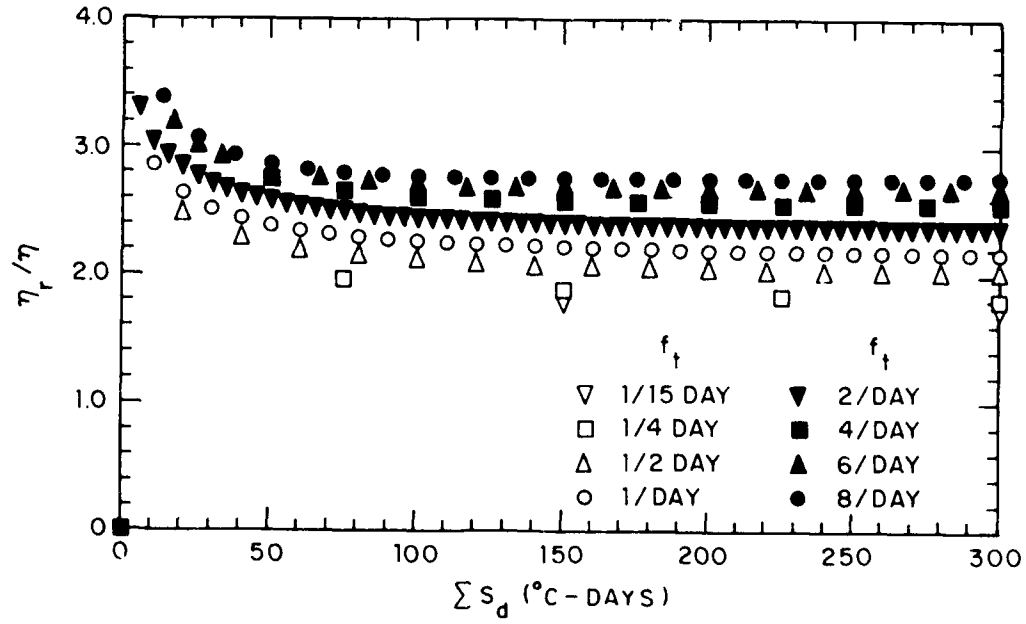

c. η_r/η.

Figure 70. Variation of normalized ice formation variables with ΣS_d *for varying* f_t.

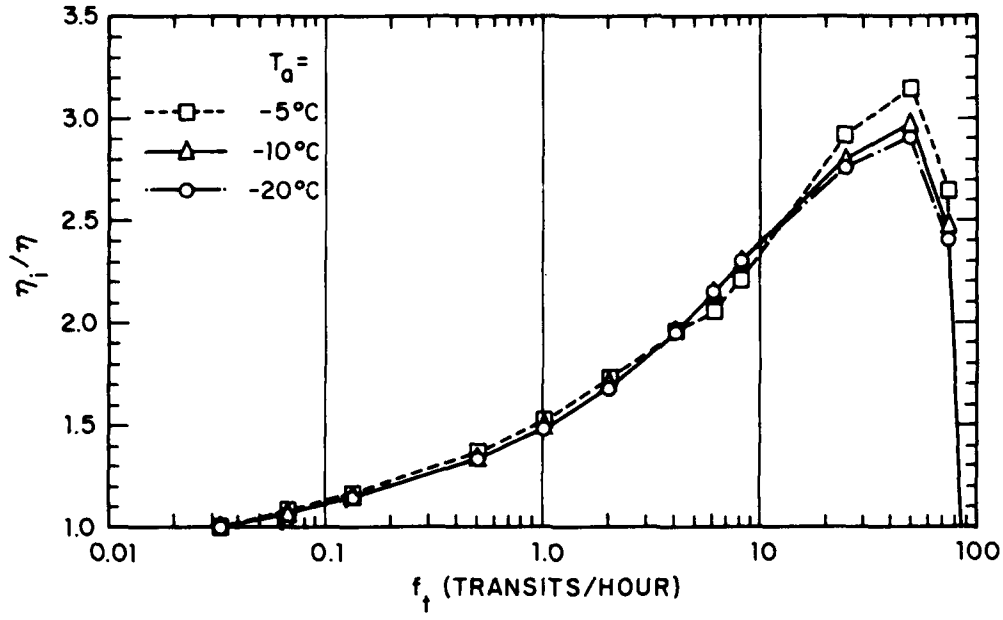

Figure 71. Variation of η_i/η with f_t.

period P_t = 0.5–12 hours; the period between navigation periods P_o = 1(day) - P_t. Additionally, T_a = –10°C and α = 24 mm/(°C-day).

The results are presented in Figure 72 for f_s = 2, 4 and 6/day. Evidently η_i/η, η_b/η and η_r/η are mildly affected by f_t, though its influence increases with increasing n and f_s. Smaller amounts of ice are produced for larger values of f_t, even though n is constant. At larger values of f_t, P_t approaches t_p such that the net period of ice regrowth decreases. A limiting condition is convoying of vessels when $P_t \leq t$. Figure 72b, for example, shows that a daily sequence of four transits, 0.5-hour apart results in about 18% less ice growth than does a daily sequence of four transits 6-hours apart. The commensurate reduction in layer thickness predicted for the two schedules is about 11%. For an ice cover thickness of about 416 mm, the additional thickness of ice growth over the track during 30 days is less than about 75 mm. The practical implication of the information presented in Figure 72 is that there is no significant advantage in scheduling transits of ice-covered channels, at least for a daily schedule involving six or fewer transits, for the purpose of minimizing the volume of additional (or brash) ice growth.

Effects of channel geometry

Many channels, especially river channels, have reaches that are narrow and shallow compared to vessel size. Approaches to locks, for instance, can be confined, and the minimum navigation depth at many sections of navigable U.S. rivers barely exceeds 10% of the maximum tow-barge draft; the minimum navigation depth in waterways maintained by the Corps of Engineers is 3.05 m (10 ft), whereas the maximum draft of tow-barges is 2.75 m (9 ft). Thus far, however, the numerical model has been exercised only for a representative channel that was wide and deep enough that channel boundaries did not have to be taken into account. An attempt is now made to assess the effects of channel width and depth on the volume of ice produced by frequent transiting. Also, so as to put the effects of frequent transiting in perspective, the volumes of ice produced at navigation channels are related to the overall volume of ice produced at channel cross sections.

Channel width

The approach taken here to evaluate the effects of channel width on ice formation is to relate the ridge geometry to the available space adjacent to a track. As indicated in Figure 67, the ridge width W_r is constrained by the width of channel such that the following relationships are needed to determine W_r and the ridge thickness:

$$W_r = 2\,\eta_r \tan\theta_r, \text{ if } W_r < 0.5\,(W\text{–}B) \qquad (32)$$

or

$$W_r = 0.5\,(W\text{–}B), \text{ if } 2\,\eta_r \tan\theta_r > 0.5\,(W\text{–}B). \qquad (33)$$

It is assumed that the curves for β and ε (Fig. 66, 68) remain valid for estimating β and ε.

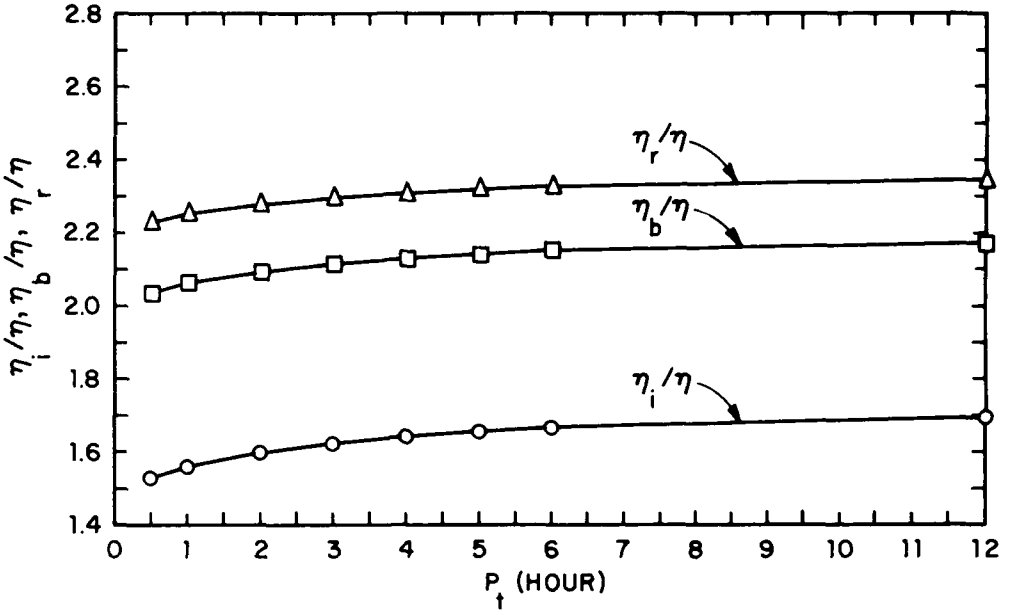

a. $f_s = 2/day$

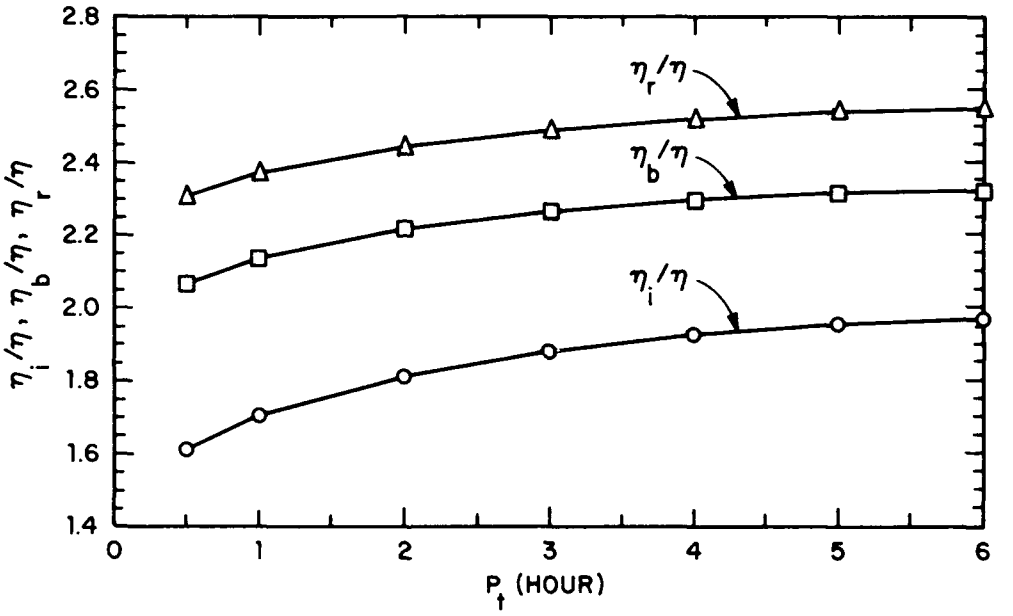

b. $f_s = 4/day.$

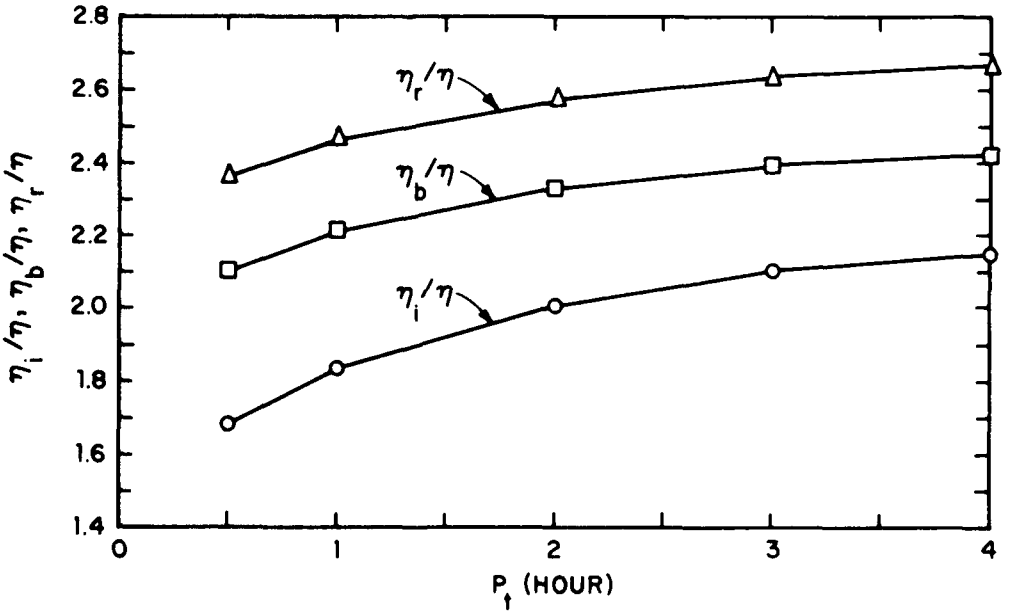

c. $f_s = 6/day.$

Figure 72. Variation of $\eta_i/\eta, \eta_b/\eta$ *and* η_r/η *with* P_t.

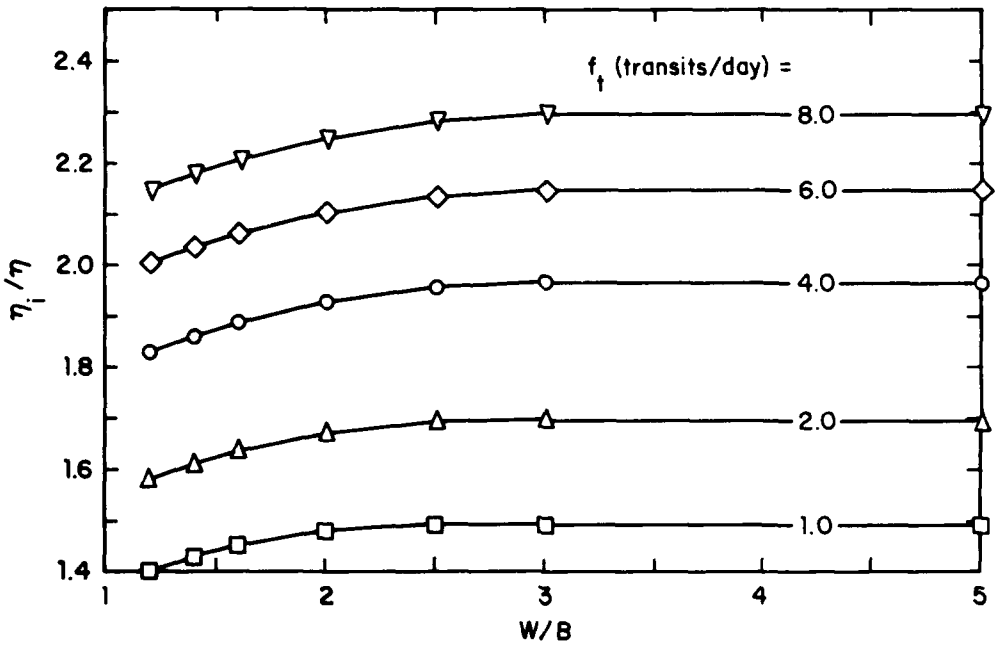

Figure 73. Variation of η_i/η with W/B and f_t.

As channel boundaries restrict the lateral displacement and accumulation of brash ice, the channel width influences volumes of ice that can be grown in frequently transited channels as shown in Figure 73, where predicted values of η_i/η are related to *W/B*. For confined channels, whose widths marginally exceed vessel beams, brash ice cannot be displaced sideways and remains in the track. Consequently, as indicated in Figure 73, less ice grows in them than in wider channels.

Frequent transits of an ice-covered channel increase the volume of ice growth, and it is useful to compare the increased ice volume with the overall volume of ice grown in a channel. Figure 74 shows that the volume of additional ice grown relative to the overall ice volume diminishes with

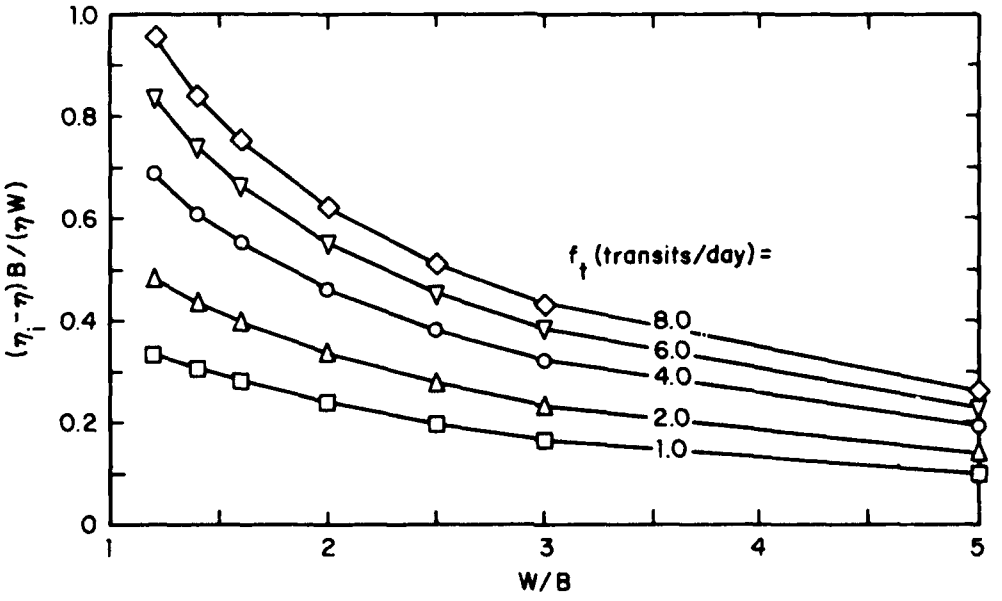

Figure 74. Variation of (η_i/η) B/ (ηW) with W/B and f_t.

increasing channel width, or $(\eta_i-\eta)B/(\eta W)$ decreases as W/B increases, as is to be expected from simple algebra. Frequent transits of a channel twice the vessel beam results in about a 50% increase in ice grown, for the given calculation scenario. The increase reduces to about 20% for a channel five times the vessel beam.

Channel depth

The principal effect of channel depth on ice formation is essentially to restrict the displacement of brash ice, thereby constraining its accumulation along a channel. A depth parameter is best included in the predictive model by modifying the relationships for β and ε, the parameters describing ice movement. Unfortunately the ice-tank experiments do not facilitate this modification. An appropriate depth parameter should be related to the draft and shape of hull, as these parameters would act concurrently in determining the trajectories of brash-ice displacement. Observations of ice displacement around the wedge hull indicate that depth effects would likely not be significant because its "keeled" profile provided adequate space for brash ice to pass around and remain in the track. On the other hand, the tow hull, being much blunter in profile, blocked the passage of brash ice and hastened ridge and plug formation. It was not possible to estimate from the few experiments with the tow hull whether shallower channels transited by tows or smaller values of η_i/η result in less ice. For keeled hulls, such as the wedge hull and deep-draft hulls, channel depth likely does not significantly affect η_i/η.

The wedge hull has been described as a physical analogy of a short tow with an under-hull accumulation of brash ice, the accumulation being, in form at least, a sort of pseudo-keel. This analogy breaks down for shallow channels (say, $y_c/D \leq 2$), because the magnitude of the accumulation diminishes and ice formation reverts to the much less predictable pattern depicted in Figure 25.

Conclusion

Although circumspection is required when appraising the predictions of numerical models of ice formation in navigation channels, the present predictions do usefully extend the information on ice formation gained from the ice-tank experiments. Admittedly they are an idealized simulation of ice formation, but they do indicate the sensitivities of ice formation to air temperature, transit frequencies and channel width. Also, the magnitudes of ice growth and distributions of brash ice concur reasonably with those formed in the ice tank and reported from field studies (e.g. Fig. 7, 8).

As pointed out earlier, predictions of ice formation are influenced by values assumed for β, ε and p, primarily because these terms affect the removal of ice from the track or the accumulation of brash ice within it. The present predictions are based on a comparatively simple predictive model supported with data on β, ε and p that were obtained from ice-tank experiments using a simplified hull form. This hull is taken to be representative of hulls generally and, in particular, of tow hulls with under-hull accumulations of ice. Different relationships to those adopted here for β and ε may prevail for different hull forms and for different speed ranges. For example, since vessels would transit thinner ice covers at greater speeds, it is possible that substantially different relationships would result for β and ε with number and frequency of transits at such high speeds. Furthermore, for actual channels the vagaries of transiting (e.g. diverse hull sizes and shapes as well as speeds, ice cover and weather conditions) are likely to cause β, ε and p to vary randomly and unpredictably. Therefore, it is doubtful that a numerical model can be sufficiently reliable to predict precisely the amount of ice produced in a channel after a period of navigation. This requirement of numerical simulation may be moot, as the problems caused by transiting are not likely to be mitigated through a predictive scheduling program.

By way of comparison with the predictions on ice growth obtained with the present model, ice growth predictions obtained using Ashton's model (eq 10) are briefly discussed in Appendix D. Equation 10 predicts comparable values of η_i/η when f_t is on the order of 1/day or less. However, for larger values of f_t, eq 10 predicts much larger values of η_i/η, and the values increase monotonically with f_t.

ICE ACCUMULATION BENEATH TOW BARGES

The objective of this part of the ancillary study is to determine the equilibrium thicknesses and forms of ice accumulations beneath and ahead of flat-bottomed tows moving through ice-covered channels. The scope of the study is limited to tow transits of ice covers comprising either an ice sheet, a thin layer of brash ice, or a layer of ice floes. Figure 75 illustrates these processes. The approach

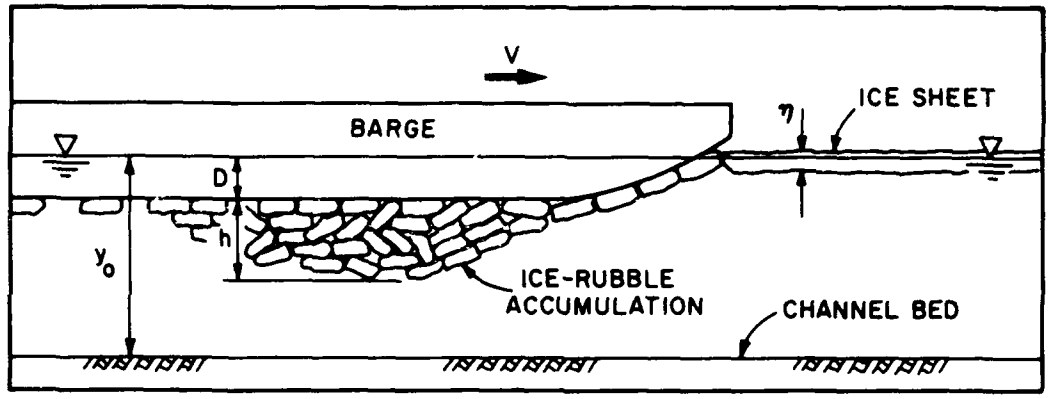

a. Moving through an ice sheet.

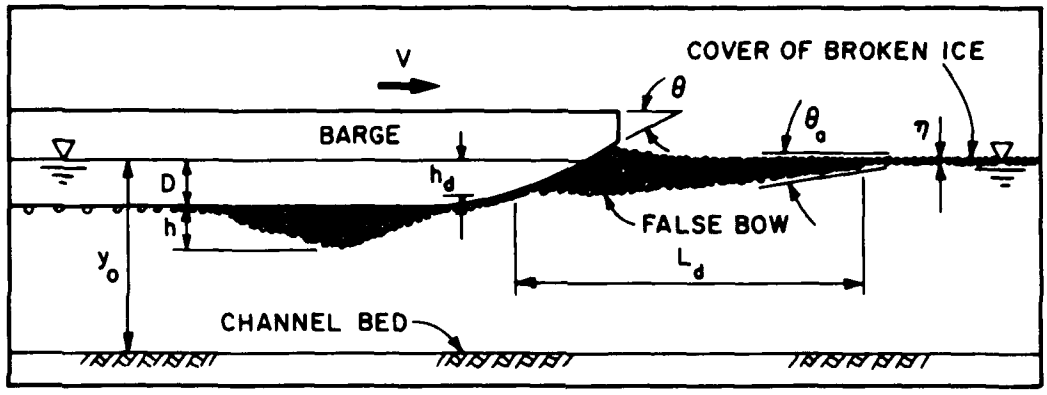

b. Moving through brash ice.

Figure 75. Ice accumulation beneath the model barge.

taken for the study is laboratory experiments guided by dimensional analysis.

Factors influencing ice accumulation

Ice accumulation beneath tows is analogous to the development of sedimentary waveforms, particularly to large-scale ripples or aeolian dunes (notably through similarity of the flow field causing wave-form accumulations).

The maximum equilibrium thickness and the form of ice accumulations beneath and ahead of a moving barge are influenced by several factors, including the barge speed relative to the water; the form, draft, beam and roughness of the barge hull; the water depth; and the dimensions and properties (e.g. strength, roughness, porosity) of the ice. Other factors, including the temperatures of the water, air and ice, may affect accumulation thickness. If the development and equilibrium forms of ice accumulations are treated as wave-like formations of particles, then the following functional relationship should be considered:

$$\frac{h}{\lambda} = \phi_1 \left[\left(\frac{u_*}{u_{*_c}} \right), \frac{u_* \ell}{\upsilon}, \frac{y_o}{\ell} \right] \tag{34}$$

where h = height of the wave
λ = wavelength of the wave
u^* = shear velocity of the water flow
u^*_c = its critical value associated with particle entrainment
ℓ = representative length dimension of ice pieces
υ = kinematic viscosity of water
y_o = water depth.

Wave forms in particulate materials are appropriately described in terms of their wavelength λ.

Wave height h (or steepness h/λ) is more complex than λ because it is determined by a larger number of variables. However, for ice accumulation beneath a barge, complications arise when attempting to predict equilibrium accumulation forms (i.e. λ and h). The rate of ice discharge beneath the barge is influenced by the barge draft and geometry (particularly the bow); the ice characteristics; the relatively small area of accumulation boundary (bottom of barges); the relatively large size of ice fragments compared to the barge size; and, for rivers and many harbors, the shallowness of the water. These factors prevent the use of a purely analytical approach to determining equilibrium thickness of ice accumulations beneath a barge. Therefore, it is appropriate to go directly to dimensional analysis to arrive at a set of parameters for describing the accumulation thickness.

Buckingham's Pi theorem yields

$$f_i\left(\frac{h}{\lambda}, \frac{\lambda}{y_o - D}, \frac{V}{\sqrt{g(1-\rho_i/\rho)\eta}}, \frac{V_\eta}{\eta}, \frac{y_o}{y_o - D}, \frac{B}{\ell}, \frac{L}{B}\frac{\ell}{y_o - D}, \frac{\eta}{\ell}, \theta, \mu_b, \mu_i, \text{ice properties}\right) = 0 \quad (35)$$

where V = barge speed relative to the water
ρ_i = density of the ice rubble
ρ = density of water
θ = stem angle of the barge bow
μ_b = coefficient of static friction between the ice and the hull
μ_i = coefficient of static friction between ice and ice
B = barge beam
D = barge draft
L = barge length
η = thickness of the ice fragments
ℓ = major length of the ice fragments.

Ice properties refer to the strength, temperature, shape, etc. of ice fragments. Strictly speaking, for describing wave topography on extensive planes, the parameter

$$\sqrt{g(1-\rho_i/\rho)\eta} = F_r$$

should be replaced by u_*/η^*_c. However, as u_{*c} is not readily determined for ice rubble beneath barges, it is more convenient to use F_r. Additionally, the second term in eq 34, a Reynolds number, need not be explicitly included in eq 35, as the flow is fully turbulent. For barge operators who wish to know the thickness of an accumulation beneath a barge, the following functional relationship is of interest:

$$\frac{h}{\eta} = \phi_2\left(F_r^*, \frac{B}{\ell}, \frac{L}{B}, \frac{\eta}{\ell}, \frac{\ell}{y_o - D}, \mu_b, \mu_i\right). \quad (36)$$

The wave-steepness parameter h/λ is replaced by h/η, as it can be argued for ripple-like waveforms, or for waveforms in infinitely deep water, that λ is proportional to η. Also, for the present study, λ could not be accurately defined, as most experiments resulted in single wave-like accumulations that commenced beneath the rounded bow of a model-scale test barge. In eq 35 the parameter $y_o/(y_o - D)$ is a blockage term and is included in eq 36 as $F_r^*[= F_r y_o/(y_o - D)]$ to account for the effects on h of water depth relative to barge draft; $\ell/(y_o - D)$ is a measure of waveform roughness relative to water depth; and B/ℓ relates barge beam to rubble size and thereby to potential wave size.

A formulation exercise similar to the one that led to eq 35 can be followed to identify a parametric relationship for accumulation slope θ_a:

$$\theta_a = f_2\left(F_r^*, \frac{\ell}{y_o - D}, \frac{\eta}{\ell}, \frac{B}{\ell}, \frac{L}{B}, \mu_b, \mu_i, \theta \text{ and ice properties}\right). \quad (37)$$

Before discussing the results of the experiments, it is helpful to consider briefly the influence of ice-rubble proportions, or the term η/ℓ, on ice-rubble accumulations beneath a moving barge. As the critical value of F_r associated with the entrainment of ice-rubble pieces lodged against the flat bottom of a barge F^*_{rc} increases with decreasing η/ℓ, it is likely that larger values of η/ℓ would lead to thicker accumulations. Tatinclaux and Gogus (1981), for example, proposed the following equation for assessing the stability of ice blocks lodged beneath a flat ice cover:

$$\overline{V}[(1-\rho_i/\rho)g\eta]^{-0.5} = [C_1(\eta/\ell)^2 + C_2(\eta/\ell) + C_3]^{-0.5} \quad (38)$$

where V is the mean velocity of the water flow

(below the cover) associated with the entrainment of blocks, and C_1, C_2 and C_3 are empirical coefficients.

Experiments

A series of experiments was conducted to determine the equilibrium thicknesses and forms of ice accumulations around barges. In particular, the relationship between h/η and F^*_r was sought for varying forms of ice cover. The experiments entailed the use of one of the 1:30-scale barges described earlier. The model barge was 1.8 m long, 0.36 m wide and of variable draft, with $\theta = 21°$. It was towed at speeds of 0.03–0.45 m/s. The experimental set-up is shown in Figure 76. Two sets of experiments were conducted: one using a glass-sided flume; the other, IIHR's ice tank. The flume was 20 m long, 0.3 m deep and 0.76 m wide. The ice tank is depicted in Figure 17.

For the flume experiments, ice covers were simulated using four sizes of polyethylene blocks or beads. In the ice tank, sheets of urea ice (4.5 and 10 mm thick) were used to simulate ice sheets and ice rubble. The dimensions of the blocks are given in Table 3. Polyethylene has the same specific gravity as ice (0.92). The coefficient of static friction μ_b for submerged polyethylene against the painted finish of the model barge was measured to be 0.15; for urea ice, $\mu_b = 0.05$. These values were obtained by pulling blocks over the surface of the model

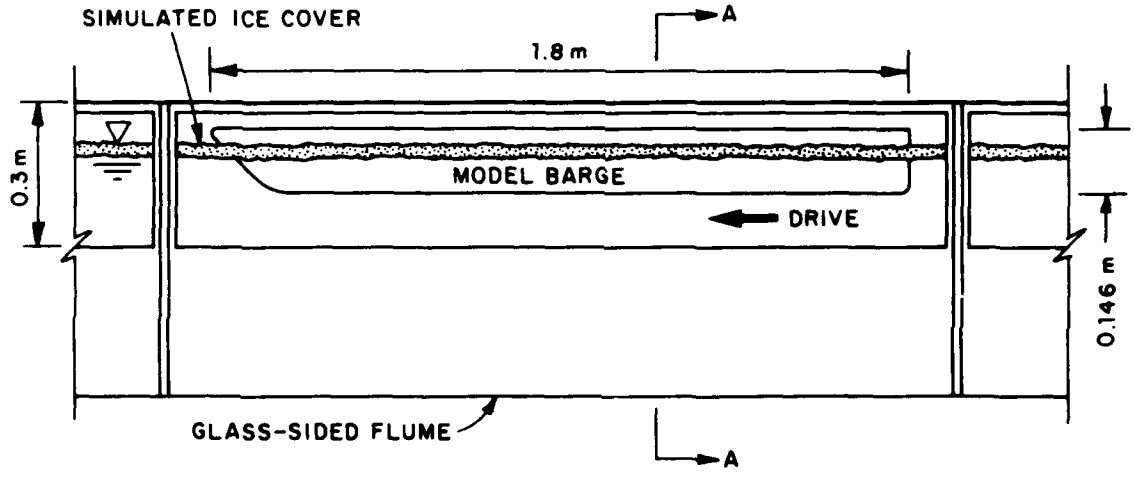

Figure 76. Experimental set-up.

Table 3. Properties of simulated ice.

Type	*Form*	*Length (mm)*	*Width (mm)*	*Thickness (mm)*	B/ℓ*
A	beads	4.8	4.8	3	74.1
B	large block	38	32	10	9.4
C	medium block	38	32	3	9.4
D	small block	13	13	3	27.4
E	urea ice	200†	50†	10	1.8
F	urea ice sheet	200†	45†	4.5	1.8
G	urea ice blocks	50†	50†	5	7.1
H	urea ice blocks	45†	45†	4.5	7.9

* $B \approx 356$ mm
† Average

barge. We realize the limitations of using plastic to simulate ice: somewhat higher values of friction coefficient, the lack of freezing between blocks, a non-wetting surface, etc. Tatinclaux and Lee (1978) discussed at length the limitations of using plastic to simulate ice. However, in addition to using urea ice, polyethylene blocks constitute an appropriate model ice material for this study because the strength properties of ice are not considered, and the accumulation processes mainly involve the movement of fully submerged blocks.

The 38-×32-×10-mm polyethylene blocks were arrayed in a tight, closely packed formation of 100% areal concentration such that they simulated an ice sheet precut into the sizes of broken ice likely to result when a barge moves through it. At a scale of 1:30 the array of plastic blocks simulated a 0.3-m-thick ice sheet breaking into ice blocks with a thickness-to-length ratio of about 1:3–4. The beads were used to simulate a cover of relatively small (0.09 m diameter, prototype) ice rubble. The areal concentration of the beads was typically about 75–78%. The two smaller sizes of ice block were used to simulate a cover of fairly small (0.4 to 1.0 m square × 0.09 m thick, prototype dimensions) ice rubble arrayed with an average areal concentration of about 66%. In the course of the experiment it was found that the areal concentration of blocks or beads affected the length of barge transit required for an equilibrium accumulation to develop beneath the model barge; lower concentrations of blocks required longer transits. This was one source of scatter in the data. Another, less significant, source was buoyancy, which, for thick accumulations of ice rubble, slightly altered the mean draft and trim of the barge.

For each experiment the barge was towed at constant speed through the simulated ice covers. Once ice accumulation below the barges had attained an equilibrium thickness, which usually occurred after about two to three hull lengths of transit, the accumulation profile was measured by means of a small-gauge hook probe. As can be appreciated from the photographs accompanying this section, the accumulation thickness could be measured to an accuracy of about one block thickness for large accumulations. Measured values of h and estimates of λ are tabulated in Table 4.

A brief set of additional experiments was performed with two barges moving in parallel along the flume. It was found that the narrowness of the flume—7% wider than the beam of the double barge configuration—occasionally caused the barges to become stuck when the simulated ice blocks wedged between the barges and the side walls of the flume. This is also a problem experienced by barges moving through locks or confined channels.

Observations

The manner in which ice rubble accumulated beneath and ahead of the model barge differed according to whether or not it transited a simulated ice sheet or a simulated layer of broken (floes or brash) ice. For both cases, ice-rubble accumulation beneath the barge was analogous to alluvium wave formation. Figures 77 and 78 illustrate accumulations under the model barge moving through simulated ice covers of sheet ice and an array of floes, respectively. The development of a false bow and a waveform accumulation of simulated brash ice (rubble with full-scale dimensions of less than about 2 m) are depicted in Figures 79 and 80, respectively. Figure 81 shows the especially troubling condition of an accumulation that extends to the channel bottom. This condition occurred when the test barge was towed at creeping speed close to the flume wall.

Table 4. List of experiments: ice accumulation beneath and ahead of the 1:30-scale model barge.

*Test no.**	*Ice type ***	V *(m/s)*	y_o *(m)*	D *(m)*	h *(mm)*	λ *(m)*
1	A	0.109	0.245	0.06	3.2	1.60
2		0.163			30.0	0.39
3		0.190			40.3	0.43
4		0.210			54.4	0.55
5		0.244			47.7	0.80
6		0.311			34.6	1.10
7		0.446			7.4	1.60
8		0.109	0.209	0.06	3.2	1.60
9		0.163			28.8	0.37
10		0.176			33.3	0.49
11		0.190			35.6	0.54
12		0.210			41.6	0.60
13		0.244			35.5	0.86
14		0.311			23.0	1.60
15		0.446			6.5	1.60
16		0.109	0.150	0.06	3.2	1.60
17		0.176			24.2	0.58
18		0.190			35.2	0.74
19		0.210			33.1	0.90
20		0.244			26.7	1.38
21		0.311			12.0	1.60
22		0.446			3.2	1.60
23		0.163	0.143	0.06	12.6	0.72
24		0.176			23.6	0.78
25		0.190			32.1	0.84
26		0.210			29.1	0.86
27		0.244			20.2	1.37
28		0.163	0.117	0.06	8.3	0.71
29		0.176			20.3	0.64
30		0.190			19.0	1.08
31		0.210			12.3	1.24
32		0.190	0.081	0.06	3.2	1.60
33		0.176			3.2	1.60
34		0.244			3.2	1.60
35		0.311			3.2	1.60
36		0.446			3.2	1.60
37	B	0.041	0.235	0.088	51.7	0.55
38		0.057			41.3	0.44
39		0.086			35.5	0.62
40		0.143			29.0	0.62
41		0.201			9.6	1.11
42		0.041	0.22	0.088	59.9	0.55
43		0.088			32.5	0.55
44		0.142			24.2	0.69
45		0.028	0.203	0.088	41.3	0.43
46		0.086			37.0	0.50
47		0.143			19.1	0.75
48		0.201			9.6	1.60

Table 4. Continued.

Test no.	*Ice type*	V *(m/s)*	y_o *(m)*	D *(m)*	h *(mm)*	λ *(m)*
49		0.041	0.178	0.088	49.0	0.44
50		0.088			32.5	0.66
51		0.143			19.1	0.86
52		0.201			9.6	1.55
53		0.041	0.168	0.088	37.8	0.56
54		0.088			29.4	0.62
55		0.142			18.8	0.86
56		0.041	0.231	0.06	65.3	0.69
57		0.088			56.9	0.75
58		0.142			40.5	0.83
59		0.203			18.5	0.95
60		0.028	0.203	0.06	62.0	0.52
61		0.143			28.6	0.74
62		0.201			19.1	0.95
63		0.041	0.178	0.06	53.2	0.45
64		0.086			41.3	0.65
65		0.143			28.6	0.70
66		0.201			9.6	0.86
67	C	0.041	0.180	0.06	30.0	0.27
68		0.075			48.0	0.50
69		0.109			66.3	0.57
70		0.244			20.8	1.60
71		0.446			13.4	1.60
72	D	0.142	0.240	0.088	21.2	0.34
73		0.159			37.7	0.48
74		0.176			34.0	0.58
75		0.244			27.6	0.86
76		0.379			19.4	1.60
77		0.446			12.0	1.60
78	E	0.042	1.067	0.088	30.5	
79		0.144			51.9	
80		0.163			54.9	
81		0.202			47.3	
82		0.245			30.5	
83		0.447			0.0	
84	F	0.042	1.067	0.088	51.9	
85		0.144			12.2	
86		0.221			12.2	
87	G	0.144	1.067	0.088	13.7	
88		0.202			41.2	
89		0.221			27.5	
90		0.245			15.2	
91		0.447			10.0	
92	H	0.144	1.067	0.088	33.6	
93		0.202			40.3	
94		0.221			70.2	
95		0.245			48.8	
96		0.447			4.5	

* Total number of experiments: 258.
** Types are illustrated in Table 3.

Figure 77. Simulated ice accumulated beneath the model barge using medium-size blocks arrayed as an ice sheet.

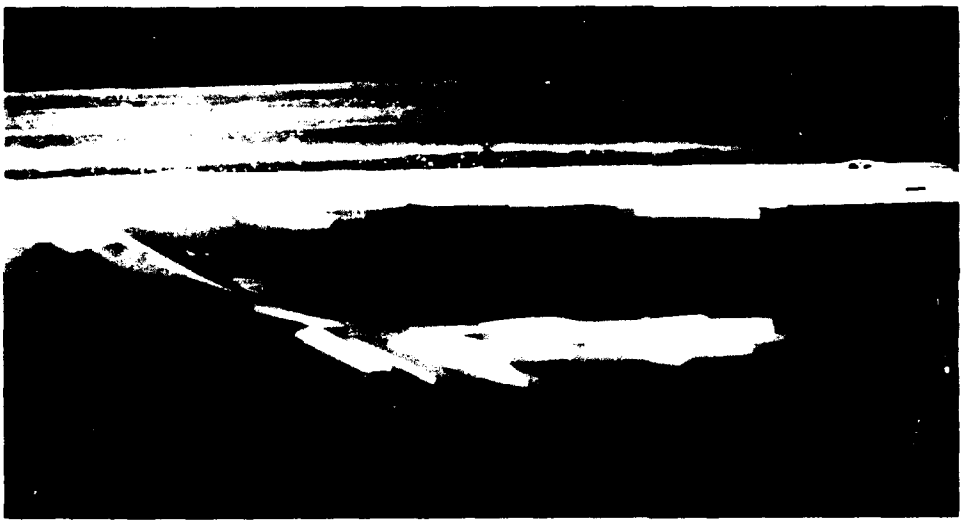

Figure 78. Simulated ice accumulated beneath the model barge using large blocks.

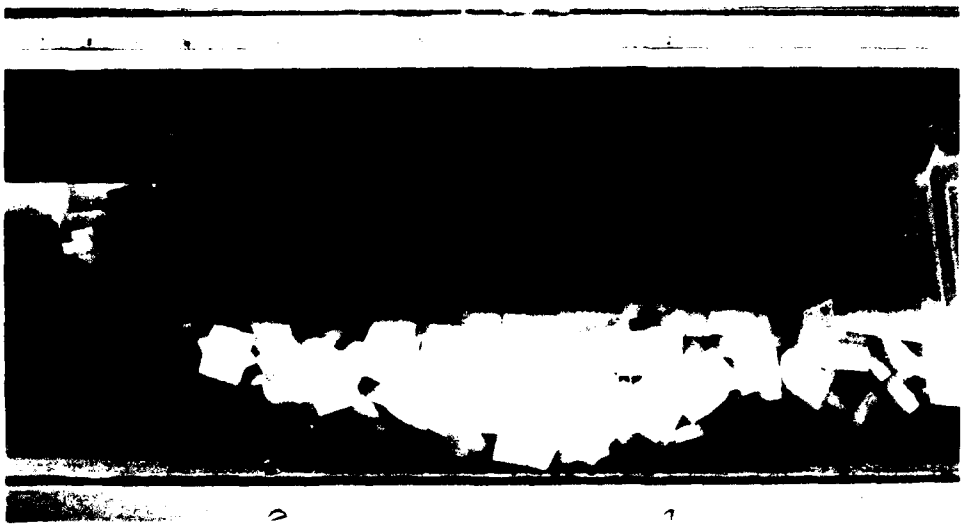

Figure 79. False-bow formation ahead of the model barge.

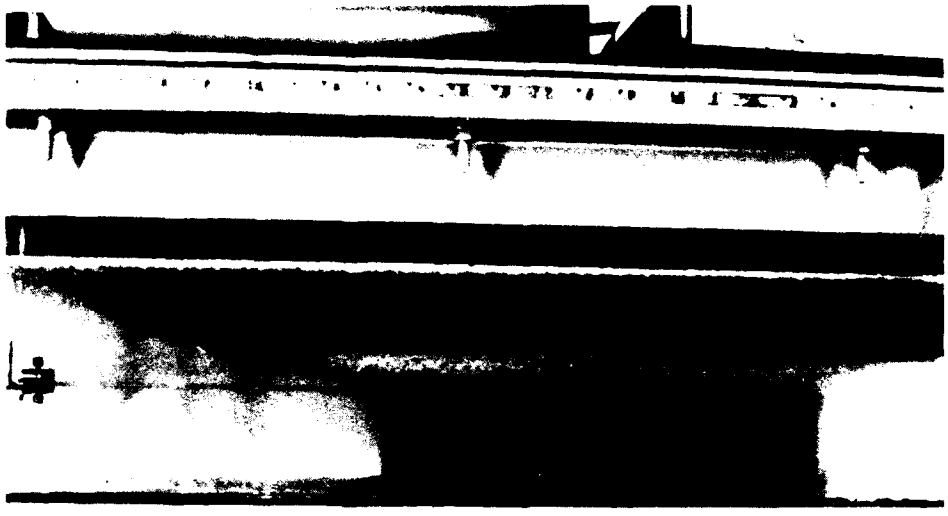

Figure 80. Dune-like accumulation of ice beneath the model barge using beads.

Figure 81. Ice accumulation extending to the channel bed when the barge crept along the flume wall.

When the model barge moved through the layer of blocks arrayed to simulate an ice sheet breaking into a more-or-less regular train of blocks, it overrode the blocks and pushed them beneath its bow. On rounding the bow and coming to the flat bottom of the barge, the initial train of blocks was dislocated, causing blocks to pile up and thereby initiating an ice accumulation. A relatively quiescent region of flow, caused by flow separation immediately downstream of the bow, aided the accumulation process such that, for relatively low values of F_r, blocks could accumulate as a more-or-less randomly oriented jumble beneath the bow. The accumulation thickened until fluid forces strengthened enough to balance the buoyancy forces acting through the blocks resting along the accumulation perimeter. With increasing hull speed, fluid forces acting on the blocks increased in magnitude such that the maximum thickness of accumulation diminished, and then the accumulation spread over a greater length of the barge. Also, the maximum thickness of the accumulation diminished with decreasing depth of water beneath the model barge. Imbrication (overlapping or shingling) of plate ice fragments may increase the resistance to erosion of an accumulation, as can be seen from Figure 78.

Small or irregularly shaped pieces of ice dislocated from one another and did not move together when shoved ahead of the test barge. Instead, when the model barge moved through the layer of beads simulating a cover of brash ice or pans of frazil ice, a false bow developed ahead of the barge without significant accumulation forming beneath it (Fig. 79). The false bow streamlined the bow, deflecting ice rubble around the barge and allowing only a trickle of ice to pass beneath it. With increasing speed the false bow shortened and thickened such that the beads could resist the fluid forces, and a greater discharge of beads passed beneath the hull, causing a dune-like accumulation to develop, as illustrated in Figure 80. For high speeds, possibly not of practical importance for conventional barge traffic, a false bow did not develop, and the accumulation thickness decreased until only a single layer of beads flowed beneath the barge. For the range of speeds associated with declining thickness of accumulation, it was not uncommon for rubble to accumulate as two or more waves beneath the test barge, though in most cases only a single wave formed under the single model barge. It may, therefore, be possible that many waveform accumulations may develop beneath the extensive bottom area of full barges or a tow comprising several barges.

The smaller blocks that simulated a cover of randomly arrayed ice pieces behaved similarly to the cover of beads. Lacking the facility to readily interlock when shoved, the smaller blocks accumulated as a conical false bow that deflected blocks around the barge. With increasing speed, the false bow shortened but thickened such that more blocks could pass beneath the barge and collect in a waveform accumulation.

Equilibrium thickness of the ice accumulation

The relationships between h/η and F_r differ according to whether or not the barge transited simulated ice sheets or layers of ice rubble. In each case, for polyethylene blocks, the maximum value of h/η was about 17–21 for $B/\ell > 9$. Barge transit through ice sheets is shown in Figure 82. Figures 83 and 84 show the variation of h/η with F_r through broken ice covers. In all three figures, $\ell/(y_o - D)$ and B/ℓ are indicated.

If the barge moved at creeping speed, the experimental set-up was truly two dimensional, and the length of simulated ice sheet transited was suitably long, ice rubble would tend to accumulate to the full water depth beneath the model barge. In other words, the maximum value of h/η should have approached $(y_o - D)/\eta$ as F_r approached zero, provided the barge or tow was large enough to accommodate the accumulation. This occurred when the test barge was towed close to the flume wall or when a double barge configuration was used, because the accumulation was confined by the flume's side walls. However, for a single barge moving slowly through the flume, whose width was 2.1 times the barge's beam, the accumulation became less two dimensional as blocks could slide or be swept from the heaped sides of the accumulations. Consequently, for a barge moving through a relatively wide channel, the values of h/η are likely to be less than $(y_o - D)/\eta$, and, for the same reason, they are likely to diminish somewhat with decreasing value of B/ℓ.

Figure 82 shows that h/η diminishes with increasing valuew of F_r, until F_r attains some critical value, in excess of about 8, beyond which all blocks swept beneath the barge move as a single layer ($h/\eta = 1$). Although the data collapse reasonably well, they vary consistently with $\ell/(y_o - D)$, reflecting perhaps the influence of accumulation roughness on local flow velocity and fluid forces.

For barge transit through broken or brash ice, the development of a false bow complicates the relationship between h/η and F_r such that h/η

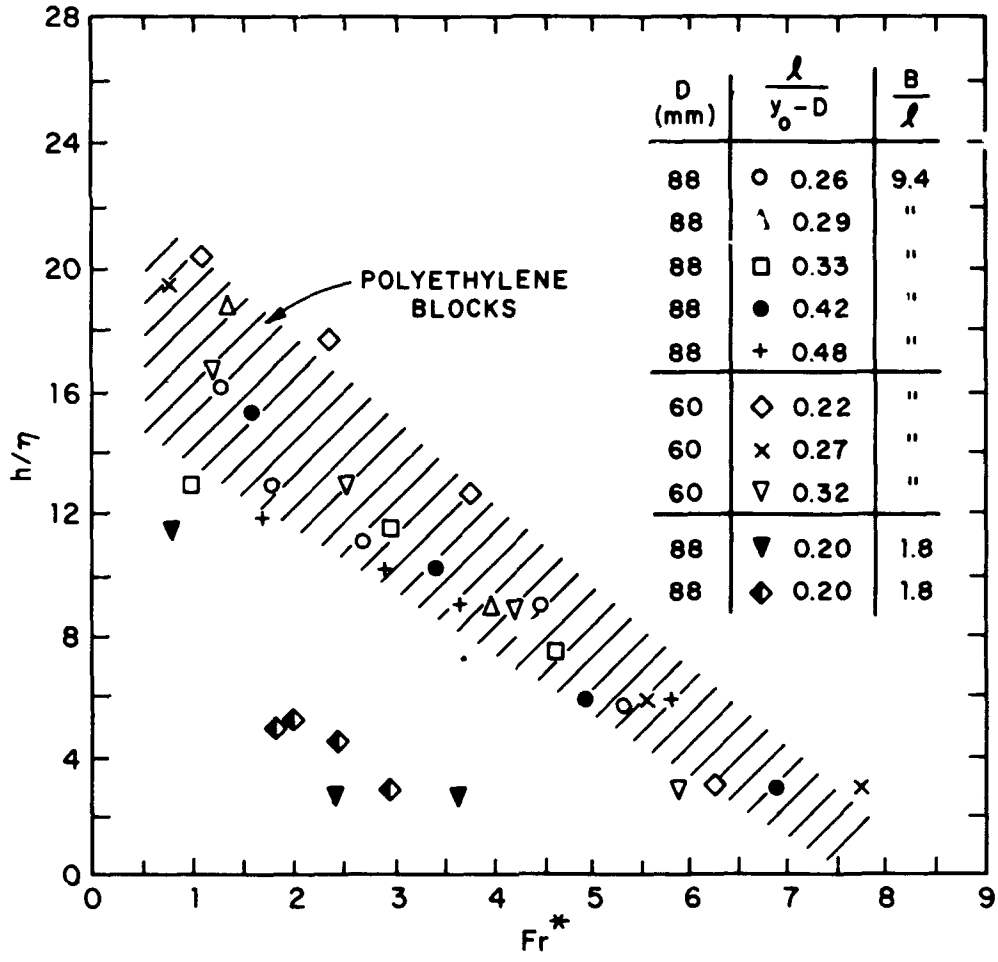

Figure 82. Accumulation thickness beneath the model barge for the simulated ice sheet.

attains a maximum value for a nonzero value of F_r, as shown in Figures 83 and 84. The relationship is analogous to that between bed-form height and flow velocity for flow over alluvial beds (e.g. Raudkivi 1976). Bow and false-bow forms affect the discharge of ice beneath a hull. As the flow of ice rubble beneath the bow increased, so did the height of the accumulation until, with further increases in both ice and water flow, the accumulation became washed out and rubble moved as a single layer beneath the barge. In Figure 83 the larger peak value of h/η that was measured for the larger B/ℓ can be ascribed to imbrication, or layering, of blocks; imbrication, which did not occur extensively for the smaller blocks (Fig. 77, 78) increases the resistance of the block to entrainment. Additionally, in accordance with eq 38, longer blocks lodged beneath a planar boundary are more resistant to entrainment and therefore may enable larger accumulations to develop.

Figure 84 should be considered together with Figure 85, which shows the variation of false-bow extent, or angle θ_a, with F_r. As the false bow diminished in size with increasing barge speed, more ice was transported beneath the barge so as to form an accumulation wave. The geometry of the false bow formed at the bow of the model barge can be described in terms of the angle θ_a, as depicted in Figure 85. With increasing hull speed F_r, θ_a increased until it was about the same value as the bow's stem angle θ. When θ_a exceeded θ, the false bow no longer developed and ice was swept beneath the barge. As described in the foregoing section, the peak accumulation beneath the model barge moving through brash ice occurred when θ_a approximately equaled θ.

An interesting result not readily apparent in Figure 84 is that, if the maximum thickness of

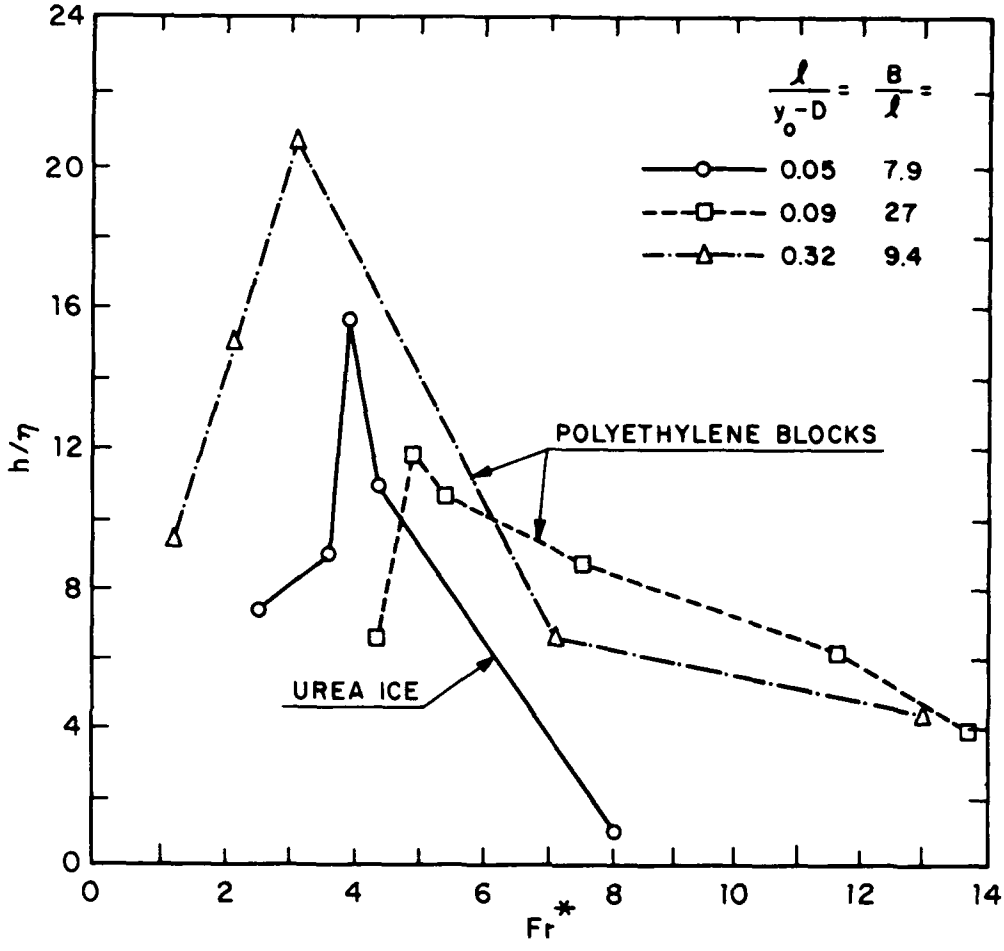

Figure 83. Accumulation thickness beneath the model barge for the simulated cover of ice floes.

accumulation h is normalized as $h/(y_o - D)$, the peak values of $h/(y_o - D)$ range from 0.26 to 0.36, with an average of 0.31. This result is remarkably similar to the maximum values of dune amplitude normalized with water depth for alluvial river channels (Raudkivi 1976).

A typical barge (9 m wide with a 2.6-m draft) moving at a speed of 0.5 m/s through a 0.2-m-thick ice sheet on a 6-m-deep pool of the Mississippi River (F_r = 2.2, $\ell/(y_o - D) \cong 0.25$) could possibly accumulate about 3 m of ice rubble beneath its bottom (Fig. 81). If the ice cover comprised brash ice with piece 0.1 m thick, and the barge were moving at speed of about 1.0 m/s (F_r = 6.1), an accumulation about 1.5 m thick may develop. These examples indicate the potential magnitudes of ice accumulations. Obviously many factors affect accumulation and its precise estimation. For example, if the barge were moving slowly through a confined channel, such as a lock approach, the accumulations may become much thicker. These estimates do not take into account the effect of ice fragments freezing to one another or the lower values of friction coefficient that occur between ice than occur between plastic. Freezing would increase the resistance of an accumulation to erosion by fluid forces and would likely result in larger accumulations. Lower values of friction coefficient may have the opposite influence.

Discussion

Several field observations cited earlier attest that significant quantities of ice do accumulate beneath flat-bottomed tows moving through ice-covered channels. The present study shows that the manner of ice accumulation varies according to whether an ice cover is an ice sheet or a layer of ice. If a cover is an ice sheet, broken ice can be directly submerged beneath a transiting tow, and the maximum thickness of the accumulation de-

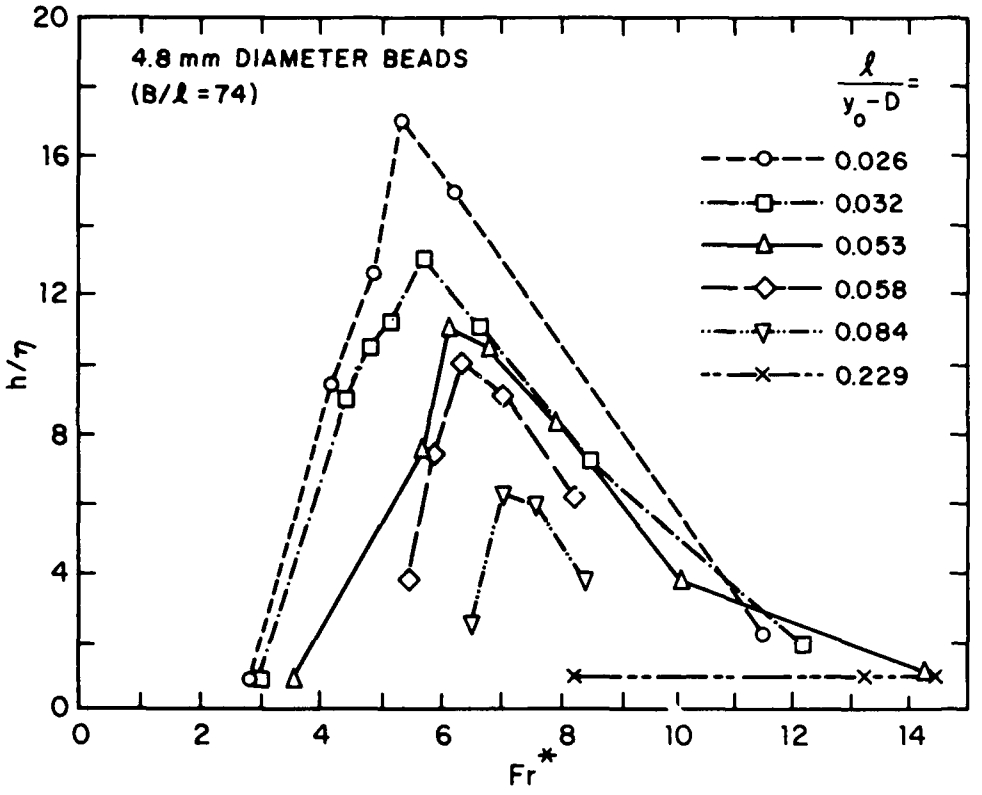

Figure 84. Accumulation thickness beneath the model barge for the simulated cover of brash ice.

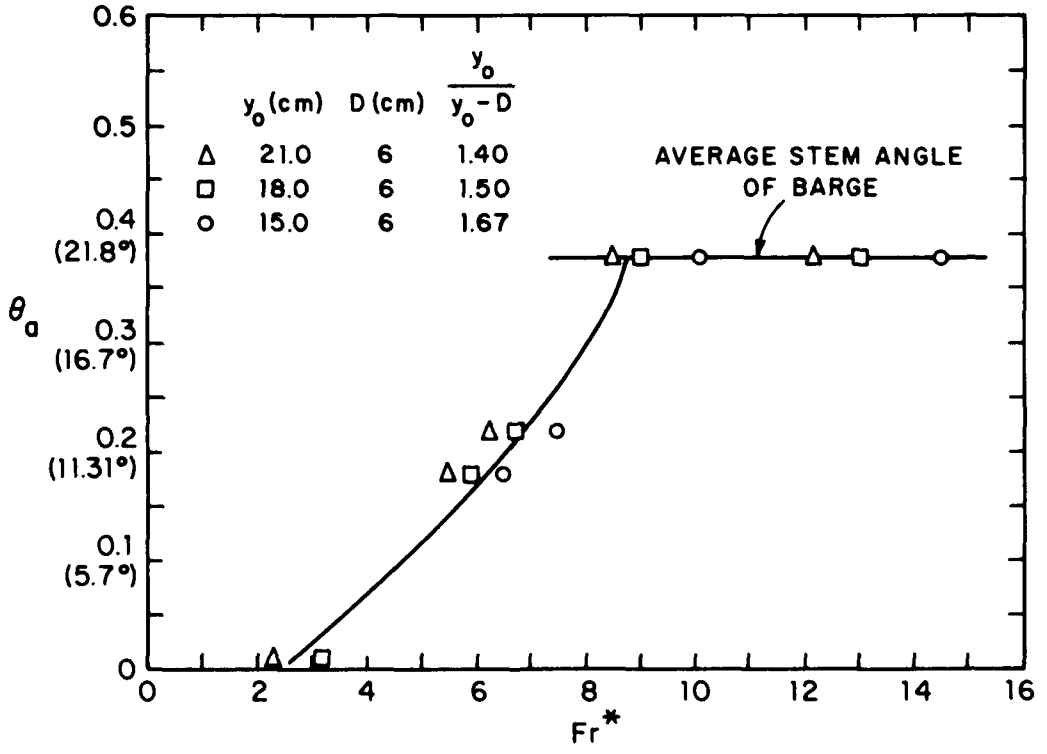

Figure 85. Variation of false-bow angle θ_a with barge Froude number F^*_r.

creases with increasing tow speed, or F_r. If an ice cover comprises comparatively small ice fragments (e.g. brash ice), a false bow may form ahead of a slow-moving tow, deflecting ice around the tow. With increasing F_r, the false-bow size diminishes such that the flow of ice beneath the tow increases and waveform accumulations develop. The accumulation thickness peaks with increasing F_r and decreases thereafter.

The thickness of an ice accumulation beneath a tow, expressed as h/η, may attain maximum values of about 17–21. However, accumulations extending to the channel bed may form beneath large, slow-moving tows in narrow or confined channels.

The use of η for normalizing h is not altogether satisfactory, but neither is any other dimension, such as y_o–D or ℓ. A drawback in using η is that measurement accuracy is on the order of η. The use of y_o–D seems attractive, especially for tow transits of loose covers of brash ice over shallow channels, for which $h/(y_o$–$D)$ attains a maximum value of about 0.31. However, for deep channels ($y_o >> D$), the water depth does not directly affect the local flow field around a hull, and therefore the use of y_o–D is not appropriate. The quandary here is the same as that faced in the appropriate description of sediment waveforms. Whereas they are often conveniently described and calculated in terms of waveform steepness (amplitude divided with wavelength), tow skippers are earnestly interested in knowing the maximum accumulation thickness relative to some familiar dimension such as ice thickness, channel depth or hull draft. They are not interested in knowing it relative to anything as nebulous as accumulation wavelength.

IMPROVED TRANSITING OF ICE-COVERED CHANNELS

Frequent transiting of navigation channels under frigid conditions incurs two fundamental problems. One problem is simply that frequent transiting causes more ice to grow than would grow without transiting. The other problem arises because transiting causes most of the ice grown along tracks opened by vessels to be broken and metamorphosed to brash ice, which may collect as thick accumulations that eventually impede transiting. The ice-tank experiments indicate that, for tow vessels, the latter problem is generally more severe, as transiting leads to the formation of thick localized accumulations that pose major impediments to sustained transiting.

A practical objective of the present study was to identify approaches that could improve transiting of ice-covered channels and to avoid or mitigate the problems caused by frequent transiting. The dual nature of these problems suggests two general approaches for ice control and problem mitigation. One approach entails minimizing ice growth and requires that the number and schedule of transits be optimized in accordance with prescribed economic constraints. This approach gives rise to the concept of optimum scheduling of transits and convoying of vessels. The other approach entails the use of mechanical methods for controlling brash-ice accumulations at specific channel locations where especially troublesome accumulations perennially form. Before outlining approaches to problem control or mitigation, it is useful to summarize the troublesome consequences that transiting may incur.

Troublesome consequences of transiting

The results obtained from the ice-tank experiments and the numerical model, together with observations cited from the field studies (reviewed earlier), show that tracks opened by transiting vessels become covered with rather porous layers of brash ice that are approximately 1.5–3 times the ice-cover thickness. The higher thickness value is associated with higher frequencies of transit. The equivalent solid volume of brash ice grown at a typical channel section is about 1.5–2.5 times the volume of ice cover that would have formed over vessel tracks. Both the experiments and the numerical model indicate that frequent transiting does not lead to as dramatic an increase in the volume of ice grown as some of the literature would suggest. The experiments do show that higher frequencies result in finer sizes of brash ice and less porous accumulations. In addition to increasing the resistance to transit, increased volumes of ice growth in river channels may exacerbate problems associated with ice-jam formation or ice passage at dams. The results of the present study show that, although transiting certainly leads to additional ice growth, the increase in the volume of ice grown on most river channels is not great. For example, transiting a channel that is five times the width of vessel beam produces about 20% more ice than would form without transiting (Fig. 73). On the other hand, transiting a narrow channel that is only twice the width of transiting vessels may double the amount of ice grown. For tow transiting of channels through shallow rivers,

possibly of greater concern than the volume of ice grown is the hazard that plugs of accumulated brash ice may precipitate ice-jam formation by being more resistant to break-up than are ice covers.

Although brash-ice layers in vessel tracks increase the resistance to transiting, ridges of brash ice formed beneath ice covers flanking the tracks pose greater impediments to transiting. For river channels transited by tows, plugs of brash ice that accumulate locally in tracks are an additional and formidable impediment. Ridges and plugs may be considerably thicker than brash-ice layers in vessel tracks. The ice-tank experiments show that ridges can be about three to five times the ice-cover thickness and that the plugs can be even thicker at about ten or more times the ice-cover thickness. The ice-tank experiments also show that ridges and plugs form more rapidly in shallower channels and may extend the entire channel depth. It is to be expected, therefore, that ridge and plug formation can create especially troublesome conditions for transiting ice-covered shallow channels. Additionally, brash-ice accumulations are likely to create severe difficulties for the winter use of small confined harbors, even if they are deep.

A further accumulation-related problem occurring for tows is their propensity to entrap and transport brash ice beneath their flat-bottomed hulls. Such accumulations not only increase the tow resistance, but they may cause tows to ground when transiting shallow channels or attempting to pass through locks.

Approaches to problem control and mitigation

Two general approaches can be implemented: minimization of ice formation through optimal scheduling of transits, or mechanical redistribution (and possibly removal) of troublesome accumulations of brash ice. The two approaches could, of course, be implemented jointly. However, the present study indicates that the latter approach is probably more practicable and promising.

Optimal schedules for transiting of ice-covered channels can ideally be identified by mathematical optimization analyses. Such analyses are beyond the scope of the present study as, in addition to the constraint of minimizing volume of ice growth, constraints related to navigation economics need to be taken into account; these constraints include minimizing the power requirements of transiting vessels, minimizing delays, and for some river channels, minimizing costs associated with locking operations. The results from both the ice-tank experiments and the exercises with the numerical model, however, indicate that sophisticated transiting schedules are not called for, especially if the vessels are river tows. This is fortunate because scheduling of transits is fraught with numerous practical difficulties, the least of which is the unpredictable nature of severe weather.

The experiments and the numerical model indicate that a basic rule for minimizing volume of ice grown in a frequently transited channel is to minimize the total number of icebreaking transits. The numerical model showed further that, for a fixed number of transits per day (or a fixed sequence frequency f_s), varying the interval between individual transits (or transit frequency f_t) had no significant effect on the volume of ice grown (Fig. 72). For example, if it is required that a channel be transited daily by four vessels (f_s = 4/day), then there is negligible difference in the volume of ice grown in the channel whether it is transited in a brief sequence during which vessels pass at a frequency of one per two hours [f_t = 1/(2 hours)], with no transits for the remainder of the day, or if the transits are equally spread over an entire day [f_t = 1/(6 hours)].

Convoying of vessels is the special case of scheduling that prevails when f_t = 0. The chief advantage of convoying is that each convoy involves only one icebreaking event. Icebreaking and the brunt of transiting resistance are borne by the lead vessel, which could be used especially for those tasks. Furthermore, because it reduces the number of icebreaking transits, convoying is likely to reduce the volume of ice grown in a navigation channel. An advantage of convoying tows is that, except for the lead tow, tows within a convoy would likely experience less under-hull accumulation of brash ice or broken ice, because they would not be transiting intact ice covers or layers of brash ice. Convoying, however, does have its practical drawbacks. A fundamental one is that convoys may be difficult to form and maintain if vessels arrive at convoy-staging locations at unpredictable and irregular intervals and if vessels then have diverse and multiple destinations. A further drawback exists for river channels that are comparatively short and are punctuated with locks, such as many channels comprising the inland waterways of North America. Erstwhile convoys transiting these channels may be disrupted by lock passage, as, in some extreme situations, the time required for a convoy to pass through a lock may exceed the time required to transit between locks. These drawbacks could be overcome by limiting the size of

convoys according to the circumstances of the channel to be transited. For example, convoys formed of two to four tows may be effective in reducing ice formation in relatively short channels. Generally, however, convoying seems more attractive for longer channels such as navigable rivers of northern Soviet Union, where convoying and scheduling of transits are the rule rather than the exception (Tronin et al. 1984).

Because the more severe problem created by transiting is the potential for thick accumulations of brash ice to develop at specific troublesome locations (such as shown in Fig. 4) in navigation channels, an alternate approach is to use mechanical methods for controlling brash-ice accumulations. This approach is probably more likely to minimize the volume of ice grown than is scheduling of transits. Although the present study did not directly examine mechanical methods of improving transiting, the insights gained from it suggest three general methods: vessel-based techniques for preventing excessive ridge formation; excavation and removal of brash ice; and modification of channel alignment and cross section, especially for relatively shallow or narrow channels. All three methods require further investigation to ascertain their effectiveness.

Vessel-based methods could be developed for controlling ice-cover formation, breaking ridges or redistributing accumulated brash ice. Sölve (1986), for example, described the use of small boats fitted with rakes for removing brash ice from entrances to lock approaches on the Trollhätte Canal. Mellor et al. (1978) and Vance (1980) assessed the physical and economic feasibilities of various methods for removing brash ice from navigation channels. The impetus for their studies was the need to control brash-ice accumulations in portions of the St. Marys River. The most attractive technique that both studies identified involved the use of a vessel for mechanically excavating brash ice from channels. Alterations to channel alignment and geometry, which may be required for recurring problem sites, are a last resort. Nevertheless, channel modifications, dredging activities and new lock approaches and river-training works should be planned with consideration of their effects on brash-ice accumulation.

CONCLUSIONS AND RECOMMENDATIONS

The major contributions of this study are detailed descriptions of ice formation in frequently transited navigation channels and the development of a predictive model. A practical objective of the study was to assess the merits of scheduling vessel transits so as to control or mitigate potential problems caused by heavy traffic. The study involved extensive laboratory experiments, which were conducted using an ice tank and model vessels, and numerical simulation using the predictive model. Although the descriptions of ice formation apply to frequently transited channels in general, the study was primarily aimed at river channels transited by tows such as those that ply the navigable inland waterways of North America. The principal conclusions derived from the study are summarized here.

A conclusion tentatively drawn from the disparate and somewhat sketchy field descriptions of ice formation in navigation channels, and confirmed subsequently during the ice-tank experiments, is that ice formation is significantly affected by the hull form and length of transiting vessels, the channel geometry and the presence of significant water currents. For example, quite different patterns of ice formation may evolve in river channels that are plied by bluff-bowed, flat-bottomed tows or have significant water currents than occur in harbor and coastal channels that are plied by ship-form hulls and are subject to comparatively weak currents. The essential difference in the patterns is that transiting tows and water currents may cause broken and brash ice to be conveyed along channels and may consequently lead to markedly nonuniform ice formation. Two general patterns of ice formation are illustrated in Figures 14 and 25. They illustrate the main differences in ice formation in channels transited by ship-form hulls and tows that move ice, respectively.

Frequent transiting of ice-covered navigation channels results in increased volume of ice growth, but the increase is perhaps not quite as dramatic as might be expected. The results from both the ice-tank experiments (Fig. 60) and the numerical model (Fig. 71) indicate that intense transiting, involving frequencies in excess of about two transits per day, produces about two to three times the volume of ice than would grow over the same area of channel opened by the track if it were not transited. Lesser volumes of ice grow with fewer than about two transits per day.

Transiting breaks ice and converts it to brash ice, which accumulates as porous layers in vessel tracks and ridges formed beneath the ice cover bordering tracks. The ice-tank experiments and the numerical model show that intense transiting

of a track leads to layers that average about two to three times the thickness of the ice cover riven by the track. This range of layer thickness corresponds to ridge thicknesses that are three to four times the ice cover thickness.

Two essential problems are created by frequent transiting. One problem is increased volume of ice growth, which increases the resistance to transiting vessels, produces more ice at ice jams and exacerbates difficulties in passing ice at dams. The other problem, which is potentially more severe, arises because brash ice may accumulate as thick layers along vessel tracks, as thicker ridges flanking them, and for channels transited by tows, as especially thick local accumulations termed plugs. Both problems (but particularly the latter one) become more troublesome for shallower channels with depths marginally greater than the vessel draft, because the lack of clearance prevents brash ice from passing beneath the vessels. Ridges and plugs may extend over the entire depth of shallow channels.

The ice-tank experiments and exercises with the numerical model indicate that sophisticated scheduling of transits to minimize ice problems is not warranted. A general conclusion is that fewer ice-breaking transits result in less ice growth. Convoying, therefore, appears attractive because it reduces the number of ice-breaking transits. However, an approach that controls ice growth and brash-ice accumulation at troublesome channel locations is more likely to mitigate problems incurred by frequent transiting. This approach would require development of appropriate mechanical means of redistributing or removing brash ice.

A problem peculiar to tow transit of ice-cover channels is the accumulation of broken ice and brash ice beneath along the flat bottoms of tows. The experiments show that accumulations on the order of 15–20 times the ice-cover or brash-ice thickness may accumulate beneath tows. For the usual range of tow speeds, the accumulation thickness decreases with increasing speed for tows transiting ice sheets. However, for transits through thin covers of brash ice, the accumulation thickness increases with increasing speed. The accumulation thickness is affected by tow dimensions and bow geometry.

As a logical extension of the present study, we recommend that sections of an actual tow or ship track be monitored so as to confirm the major conclusions drawn from the present study. Ideally such field monitoring might comprise field tests conducted with sections of navigable channels being transited at regular frequencies. A further extension would be to survey important navigation channels to identify locations where troublesome accumulations of brash-ice form. A practical extension would then be to investigate effective methods for moving and "storing" brash ice accumulated at these channel locations. Among the more fundamental aspects of ice formation to be studied further is ice grown through porous layers of brash ice.

LITERATURE CITED

Argiroff, C. and L.E. Weigum (1986) Great Lakes—Limited season extension. In *Proceedings of International Association for Hydraulic Research Symposium on Ice, The University of Iowa, Iowa City, Iowa.*

Ashton, G. (1974) Evaluation of ice management problems associated with operation of a mechanical ice cutter on the Mississippi River. USA Cold Regions Research and Engineering Laboratory, Special Report 214.

Ashton, G. (Ed.) (1986) *River and Lake Ice Engineering*. Littleton, Colorado: Water Resources Engineering.

Ashton, G., S.L. DenHartog and B. Hanamoto (1973) Icebreaking by tow on the Mississippi River. USA Cold Regions Research and Engineering Laboratory, Special Report 192

Bérenger, D. and B. Michel (1975) Algorithm for accelerated growth of ice in a ship's track. In *Proceedings, 3rd International Symposium on Ice Problems, Hanover, New Hampshire, 18–21 August.* International Association of Hydraulic Research, p. 127–132.

Beurket, R.T. and C. Argiroff (1984) Great Lakes limited season extension operation of Sault Ste Marie Locks, Michigan, USA. In *Proceedings of International Association for Hydraulic Research Symposium on Ice, Hamburg, W. Germany*, p. 267–276.

Borland, S.L. (1987) Progress report on the barge profiling system at Lock 26, Mississippi River. USA Cold Regions Research and Engineering Laboratory, Internal Report (unpublished).

Calkins, D.J. (1979) Accelerated ice growth in rivers. USA Cold Regions Research and Engineering Laboratory, CRREL Report 79–14.

Enkvist, E. (1972) On the ice resistance encountered by ships operating in the continuous mode of icebreaking. Swedish Academy of Engineering Sciences in Finland, Report No. 24.

Eranti, E., E. Leppanen and M. Penttinen (1983a)

Ice control in Finnish harbours. In *Proceedings, 7th International Conference on Port and Ocean Engineering under Arctic Conditions, 5–9 April, Helsinki, Finland*. Espoo, Finland: Valtion teknillinen tutkimuskeskus, vol. 1, p. 370–380.

Eranti, E., M. Penttinen and T. Rekonen (1983b) Extending the ice navigation season in the Saimaa Canal. In *Proceedings, 7th International Conference on Port and Ocean Engineering under Arctic Conditions, 5–9 April, Helsinki, Finland*. Espoo, Finland: Valtion teknillinen tutkimuskeskus, vol. 1, p. 381–391.

Eskola, H. (1983) Propulsion tests of a ship model in conditions simulating an old ice-clogged channel. In *Proceedings, 7th International Conference on Port and Ocean Engineering under Arctic Conditions, 5–9 April, Helsinki, Finland*. Espoo, Finland: Valtion teknillinen tutkimuskeskus, p. 494–504.

Ettema, R., M. Matsuishi and T. Kitazawam (1985) Model tests on ice-rubble size and ship resistance in ice rubble. Iowa Institute of Hydraulic Research, The University of Iowa, Iowa City, Iowa, Report No. 293.

Forsman, B. and J. Sandkvist (1986) Brash ice effects on ship operators—A presentation of the SSPA maneuvering simulation model and other brash ice related projects. *International Offshore and Navigation Conference and Exhibition at the Finlandia Hall, Helsinki, Finland*, p. 1021–1038

Greisman, P. (1981) Brash ice behavior. U.S. Coast Guard Research and Development Center, Avery Point, Groton, Connecticut. Report No. USCG-D-30-81

Hamza, H. (1985) Numerical predictions of ice build-up in ships tracks. In *Proceedings, 8th International Conference on Port and Ocean Engineering under Arctic Conditions (POAC '85), 7–14 September, Narssarssuaq, Greenland*. Hörsholm, Denmark: Danish Hydraulic Institute, p. 797–810.

Hausser, R. and F.E. Parkinson (1986) Thin sheet ice generation on cold water. *Proceedings, 4th Workshop on Hydraulics of River Ice, Montreal, Canada.*

Kannari, P.S. (1983) Measurements of characteristics and propulsion performance of a ship in old ice-clogged channels. In *Proceedings, 7th International Conference on Port and Ocean Engineering under Arctic Conditions, 5–9 April, Helsinki, Finland*. Espoo, Finland: Valtion teknillinen tutkimuskeskus, vol. 2, p. 600–609.

Kashteljan, V.I., I.I. Posnjak and A.Y. Ryvlin (1968) Ice resistance to motion of a ship. Sudostroyeniye, Leningrad.

Keating, B. (1970) *The Northwest Passage*. New York: Rand McNally and Company.

Kitazawa, T. and R. Ettema (1985) Resistance to ship–hull motion through brash ice. *Cold Regions Science and Technology*, **10**(3):219–234.

Kotras, T.V., P.P. Kosterich and R.P. Voelker (1977) Ice impact forces on the bow of a Great Lakes bulk carrier. Maritime Administration, U.S. Department of Commerce, Washington, D.C. Report No. 160C-2.

Levine, G.H., R.P. Voelker and P.B. Mentz (1974) Advances in the development of commercial ice-transiting ships. In *Proceedings of Annual Meeting of the Society of Naval Architects and Marine Engineers, New York.*

Lewis, J.W. and R.Y. Edwards (1970) Methods for predicting icebreaking and ice resistance characteristics of icebreakers. *Transactions of the Society of Naval Architects and Marine Engineers*, vol. 78.

Lunardini, V. (1981) *Heat Transfer in Cold Climates*. New York: Van Nostrand Rheinhold Co.

McKindra, C.D. and T.C. Lutton (1981) Statistical analysis of broken ice dimensions generated during 140 ft WTGB icebreaking trials. In *Proceedings, 6th International Conference on Port and Ocean Engineering under Arctic Conditions (POAC '81), 27–31 July, Quebec, Canada. Université Laval, p. 235–243.*

Mellor, M. (1980) Ship resistance in thick brash ice. *Cold Regions Science and Technology*, **3**: 305–321.

Mellor, M., Vance, G.P., Wuebben, J.C. and G.E. Frankenstein (1978) An investigation of ice-clogged channels in the St. Marys River. U.S. Coast Guard Research and Development Office, Washington, D.C., Report No. CG-D-22-78.

Michel, B. (1971) Winter regime of rivers and lakes. USA Cold Regions Research and Engineering Laboratory, Monograph III-B1a.

Naegle, J. (1980) Ice resistance predictions and motion simulation for ships operating in the continuous mode of icebreaking. University of Michigan, Ann Arbor, Michigan, Ph.D. thesis.

Raudkivi, A.J. (1976) *Loose Boundary Hydraulics*. Pergamon Press.

Sandkvist, J. (1978) Problems in keeping year-round navigation in the Luleä Harbour. *Proceedings, IAHR Symposium on Ice Problems, Luleä, Water Resources Engineering, University of Luleä, Luleä, Sweden*. Research Report Series A, No. 13.

Sandkvist, J. (1980) Observed growth of brash ice in ship's tracks. Water Resources Engineering, University of Luleä, Luleä, Sweden, Research Report Series A, No. 42.

Sandkvist, J. (1981) Conditions in brash ice covered channels with repeated passages. *Proceedings, 6th International Conference on Port and Ocean Engineering under Arctic Conditions (POAC '81),*

27–31 July, Quebec, Canada. Université Laval, p. 244–252.

Sandkvist, J. (1982) Vertical block sizes in brash ice covered channels. Water Resources Engineering, University of Luleä, Luleä, Sweden, Research Report Series A, No. 101.

Sandkvist, J. (1986) Brash ice behaviour in frequented ship channels. Water Resources Engineering, University of Luleä, Luleä, Sweden, Research Report Series A, No. 139.

Sölve, T. (1986) Winter traffic on the Trollhätte Canal and the Lake Vänern. *Proceedings of International Association for Hydraulic Research Symposium on Ice, The University of Iowa, Iowa City, Iowa,* vol. 2, p. 63–74.

Tatinclaux, J.-C. and S.T. Cheng (1978) Characteristics of river ice jams. In *Proceedings of International Association for Hydraulic Research, International Symposium on Ice Problems, Luleä, Sweden,* p. 461–475.

Tatinclaux, J.-C. and M. Gogus (1981) Stability of floes below a floating ice cover. In *Proceedings of International Association for Hydraulic Research, International Symposium on Ice, Quebec, Canada,* vol. 1, p. 298–308.

Tatinclaux, J.-C. and C.L. Lee (1978) Initiation of ice jams—A laboratory study. *Canadian Journal of Civil Engineering,* 5(2):202–212.

Tronin, V.A., V.A. Malinowsky and Y.A. Sandakov (1984) Problems of river shipping in ice-bound conditions. In *Proceedings of International Association for Hydraulic Research Symposium on Ice, Hamburg, W. Germany,* vol. 2, p. 255–266.

Tuovinen, P. (1978) The size distribution of ice blocks in a broken channel. Helsinki University of Technology, Ship Hydrodynamics Laboratory, Otaniemi, Finland, Memorandum M-78.

Urroz, G.E. and R. Ettema (1987) Simple-shear box experiments with floating ice rubble. *Cold Regions Science and Technology,* **14**(2):185–199.

U.S. Army Corps of Engineers (1976) L & D No. 26—Barge lockage under ice conditions. USA Cold Regions Research and Engineering Laboratory, Disposition Form LMSED-DA.

U.S. Army Corps of Engineers (1978) Ohio River Division Ice Committee Ohio River Division, Cincinnati, Ohio, Summary Report, Appendix I (Memo To Record).

Vance, G.P. (1980) Clearing ice-clogged shipping channels. USA Cold Regions Research and Engineering Laboratory, CRREL Report 80-28.

Voelker, R.P. and G.H. Levine (1972) Methods to improve Great Lakes bulk carrier performance in mush ice fields and clogged channels. Maritime Administration, U.S. Department of Commerce, Washington, D.C., Technical Report No. 371.

Welsh, J.P. and B.T. Kingsbury (1975) Characterization of slush ice in the Great Lakes. USCG Research and Development Center, Avery Point, Groton, Connecticut, Report No. CG-D-45-75.

APPENDIX A. BRASH-ICE RESISTANCE TO TOW TRANSIT

Introduction

As part of their study on the icebreaking performance of tows on the Mississippi River, Ashton et al. (1973) estimated mean values of resistance experienced by tows transiting brash-ice covers. Their resistance data, reproduced in Figure A1, show a curious if not controversial trend: the total resistance generally decreased with increasing tow speed and brash-ice thickness, and the ice resistance (evaluated as total resistance minus open water resistance) decreased with increasing tow speed. Ashton et al. suggested that with increasing tow speed, less ice was accumulated either as a false bow or beneath its hull. Less ice accumulation would result in less resistance. However, the trend shown by their data is counter to those reported for other hulls (e.g. Ettema et al. 1985).

A brief series of experiments was conducted to assess the levels of resistance and power requirements for tow transit of navigation channels that are covered with brash ice.

Experiments

The experiments were conducted using IIHR's ice tank and the 1:30-scale tow model described earlier. The model was towed at speeds ranging from 0.05 to 0.75 m/s along a channel containing a preformed layer of brash ice, as illustrated in Figure A2. Two configurations of tow model were used. For one the towboat pushed two barges aligned in parallel (model length and beam = 3.05 and 0.71 m, respectively). For the other the towboat pushed two barges in series (model length and beam = 4.88 and 0.36 m, respectively). For both configurations the model draft was 92 mm. The tow models were connected by a towing shaft to a dynamometer mounted on the towing carriage. A guide fitted to the lead barge(s) ensured that the model held course along the channel. In this towing harness the tow model was free to pitch and heave as well as undergo slight roll and yaw. Towing forces were

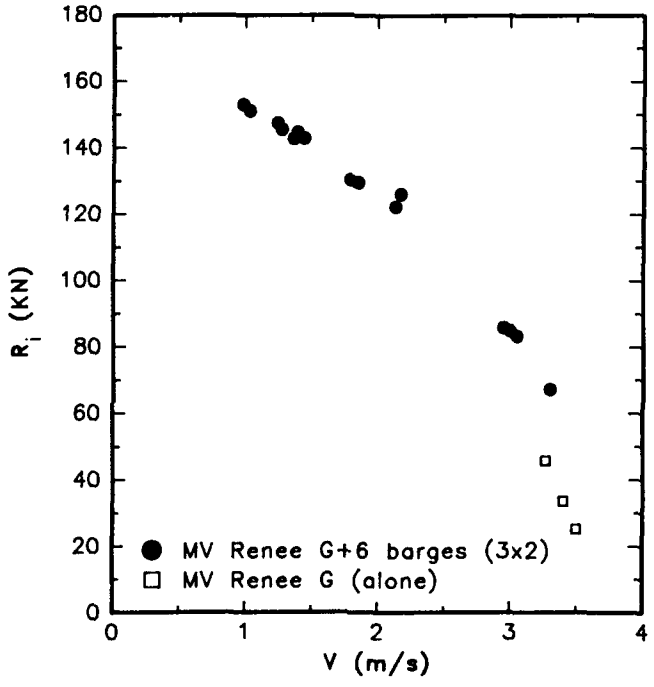

Figure A1. Variation of ice resistance R_i with tow speed V (Ashton et al. 1973).

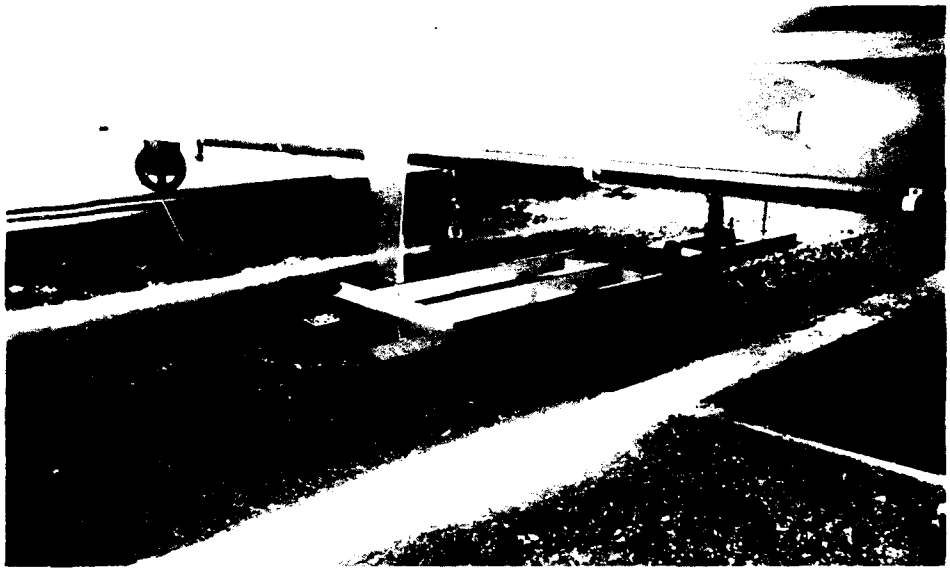

a. Hull towed through a preformed layer of brash ice

b. View of the track left by the tow. The markers indicate the shear deformation of the layer.

Figure A2. 1:30-scale tow hull.

measured using a 45-N load cell fitted to the towing dynamometer.

For most of the experiments the channel width was 2.13 m. A subset of experiments was performed with the channel width at 0.84 m. In other words, the channel was 1.2 and 3.0 times the beam of the tow model configured with two barges in parallel, and 2.4 and 6.0 for the series configuration. Since the water depth for all the experiments was maintained at 1.07 m, such that $y_o/D \equiv 12$, the effects of shallow water on resistance were not investigated. The tow resistance was examined for three layer thicknesses h: 4 (single layer), 50 and 100 mm. Values of h/D ranged from 0.05 to 1.14. The brash ice was formed by fragmenting 4-mm-thick sheets of unseeded urea. The average dimension of the brash ice was 19 mm, with a geometric standard deviation of $\sigma_g = 1.31$. The brash ice was confined as a layer over a channel formed by means of two floating side panels, which are visible in Figure A2.

For each experiment the brash-ice layer was leveled such that it was of the requisite average thickness; at some points the thickness varied by as much as 4 mm, the thickness of a single piece of brash ice. The model was then accelerated to speed and towed at a constant speed for about 12 m along the ice tank. Each transit of the model through the channel was videotaped to record the manner of brash-ice movement around the model. Of particular interest was the influence of model speed on the formation and areal concentration of open water in the track left by the model.

Results

The relationships between the mean total resistance R and the hull speed V for the tow in parallel and series configurations are shown in Figures A3 and A4, respectively. The third variable in these figures is h/D. The general trend apparent in these figures is that R increases with increasing V, though, for the model configured with tows in parallel, R decreased mildly as V increased to about 0.2 m^2 (1.1 m^2 at full scale). No such decrease occurred for the model configured with the two barges in series. The difference in the trends for R can be attributed to the influence of false-bow formation. The broader parallel-barge arrangement created a larger false bow than did the series-barge arrangement. Figure A2b illustrates the lateral extent to which false-bow formation generates shear stresses through a layer of brash ice and thereby increases layer resistance. The extent of false-bow formation decreased with increasing V, and so did the component of resistance attributable to false-bow formation.

Figures A3 and A4 show that the relationship between mean ice resistance R_i (= $R-R_o$) and V is similar to that between R and V. On the whole, R_i increased, albeit mildly, with increasing V. However, it did not decrease with increasing V as it did in the data presented by Ashton et al.

When the channel was narrowed from $W/B = 3.0$ to $W/B = 1.2$, the tow with two barges in parallel encountered increased resistance, except when transiting the thinnest layer ($h/D = 0.05$) at creeping speeds. For those transits the width of the false bow was limited to the channel width, causing less ice to be shoved and therefore resulting in diminished R.

Other than indicating that R generally increased with increasing h/D and V, further discussion of the data presented in Figures A3 and A4 is complicated by variations in the processes contributing to resistance.

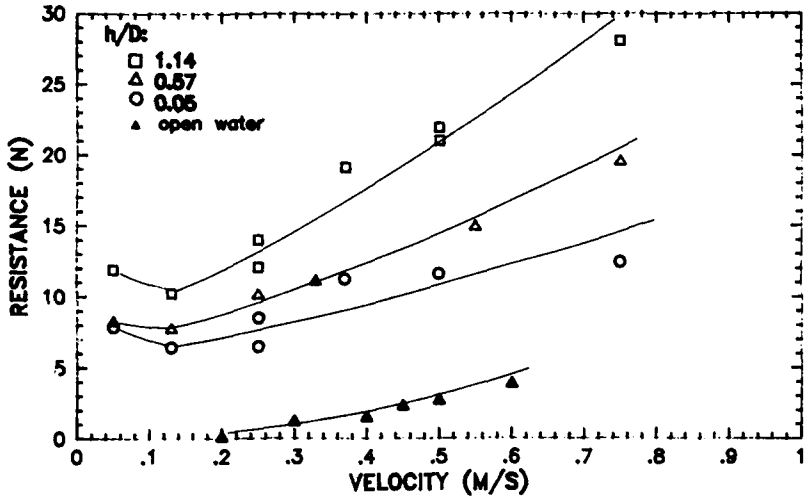

a. Wide channel.

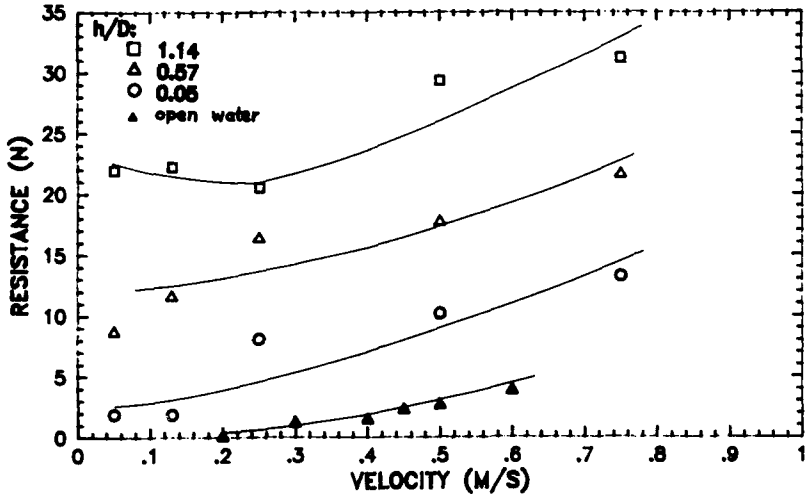

b. Narrow channel.

Figure A3. Variation of mean resistance R *with barge speed (parallel configuration).*

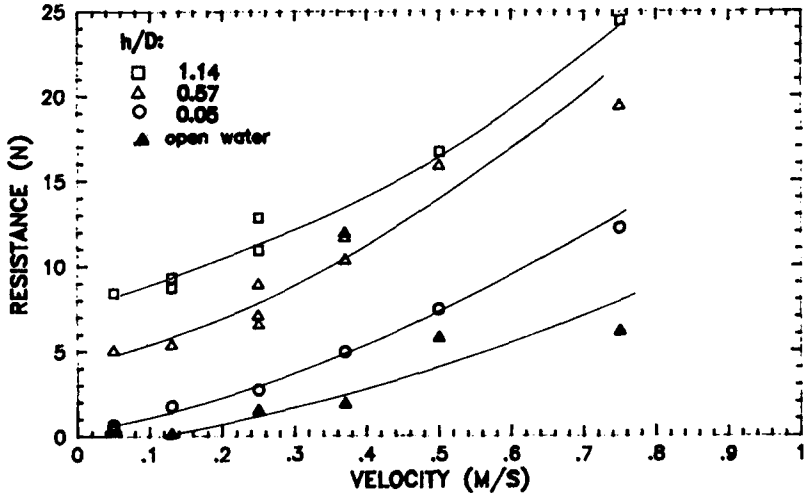

Figure A4. Variation of mean resistance R *with barge speed (series configuration).*

Conclusions

The following conclusions concerning the relative resistance for each tow configuration can, however, be made from the data. The tow comprising two parallel barges generally encountered greater resistance than did the tow comprising two barges in series. For transits at creeping or slow speed, the difference of R values diminished with increasing h/D. The difference in R values also decreased with increasing V such that, at the highest speed tested, the resistances are of comparable magnitude. Essentially, when brash ice significantly accumulated beneath the hull or formed as a false bow, the wider hull encountered about three times more resistance.

APPENDIX B: PHOTOGRAPHS OF BRASH-ICE SAMPLES

Figure B1. 1:15-scale tow; f_t = 1/(2 hours).

Figure B2. 1:15-scale tow; f_t = 1/(4 hours).

Figure B3. 1:15-scale tow; f_t = 1/(0.5 hour) and f_n = 1/(7.5 hours).

Figure B4. 1:15-scale tow; f_t = 1/(8 hours).

Figure B5. 1:15-scale tow; f_t = 1/(4 hours) and y_o/D = 2.78.

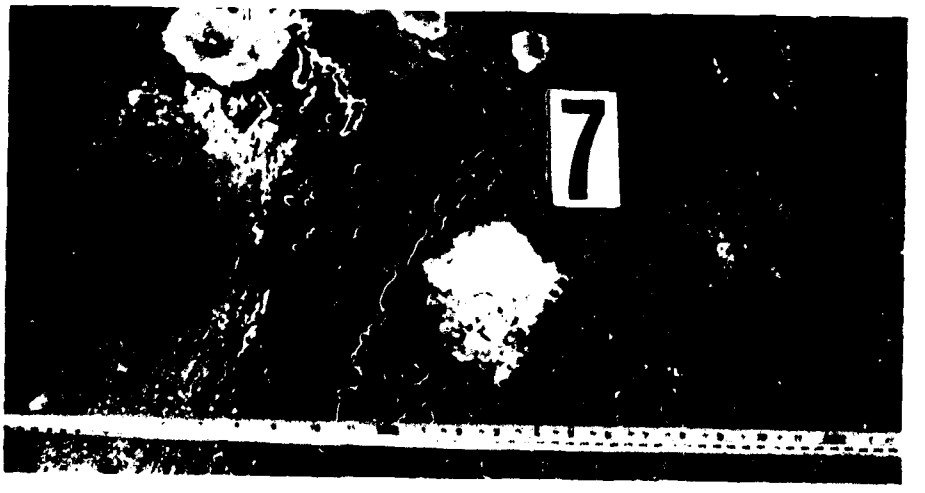

Figure B6. 1:15-scale tow; f_t = 1/(2 hours) and y_o/D = 1.16.

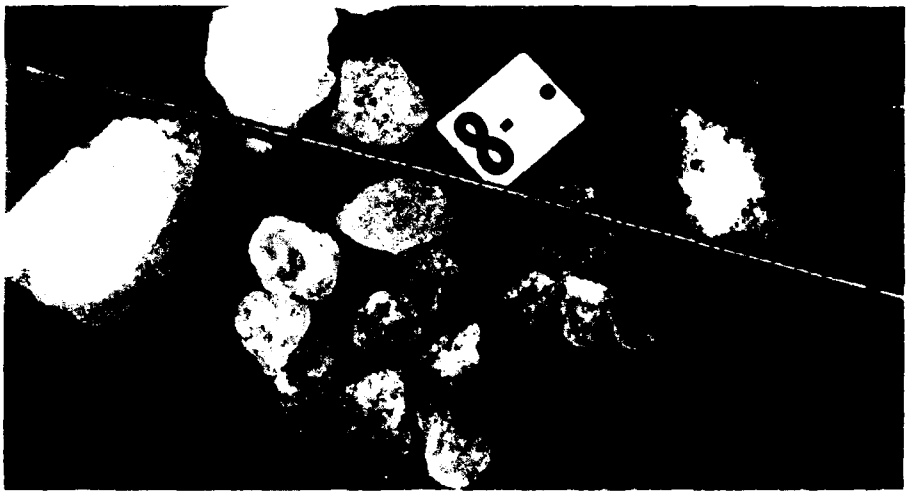

Figure B7. 1:15-scale wedge; f_t = 1/(4 hours).

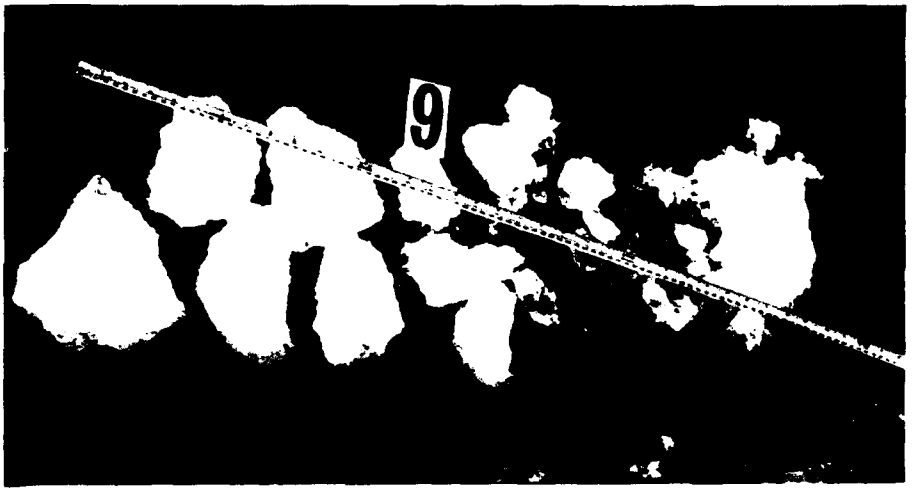

Figure B8. 1:15-scale wedge; f_t = 1/(2 hours).

Figure B9 1:15-scale wedge; f_t = 1/(0.5 hour) and f_n = 1/(7.5 hours).

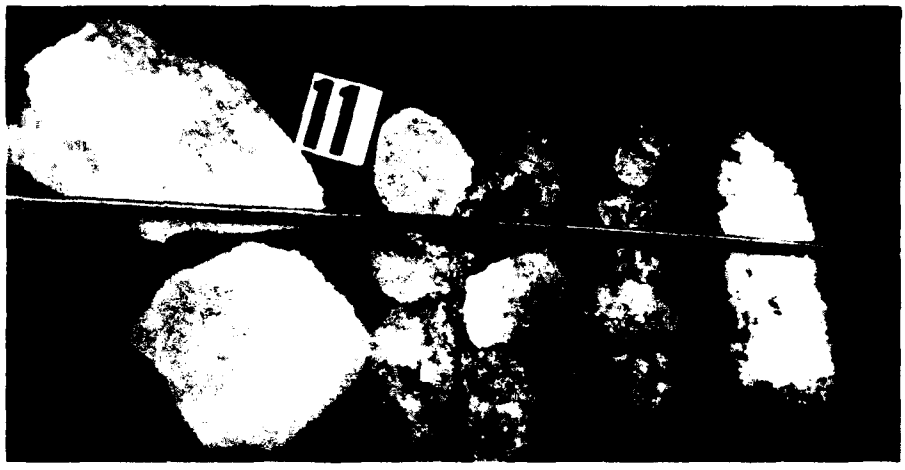

Figure B10. 1:15-scale wedge; f_t = 1/(8 hours).

Figure B11. 1:15-scale wedge; f_t = 1/(0.5 hours).

APPENDIX C: VOLUMES OF ICE GROWN ALONG EACH TRACK TRANSITED BY THE WEDGE HULL AND THE THICKNESS OF BRASH-ICE ACCUMULATION IN EACH TRACK, BOTH NORMALIZED WITH η.

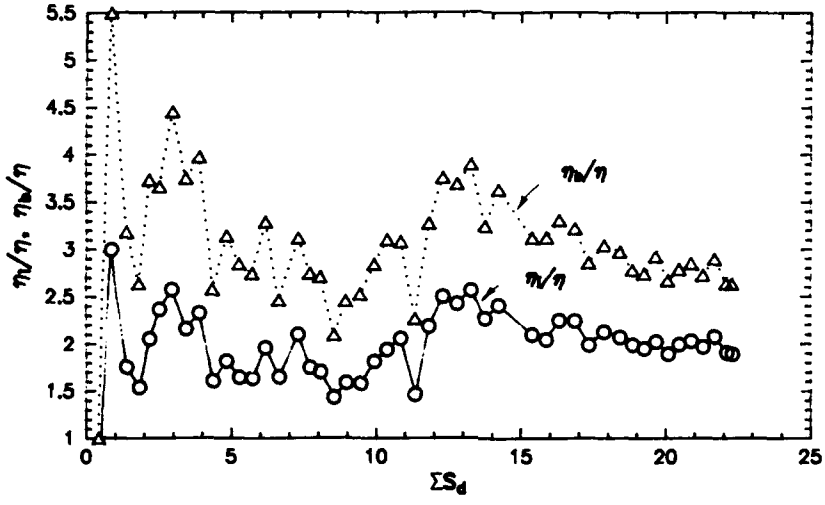

Figure C1. Variation of η_t/η and η_b/η with ΣS_d; f_t = 1/(0.5 hour).

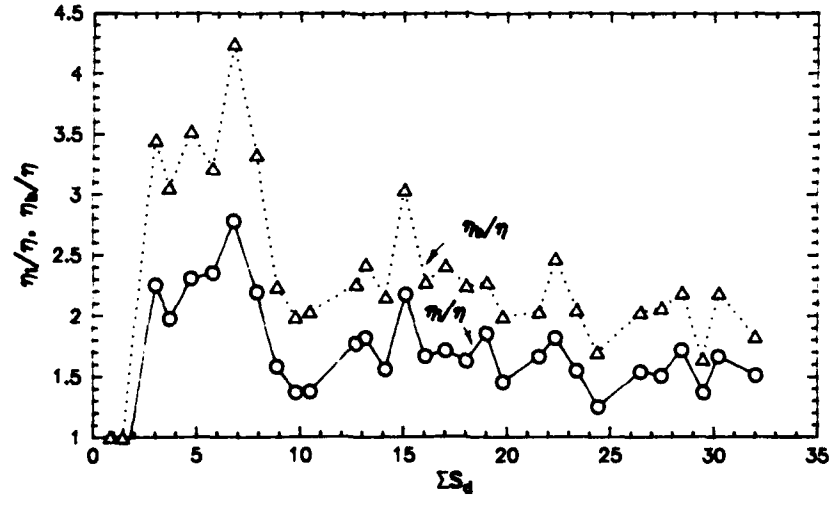

Figure C2. Variation of η_t/η and $\eta_b/$ with ΣS_d; f_t = 1/(2 hours).

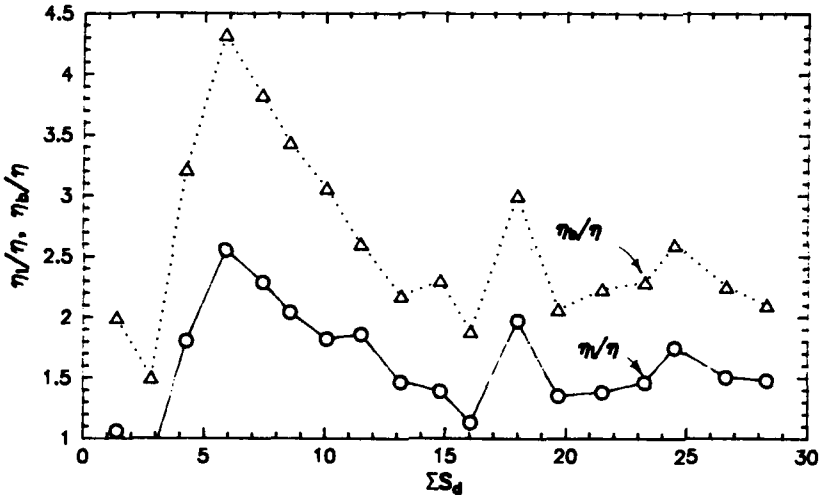

Figure C3. Variation of η_i/η and η_b/η with ΣS_d; $f_t = 1/(4$ hours).

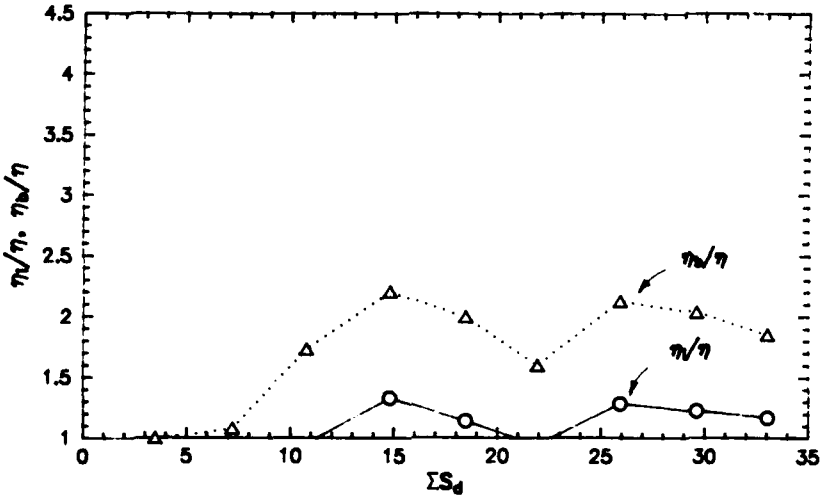

Figure C4. Variation of η_i/η and η_b/η with ΣS_d; $f_t = 1/(8$ hours).

APPENDIX D. PREDICTIONS FROM ASHTON'S FORMULATION

Ashton's formulation of ice formation in frequently transited navigation channels is exercised here to compare its predictions with those obtained with the formulation presented earlier. For Ashton's formulation, α = 24 mm/(°C-day) and β = 0.25. Figures D1–D3 are to be compared with Figures 69–71.

For transit frequencies less than about 1/day, Ashton's formulation predicts values of η_i/η that are comparable with those predicted using the authors' formulation. For f_t exceeding 1/day, eq 10 predicts even increasing values of h_i/h. The predictions obtained using the authors' formulation are also indicated for comparison on Figure D2.

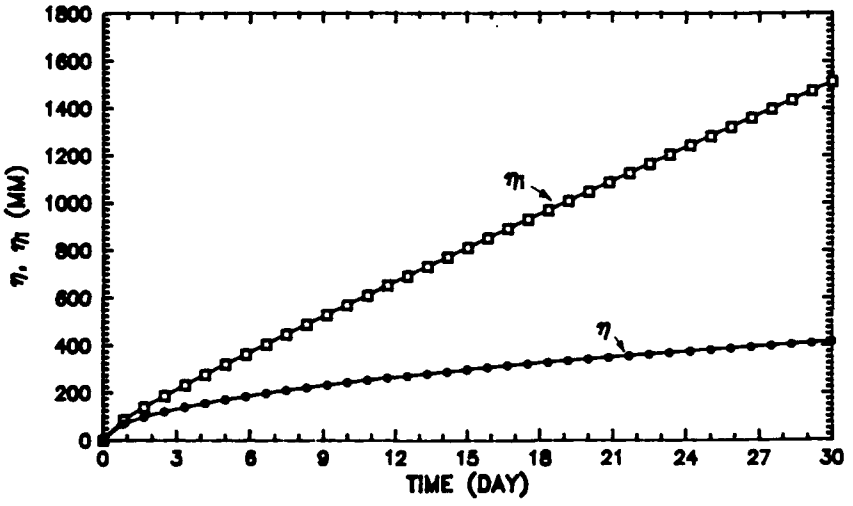

Figure D1. Variation of η_i with time.

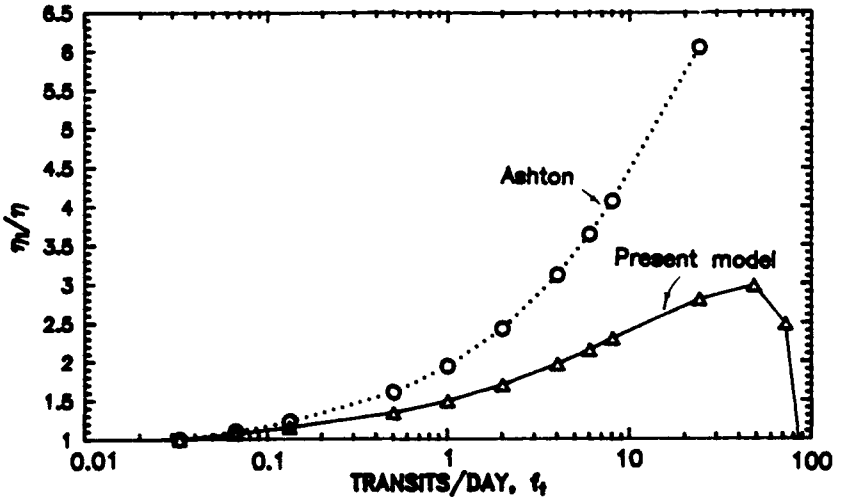

Figure D2. Variation of η_i/η with f_t.

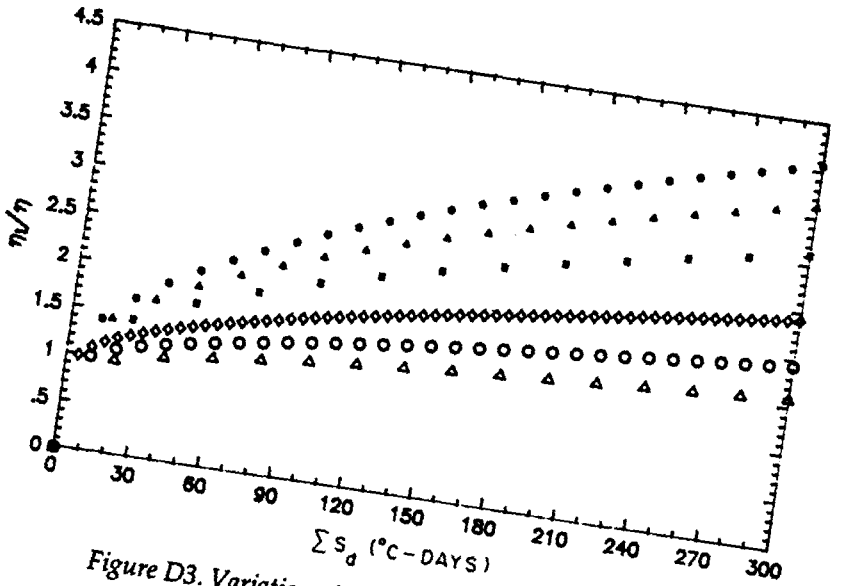

Figure D3. Variation of η_i/η with ΣS_d for varying f_i.

REPORT DOCUMENTATION PAGE

Form Approved
OMB No. 0704-0188

1. AGENCY USE ONLY (Leave blank)	2. REPORT DATE	3. REPORT TYPE AND DATES COVERED
	December 1990	

4. TITLE AND SUBTITLE
Ice Formation In Frequently Transited Navigation Channels

5. FUNDING NUMBERS
WU: CWIS 32292

6. AUTHORS
Robert Ettema and Hung-Pin Huang

7. PERFORMING ORGANIZATION NAME(S) AND ADDRESS(ES)
Iowa Institute of Hydraulic Research
University of Iowa
Iowa City, Iowa

8. PERFORMING ORGANIZATION REPORT NUMBER

9. SPONSORING/MONITORING AGENCY NAME(S) AND ADDRESS(ES)
Office of the Chief of Engineers
Washington, D.C. 20314

U.S. Army Cold Regions Research and Engineering Laboratory
72 Lyme Road
Hanover, New Hampshire 03755-1290

10. SPONSORING/MONITORING AGENCY REPORT NUMBER
Special Report 90-40

11. SUPPLEMENTARY NOTES

12a. DISTRIBUTION/AVAILABILITY STATEMENT
Approved for public release; distribution is unlimited.

Available from NTIS, Springfield, Virginia 22161

12b. DISTRIBUTION CODE

13. ABSTRACT (*Maximum 200 words*)

Results are reported of a study aimed at determining and documenting the effects of frequent vessel transit on ice-cover formation over navigation channels. A practical objective of this study was to evaluate the merits of scheduling vessel transits as a means of mitigating problems caused by transiting of ice-covered channels. Vessels transiting through ice covers lead to increased ice growth and transform ice to brash ice, which collects in thick accumulations that may halt traffic. The study entailed extensive laboratory experiments conducted with an ice tank and model hulls that simulated river tows and ships. It also included the formulation and use of a numerical model of ice formation. Another brief study examined the mechanics of ice accumulation beneath flat-bottomed tows.

The results from the ice-tank experiments and the numerical model indicate that, except for convoys of vessels, the problems incurred by frequent transiting are not readily mitigated by a sophisticated transiting schedule. Convoying does hold promise of reducing the severity of problem because it reduces the number of icebreaking transits. Of greater promise, however, is an approach involving mechanical methods for controlling brash-ice accumulations at perennially difficult channel locations.

14. SUBJECT TERMS
Ice-covered channels
Ice formation
Navigation channels
River navigation

15. NUMBER OF PAGES
120

16. PRICE CODE

17. SECURITY CLASSIFICATION OF REPORT	18. SECURITY CLASSIFICATION OF THIS PAGE	19. SECURITY CLASSIFICATION OF ABSTRACT	20. LIMITATION OF ABSTRACT
UNCLASSIFIED	UNCLASSIFIED	UNCLASSIFIED	UL

NSN 7540-01-280-5500

☆ U. S. GOVERNMENT PRINTING OFFICE: 1991--500-063--.2055

Standard Form 298 (Rev. 2-89)
Prescribed by ANSI Std. Z39-18
298-102